THE PARNAÍBA RIVER DELTA - FROM MODERN HYDRO AND MORPHODYNAMICS TO SEA LEVEL CHANGE

Dissertation

Zur Erlangung des Doktorgrades

der Mathematisch-Naturwissenschaftlichen Fakultät

der Christian-Albrechts-Universität

Kiel

vorgelegt von

André G. Aquino da Silva

Kiel, 2015

THE PARNAÍBA RIVER DELTA - FROM MODERN HYDRO AND MORPHODYNAMICS TO SEA LEVEL CHANGE

Dissertation

Zur Erlangung des Doktorgrades

der Mathematisch-Naturwissenschaftlichen Fakultät

der Christian-Albrechts-Universität

Kiel

vorgelegt von

André G. Aquino da Silva

Kiel, 2015

Referent: Prof. Dr. K. Stattegger

Korreferent: Prof. Dr. Helenice Vital

Tag der mündlichen Prüfung: May 11th, 2015

Zum Druck genehmigt: May 11th, 2015

gez. Prof. Dr. Wolfgang J. Duschl, Dekan

I affirm in lieu of oath that:

i) apart from the supervisor's guidance the content and design of the paper is all the candidate's own work,

ii) the present thesis has not been submitted either partially or wholly as part of a doctoral degree to another examining body and whether it has been published or submitted for publication;

that the thesis has already been prepared subject to the Rules of Good Scientific Practice of the German Research Foundation;

Date of official submission:

Kiel, February 24th 2015 Signature: _____

ABSTRACT

This study presents the first findings regarding the hydrography, morphodynamics, hydrodynamics and sea-level change on Parnaíba River (PR) and its delta. The PR is 1,400 km long and located in NE Brazil. It forms an asymmetric wave dominated delta, the Parnaíba River Delta (PRD). The delta region is approximately 100 km wide and has tidal channels forming an estuarine-lagoonal system, west of PR. The delta is located in a transition zone in terms of climatic and oceanographic conditions. Despite the existence of a river dam on its mid-course, the river has a moderate (approximately 91 mg/l, in average) suspended sediment load which is mainly attributed to the geology and the climatic conditions of its drainage basin.

Rainfall data from 1965 to 2009 revealed seasonal variations on rainfall and suspended sediment concentration (SSC). Moreover, harmonic analysis of time series revealed a correlation of both, rainfall and SSC, with El Niño-Southern Oscillation (ENSO).

The suspended sediment concentration was calculated from a set of 12 multispectral satellite images (CBERS 2-B and LANDSAT TM 5), which were calibrated using in situ measurements. Using averaged river discharge and remote sensed suspended sediment concentration it was possible to estimate the amount of sediment that is transported through the PR to the continental shelf.

The PR is the primary sediment source to the adjacent coast and this is evidenced by the shoreline stability and progradation noticed at the vicinities of the river mouth (observed on decadal time scale using satellite images).

The river runoff interferes on the direction of the offshore bottom currents on the continental shelf up to 4 km in front of the river mouth. It acts as a hydrodynamic groin preventing sediment bypass.

Offshore bathymetry and seismic profiles depicted evidences of past sea level on the continental shelf offshore PRD in the form of incised valley and paleo-channels. Interpretations of architectural elements, seismic facies and seismic boundaries were related to extreme events of sea level such as sea level low- and highstand providing relative age control for the formation and complete burial of the paleo-channels.

Relating worldwide reconstructions of sea level curves to the interpretations it is suggested that the valley incision occurred during the Late Pleistocene sea-level drop and lowstand (70,000 – 20,000 years BP). Moreover, the valley infill indicates the

flooding of the shelf during deglacial sea-level rise that reached the mid-Holocene highstand around 5,500 years BP.

ZUSAMMENFASSUNG

Diese Arbeit präsentiert neue Erkenntnisse über die hydrographischen, hydrodynamischen und morphodynamischen Verhältnisse, sowie Meeresspiegeländerungen im Parnaiba Fluss (PR) und seinem Delta (PRD). Der PR ist etwa 1,400 km lang und befindet sich in NE Brasiliens. Sein Mündungsbereich zeichnet sich durch ein asymetrisches, wellendominiertes Delta aus. Bezogen auf die klimatischen und ozeanographischen Randbedingungen liegt das Delta in einem Übergangsbereich. Die Suspensionsfracht ist trotz eines im zentralen Teil des Flusslaufs befindlichen Staudamms relativ hoch (bis zu 91 mg/l, im Durchschnitt), was durch die anstehenden Gesteinen und den vorherrschenden Klimabedingungen hervorgerufen wird.

Niederschlagsdaten aus den Jahren 1965 bis 2009 zeigen eine deutliche saisonale Variation in Niederschlagsmenge und Suspensionskonzentration (SSC). Zudem kann mit Hilfe einer harmonischen Analyse der Datenreihe eine Korrelation der Niederschlagsmenge und der SSC mit der El Ninõ Southern Oscillation (ENSO) beobachtet werden.

Basierend auf einem Datensatz aus 12 multispektralen Satellitenbildern (CBERS 2-B und LANDSAT TM5) wurden SSCs errechnet und mittels in situ Messungen kalibriert. Die ermittelten SSCs und der durchschnittlichen Abflussraten erlaube eine Abschätzung der Sedimentmengen, die durch den PR auf den Schelf transportiert wird
Der PR ist die primäre Sedimentquelle für die angrenzenden Küstengebiete. Dies wird durch die über einen Zeitraum von mehreren Jahrzehnten in Satellitenbildern beobachtete Stabilität und Progradation der Küstenlinie nahe der Flussmündung deutlich.

Aus dem Fluss strömende Wassermassen haben einen Einfluss bis zu 4 km vor der Flussmündung auf die Bodenströmungen im vorgelagerten Schelf und wirken dabei wie eine hydrodynamische Buhne, die in den küstenparallelen Sedimenttransport eingreift. Das PRD ist in etwa 100 km breit und zeigt im Westen eine Vielzahl von Tidekanälen, die sich durch ästuarin-lagunäre Bedingungen auszeichnen.

Bathymetrische Daten und seismische Profile ermöglichen Rückschlüsse auf frühere Meeresspiegelphasen entlang des vorgelagerten Schelfs, da sie alte, eingeschnittene Flusstäler und Paläo-Rinnen im Untergrund zeigen. Die Architektur des Untergrunds mit den darin beobachteten seismischen Fazies und Reflektoren kann auf

extreme Meeresspiegelereignisse, wie Meeresspiel-Hoch und Niedrigstände zurückgeführt werden und können somit als relative Alterseinstufung dienen.
Im Zusammenhang mit bekannten weltweiten Meeresspiegelrekonstruktionen lassen die Daten den Schluss zu, dass die beobachteten eingeschnittenen Täler und Kanäle mit dem auftretenden Meeresspiegelrückgangs und Niedrigstand im späten Pleistozän zusammenhängen (70,000-20,000 Jahre BP). Desweiteren deuten die Verfüllungen dieser Täler und Rinnen auf eine anschließende Flutung des Schelfs während des postglazialen Meeresspiegelanstiegs hin, welcher seinen Höchststand im mittleren Holozän erreicht (ca. 5,000 Jahre BP).

RESUMO

Este trabalho apresenta as primeiras descobertas com relação à hidrigrafia, morfodinêmica, hidrodinâmica e variações de níveis do mar no rio Parnaíba e seu delta. O rio Parnaíba (RP) tem aproximadamente 1.400 km de extensão, localizado no nordeste do Brasil, que forma um delta assimétrico dominado por ondas, o Delta do Rio Parnaíba (DRP). A região do delta tem aproximadamente 100 km de extensão e tem canais de maré que formam um sistema estuarino-lagunar, a leste do RP. O delta está localizado em uma zona de transição, de acordo com suas condições climáticas e ocenográficas. Apesar de haver uma represa no seu médio-curso, o rio tem uma moderada descarga de sedimento em suspenção (média de aproximadamente 91 mg/l) a qual é principalmente atribuída a geologia e condições climáticas da sua bacia de drenagem. Dados de chuvas entre 1965 e 2009 revelaram uma variação sazonal tanto de chuvas quanto de concentração de sedimento em suspenção (CSS). Além disso, análises harmônicas de séries temporais revelaram a correlação de ambos, chuvas e CSS, com El-Niño Southern Oscillation.

A concentração de material em suspensão foi calculada a partir de 12 imagens de satélite multiespectral (CBERS-2B e LANDSAT TM-5) que foram calibradas usando dados de medições *in situ.* Utilizando médias de vazão e concentração de sedimento em suspensão por sensores remotos foi possível estimar a descarga de sedimento em suspenção do RP para a plataforma continental.

O RP é a principal fonte de sedimento para a costa adjacente, isto é evidenciado pela estabilidade e progradação da linha de costa observada nas proximidades da sua foz (observada em escala de decadal utilizando imagens de satélite).

A descarga do rio interfere na direção das correntes de fundo *offshore*, na plataforma continental até uma distância de 4 km da foz. Isto funciona como uma barreira hidrodinâmica impedindo o transporte longitudinal de sedimento.

Perfis sísmicos e a batimetria da plataforma mostram evidencias de níveis do mar pretéritos, na plataforma continental próxima ao DRP, na forma vales incisos. A interpretação de unidades sísmicas, elementos arquiteturais, fácies sísmicas e limites sísmicos, foram relacionados a mudanças do nível do mar, tais como níveis de mar baixo e alto, proporcionando controle temporal relativo para a formação e completo soterramento dos páleo-canais. Relacionando curvas de reconstrução de nível do mar de escala mundial as interpretações, foi possível sugerir que a incisão do vale ocorreu

durante a queda do nível do mar no Pleistoceno tardio e nível de mar baixo (70.000 – 20.000 anos B.P.). Além disso, que o preenchimento do vale indica a inundação da plataforma continental durante a subida do nível do mar pela completa deglaciação, quando o nível do mar atingiu seu nível mais alto em meados do Holoceno, aproximadamente 5.500 anos BP.

TABLE OF CONTENTS

Chapter 1 - INTRODUCTION

1.1. – Description and Objectives

The three major rivers of N and NE Brazil are the Amazon, São Francisco and Parnaíba. Despite its importance, Parnaíba River has never been subject of a proper scientific research due to several reasons and one of them is its geographic location. It is located in a very poor area of Brazil, Piauí (PI) and Maranhão (MA) states, which have a very low human development index (HDI) with average of 0.713 e 0.683, to Piauí (PI) and Maranhão (MA), respectively. During the last 5 years, wind power has grown and wind farms were installed on PI's coast. The underdevelopment of the region also represents the absence or incipient human interference that results on modifications on the natural development of the coastline. The natural states of the region led to the interest on develop a scientific research aiming the understanding of the geological formation of this area. On this frame this research is inserted on the objectives of the project "Northern Brazilian river deltas: River impacts versus pristine discharge" is sponsored by the German Research Foundation (DFG), grant number: STA 401/16-1. In this project the main objectives have been the analysis of hydrodynamic and sediment dynamic processes in the Parnaíba delta and its adjacent shelf areas in the framework of the Holocene evolution of this wave- and tide-dominated delta.

This thesis is organized as follows:

Chapter 1 gives an introduction about the research and the research area, chapter 2 summarizes the methodology and the data set used and chapter 3 describes the geological background.

Chapter 4 describes the general settings of the study area characterizing its major physical, geological and meteorological settings.

Chapter 5 covers the approach used to estimate suspended sediment concentration, on Parnaíba River (PR) using multispectral satellite images calibrated using ground controlling samples.

Chapter 6 describes the findings resulted from the high resolution seismic survey done on the entire area of the delta.

Chapter 7 summarizes the results and Chapter 8 gives the general conclusions.

1.2. - The Parnaíba River and its Delta

The PR is the second major river in NE Brazil in length and water discharge. It marks the border between PI and MA States. PR is formed by the confluence of the two rivers:

Água Quente and Lontra do Piauí, and has its source at Mangabeiras Plateau at approximately 280m above sea level (Figure 1). PR is approximately 1,400 km long and has a catchment area of 344,000 km^2 comprising the entire PI State and part of MA and Ceará (CE) States (Figure 1).

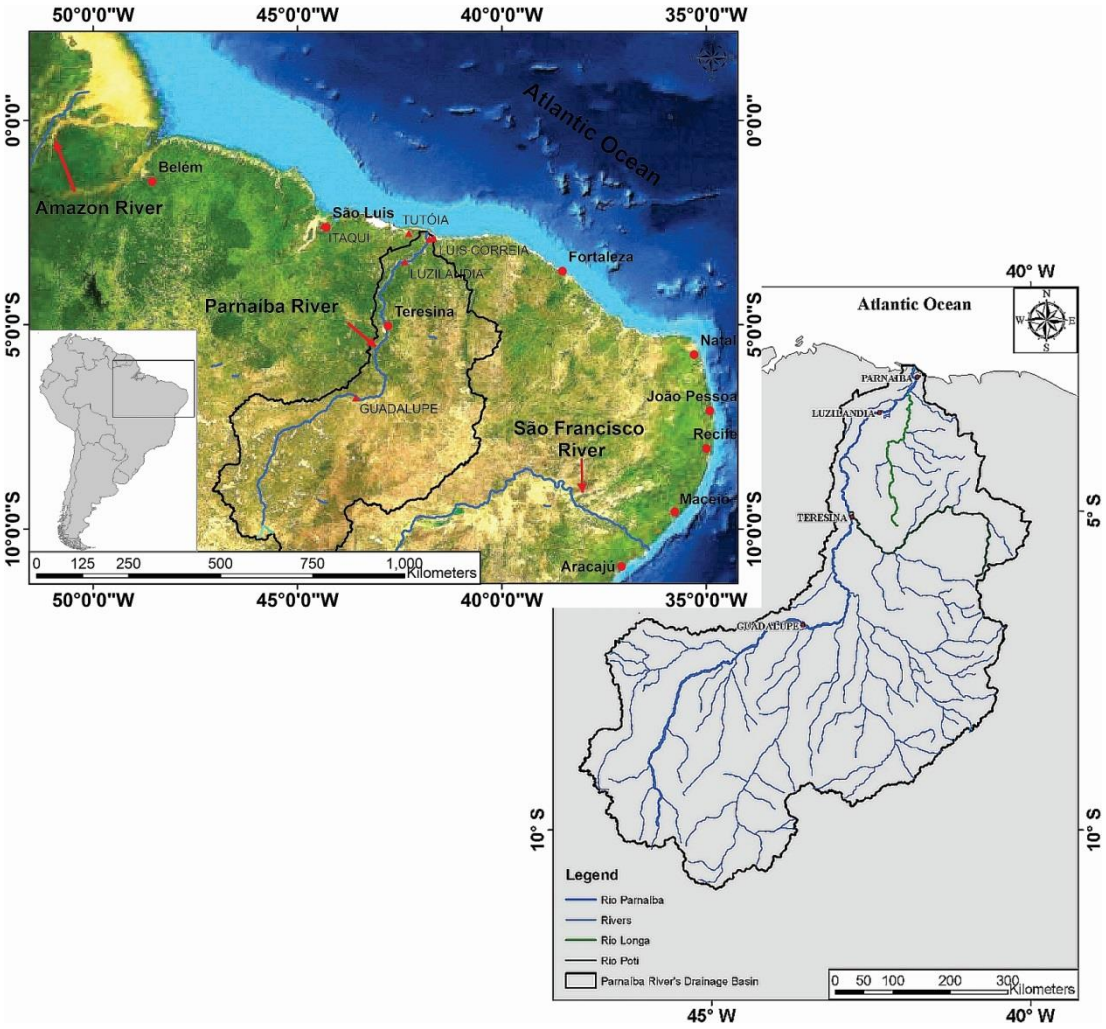

Figure 1- Location of Parnaíba River, its position related to Amazon and São Francisco Rivers and the dimension of its drainage basin.

It is divided in sector named as High Parnaíba, Medium Parnaíba and Low Parnaíba. This classification is done as follows: High Parnaíba: From its source until Boa Esperança water reservoir. Medium Parnaíba: from Boa Esperança until the confluence with Potí River, on Terezina. Low Parnaíba: from Terezina until its mouth on the Atlantic Ocean. The River has an approximate average discharge of 16 billion m^3/year, has an averaged slope of 0.027° and passes through 42 cities along its way to the Atlantic Ocean. Along its course PR passes through Parnaíba and Barreirinhas sedimentary Basins, leaching sediment from both. The deposition of these sediments on the continental shelf, along the geologic time, led to the formation of a 100 km long, wave dominated asymmetric delta called Parnaíba River Delta (PRD).

The delta is divided in two parts by its main distributary. Tidal channels are the major feature of the west part, which has is only one artificial connection to the PR that is located 13 km upstream. On the east part there is a distributary of PR called Igaraçú River which passes through the cities of Parnaíba and Luiz Correia (Figure 2).

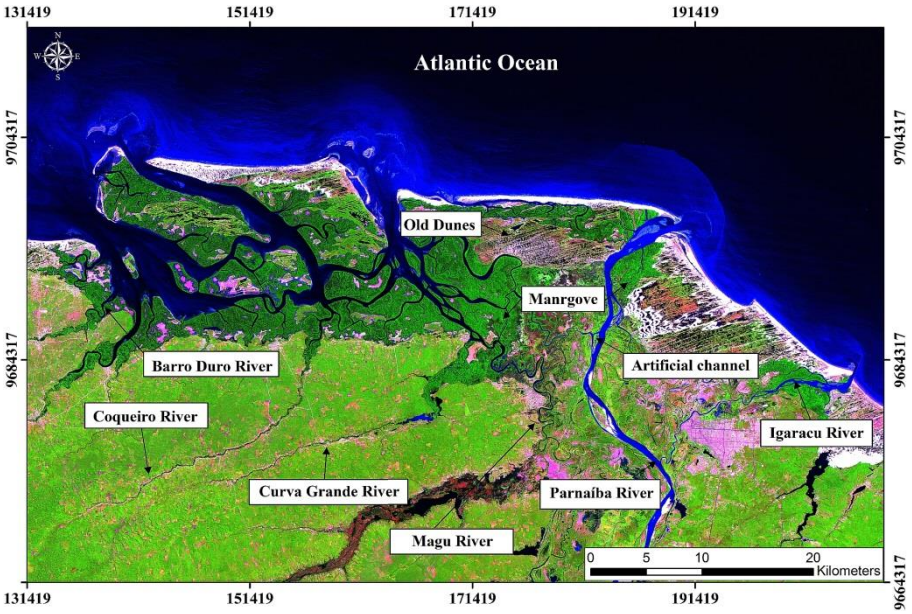

Figure 2 – This figure is an overview of PRD. West of PR, it depicts the tidal channels on and the rivers that drain into this part of the delta. East of PR, it displays the Igaraçú river that is the last distributary of PR. In addition, the dark green areas represent the mangrove coverage at the vicinities of the rivers and tidal channels.

The continental shelf offshore PRD is shallow and narrow which is a characteristic of NE Brazilian continental shelves (Gomes and Vital, 2010). In this region the continental shelf is approximately 50 km wide with the shelf break at 40 m water depth (Figure 3). The region is in meso-tidal range with maximum amplitude of 3.06 m occurring in semi-diurnal regime. Due to the shallow character of the shelf, there is no salinity stratification and salinity ranges from 33 PSU to 36 PSU. Similarly, temperatures do not vary with depth and ranges from 28^0 C to 31^0 C.

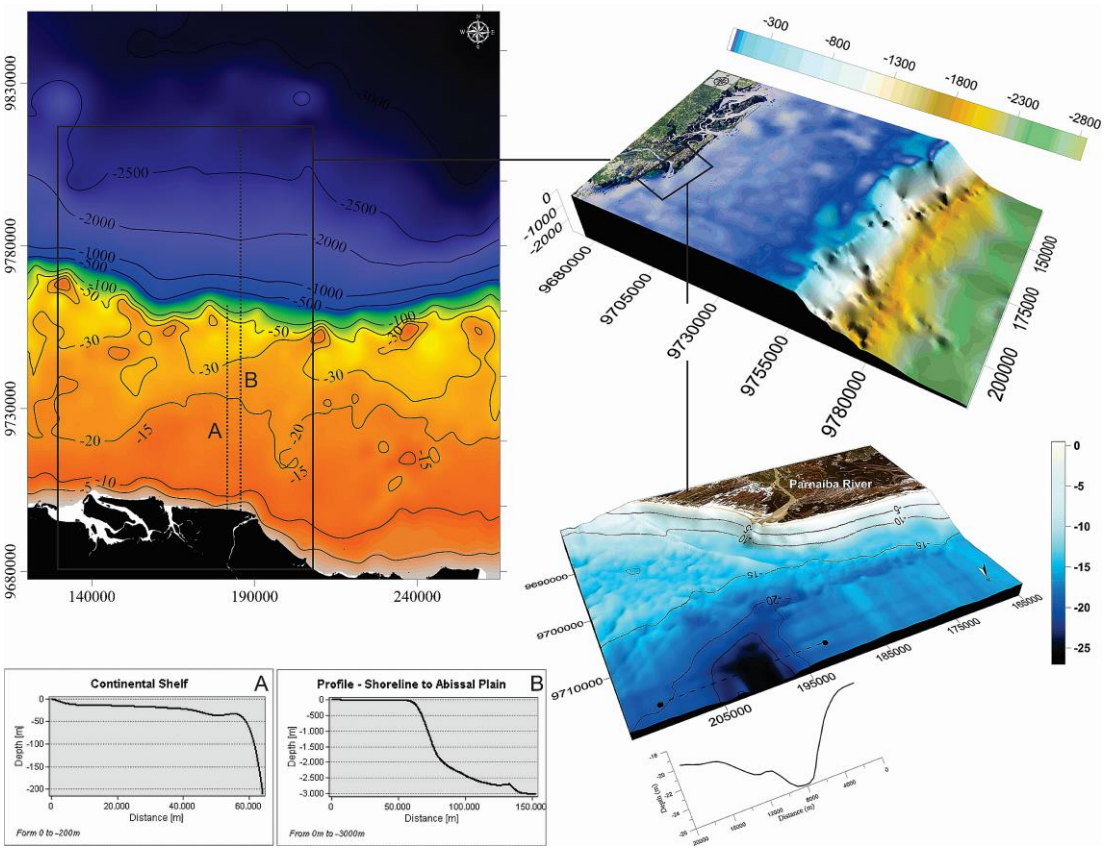

Figure 3 – Bathymetric and 3D map of the continental shelf (left) and the detail of the incised-valley (right) offshore PR.

Chapter 2 – MATERIAL AND METHODS

This chapter aims to give a brief summary of the methods and data sets used on this project. The specifics of each method will be discussed in detail in each chapter.

The data set analyzed on this work comprises measurements performed in two field campaigns (February of 2009 and March of 2010) and data provided from Brazilian governmental agencies, such as: INMET, IBGE, ANA, INPE, CHESF, CPRM, PETROBRAS, between others. The data acquired on the field campaigns cover measurements of physical water properties (salinity and temperature), suspended sediment concentration (SSC), offshore bottom currents, tidal variation, offshore bathymetry and high resolution shallow seismic. The data provided by the Brazilian governmental agencies were meteorological information of the area and riverine related data (drainage basin, river discharge and suspended sediment concentration).

The physical water properties (salinity and temperature) of the PR as well as of the tidal channel area on the west were measured using one CTD profiler. A CTD station was located approximately 5 km upstream of PR moth where were performed 25 vertical profiles, one at each hour. Moreover, in the west most tidal channel was made

one transect composed of 7 vertical CTD profiles, which were spaced one nautical mile from each other. During the measurements were collected surface water samples (0.5 m bellow water surface) to measure SSC though filtering. The filtering process was carried out using a vacuum pump and previously weighted 4 µm fiber glass filters. Measured SSC were used as *in situ* data for calibrating Tasan's algorithm and retrieving SSC using multi-spectral satellite images (Tasan, 1987).

Offshore bottom currents were measured using one S4 oceanographic buoy, positioned at 1 m above sea floor. The buoy measured current velocity and direction for 28 days (March 7th to April 4th) with 30-minute standby period, which results in two data per hour.

Tidal information was obtained from the Brazilian Navy and measured, from 16–19 March 2010 (spring tide), using a tidal gauge that was installed 5 km upstream of the mouth of the PR to record tidal variation with 5-minute record interval.

Over 500 km of high resolution shallow seismic profiles were acquired using the sub-bottom profiler SES 2000 Standard from INNOMAR, which uses dual frequency chirp technology recording both low and high frequency signals (LF and HF, respectively). A dynamic motion sensor (DMS) was used to compensate pitch and roll originated by wave interference, which was installed immediately aside the SES 2000 Standard transducer as well as the GPS antenna, in order to minimize post-acquisition positioning corrections. Seismic lines were surveyed along the entire area offshore PRD (Figure 1) to acquire substantial data about the sub-bottom features. Processing of the seismic lines was restricted to the use of bandpass filters and time-varying gain to minimize the spherical divergence effects. For depth calculation the sound velocity for average sea water (1,500 m/s) was used, given the simplicity of the depth conversion which was successfully applied in other areas (Schwarzer *et al.,* 2000; Schwarzer *et al.,* 2006). The positions of the features found were plotted on map, wherever they occur, for visualization of their spatial distribution.

The bathymetric information was acquired from single beam echosounder and remotely sensed data (SRTM-30 plus). The single beam data was acquired concomitantly to the seismic data and covers the entire delta area. However, given the size of the area of investigation was necessary to complement this data using data from SRTM-30 plus which provide a depth measurement at each 30 arc second, which at 2º S of latitude is approximately half of a nautical mile (Becker *et al.,* 2009).

Chapter 3 – SETTINGS

3.1. – Geological Settings

PR flows mostly over sedimentary deposits from Parnaíba Basin and only on its lowermost section and its mouth on Barreirinhas Basin.

The Parnaíba Basin covers an area of approximately 400,000 wide km^2 and 3,000 m thick of siliciclastic and carbonatic rocks which are remnants of Afro-Brazilian sedimentation, occurred in three transgressive-regressive cycles. These cycles started on the Silurian and lasted until the continentalization of the basin during the Triassic and are represented by Serra Grande, Canindé and Balsas groups (Goes & Feijó, 1994). The installation of one rift system with rocks deposited in fluvial-lacustrine environment with volcanic rocks associated (Jurassic and Eo-Cretacic) were correlated to the opening of the South Atlantic Ocean. The effective opening of the South Atlantic Ocean, on Cretaceous, new depocenters were created: To the north, predominated deposition in eolic-lacustrine environment and to the south predominated sedimentation in fluvial-eolic environment. Therefore, according to Goes & Feijó (1994), Parnaíba Basin is represented only by Paleozoic rocks corresponding to the groups Serra Grande, Canindé and Balsas. They had a tectonic-sedimentary development associated to the basin basement subsidence in the evolutionary context of the Gondwana Paleo-continent. The tectonic and sedimentary aspects observed after Balsas group deposition are directly related to the rupture process of Gondwana, hence, considered as having distinct evolutionary context to the Parnaíba Basin (Rosseti *et al.,* 2001).

The area of Parnaíba River Delta is located at the NE Brazilian coast on the border of the PI and MA States. It is located approximately 1,100km east from Amazon River and around 1,200km northwest from Sao Francisco River (Figure 1). It is inserted in the domains of the Barreirinhas basin which formation's is referred to the Albian and is composed by three Groups: Canárias, Cajú e Umberto de Campos. Barreirinhas basin is a coastal basin which has as its basement the whole stratigraphic column of the Parnaíba Basin that was developed between the Silurian and meddle Cretaceous approximately.

Barreirinhas Basin comprises an area of approximately 40,000km^2 of the coastal and continental shelf portion of the MA and PI States. The sedimentary fulfillment is represented by two stratigraphic sequences deposited in rift and passive margin systems. The rift sequence is dated from Eoalbiano and is represented by the Canárias group. The

passive margin sequence is represented by Cajú and Humberto de Campos Group and by Pirabas and Barreiras formation (Feijó, 1994).

This basin has onshore and offshore parts. The onshore part is the west continuation of the Ilha Nova Basin and is formed by listrics normal faults of WNW-ESE and NW-SE directions, which defines a distensive system cut by younger NE-SW strike-slip faults. It is west limited by the Parnaíba Platform, shoulder of the CE Basin. Its offshore part is linked to Pará-Maranhão Basin and is formed by NW-SE normal faults. Its oriental limit is the Tutóia High which separates Barreirinhas from CE Basin. Its occidental limit is not marked by any geologic feature and it mingles with Pará-Maranhão Basin.

The tectonic influence on this region can be noticed by the course of PR, with strait section, aligned according to the tectonic framework of Barreirinhas and Parníba Basins, changing directions in an "elbow" like shape. Almeida Filho *et al.* (2009) recognized the differences in drainage pattern from eastern and western sides of Pirapemas lineament.

3.2. Environmental Settings

The Parnaíba River is the second major river in NE Brazil (according to data provided from CHESF). It is formed by the confluence of two rivers Água Quente and Lontra do Piauí (Figure 4). The Parnaiba River extends from the Mangabeira's Plateau to the Atlantic Ocean where it forms a delta close to Parnaiba city. The catchment area covers approximately 344,112 km^2 (ANA) involving the entire PI and parts of MA and CE States.

The Parnaiba River Delta (PRD) is at the NE Brazilian coast at the border of Piauí and Maranhão states. It is located approximately 1,100km east from the Amazon River and 1200km northwest of the Sao Francisco River (Figure 1). The tidal conditions are semidiurnal reaching 3.3 m tidal range during spring tide and 1.7 m during neap tide.

Piauí State marks a climatic transition zone between the Pre-Amazon Wet and NE Semi-Arid (Andrade Jr. *et al.*, 2005) where the influence of both domains can be observed. This region has a short rainy season lasting from March only to April, although, it can vary from year to year. The duration of each season depends on the position of the Intertropical Convergence Zone and the occurrence and intensity of ENSO (El Niño-Southern Oscillation) phenomena (Hastenrath, 2006).

Chapter 4

THE INFLUENCE OF CLIMATIC VARIATIONS ON RIVER DELTA HYDRODYNAMICS AND MORPHODYNAMICS, THE EXAMPLE OF THE PARNAÍBA DELTA (NE BRAZIL)

André G. Aquino da Silva[†], Karl Stattegger[†], Klaus Schwarzer[†], Helenice Vital[‡], Bjorn Heise[†]

[†]Department of Sedimentology
Coastal and Continental Shelf Research Group
Christian-Albrechts-Universität zu Kiel
[‡]Programa de Pós-Graduação em Geodinâmica e Geofísica
Departamento de Geologia
Grupo de Pesquisa em Geologia Marinha e Monitoramento Ambiental
Universidade Federal do Rio Grande do Norte

Published on Journal of Coastal Research, reprinted with the permission from the Publisher JCRonline.org

ABSTRACT

In this work, we present a baseline study on the geo-environmental, morphodynamical, and hydrodynamical conditions of the Parnaíba River and its mouth, the Parnaíba River Delta (PRD). The outline of the PRD indicates that waves are the major forcing factor for delta development. Furthermore, the shape of the delta suggests that there is a considerable degree of asymmetry in its formation. The asymmetry is the result of coastal current influence on the reworking of the sediments that are discharged by the river. To investigate the hydrodynamic conditions of the area, field measurements were conducted on the river, offshore of the PRD, and on the tidal channels of the west part of the delta. At these locations, the currents, salinity, temperature, and tidal dynamics were measured. In addition, a time series of rainfall, river discharge, and suspended sediment concentration (SSC) were obtained from Brazilian governmental agencies. The interpretation of all of the data was used to determine how they interact to characterize the hydro- and morphodynamics of the PRD. Harmonic analysis was of high importance in the analysis of the time series, and it was employed to identify longer periods presenting similarities in terms of

meteorological conditions. This allowed determination of the interconnection between rainfall, river discharge, and SSC with the occurrence and intensity of the El Niño-Southern Oscillation. The influence of river discharge, rainfall, and SSC on shoreline change was demonstrated through the analysis of decadal shoreline evolution using a series of LANDSAT images covering the period from 1981 to 2009. The analysis revealed that most changes occurred westward from the PR mouth. Changes in spit migration velocity were correlated to variations in riverine sediment yielded as a result of variations of river discharge and SSC.

4.1. INTRODUCTION

Rivers are the major sediment suppliers to continental shelves (Milliman and Farnsworth, 2011; Milliman and Meade, 1983; Milliman and Syvitski, 1992; Vital *et al.*, 1998). Sediment type and grain size depend on weathering conditions, river flow pattern, land use, geological setting, and the drainage basin steepness. Suspended sediment load is the result of the combination of river discharge and suspended sediment concentration (SSC), which are greatly influenced by the amount of rainfall in the drainage basin. The amount of sediment that is discharged by river-runoff settles or is reworked depends upon the hydrodynamic conditions at the river mouth. In cases of river systems draining into the oceans, the capacity of the marine processes for reworking the sediments discharged by the river will determine the geomorphology of the coastline as well as the submarine conditions offshore of the river mouth. Marine deltas are formed when riverine sediment supply overcomes marine processes in reworking the discharged material (Bhattacharya and Goisan, 2003). The manner in which the sediment flushed by the river will be deposited and reworked depends on the local hydrodynamic conditions. The shape of the delta will be defined by the dominance of river discharge, tidal range, or wave energy over one another and the grain size distribution of the sediment (Galloway, 1975; Orton and Reading, 1993). Recently, sea-level rise (Goisan *et al.*, 2006) and human engineering (Syvitski *et al.*, 2005) have been reported as contributors to the modification of deltas. Channel switching is a common process that occurs with deltaic systems, and it is related to changes in river discharge, sediment supply, or tectonics. The Parnaíba River (PR) is the largest river system between the Amazon and São Francisco Rivers in terms of river discharge and drainage basin size. The river mouth is composed of a deltaic system approximately 100 km wide that, up to now, has not been a target of any oceanographic and geoscientific

investigations. This research presents a baseline study regarding the hydrodynamic and morphodynamic conditions of the Parnaíba River Delta (PRD). This information will provide the first characterization of this deltaic system in terms of the delta type and the dominant forces acting on it. This study also discusses the interconnection between the river dynamics and climatic Parnaíba conditions. In addition, it is demonstrated how climatic controlling events, such as El Niño-Southern Oscillation (ENSO), affect the morphological configuration of the coastline at the vicinities of the river mouths.

4.1.1. Study area

The PR is the second major river of NE Brazil in terms of length, river discharge, and drainage basin size. It is approximately 1400 km long and is formed by the confluence of the Água Quente and Lontra do Piauí Rivers (Figure 1). The PR is divided into three sectors: the high, medium, and low Parnaíba (Figure 1).

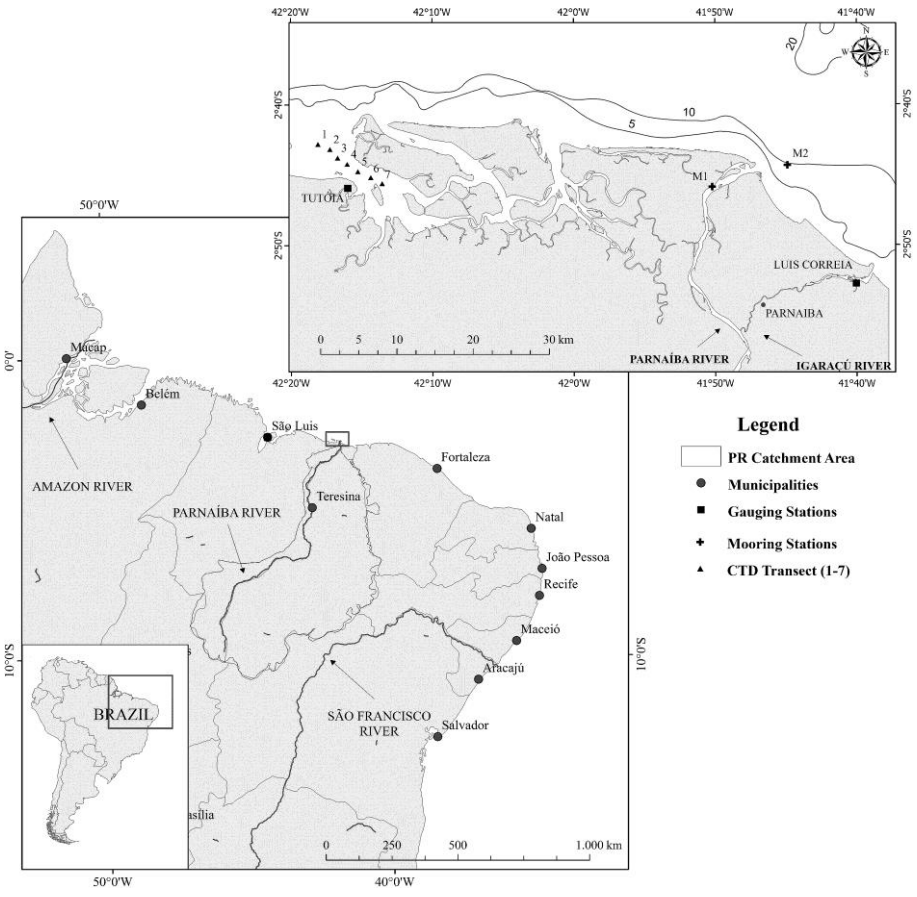

Figure 1 - Location of the Parnaíba River, highlighting its position related to the Amazon and São Francisco Rivers, the dimension of its drainage basin, and the dimension of its drainage basin, and the position of the mooring stations M1 and M2, as well as the CTD profile (1–7) taken on the lagoonal area.

At the low Parníba, the Igaraçu River springs out, which is the last distributary of the PR before it reaches the ocean (Figure 1). The catchment area has a dendritic pattern and covers approximately 344,112 km2, including the entire Piauí and parts of Maranhão and Ceará states. Most PR hydrographic parameters (catchment area, length, average discharge, and average SSC) are small compared with other Brazilian rivers such as the Amazon, São Francisco, and Paraná, as well as other examples around the world (Table 1).

Table 1 - Examples of river hydrographic parameters on different geological and climatological environments of distinct locations.

River	Country	Catchment Area (km^2)	Length (km)	Water Discharge (m3/s)	ssc (mg/l)
Parnaíba	Brazil	344,112	1,400	841	50
São Francisco	Brazil	638,576	2,700	2,528	34
Amazon	Brazil	6,183,507	6,516	198,676	190
Paraná	Brazil	2,887,069	4,500	14,506	180
Arno	Italy	7,969	240	57	680
Danube	Italy	778,499	2,850	6,420	330
Ebro	Spain	756,86	930	1,400	1,040
Ganhes/Brahma	India	1,568,702	2,840	31,000	1,120
Mekong	Vietnam	792,245	4,425	17,345	340
Mississipi	United States	3,208,025	6,020	15,452	1,110
Nile	Egypt	2,786,902	6,669	3,484	1,400
Orinoco	Venezuela	962,373	2,500	34,500	160
Rhone	France	87,857	820	1,700	1,310
Yagtze	China	1.810.000	6,300	28,278	540

The Parnaiba River Delta (PRD) is located in the NE Brazilian coast at the border of the Piauí and Maranhão states. It is located approximately 1100 km east from the Amazon River and 1200 km NW of the Sao Francisco River (Figure 1). The tide is semidiurnal, reaching amplitudes of 3.3 m during spring tide and 1.7mduring neap tide. The NE trade winds are fairly constant along the year with average velocities ranging from 2 m/s to 6 m/s (Bittencourt *et al.,* 2005). In this part of the Brazilian NE coast, the wave climate is dominant in the SW direction, with a significant wave height of 1 m and average period of 5 seconds. The combination of wind and waves produces an east to west longshore current, which is a characteristic of the entire NE Brazilian coast (Bittencourt *et al.,* 2005). The western part of the PRD is composed of a tidal channel systemwith estuarine lagoonal conditions (Holz, 2003; Kim and Montagna, 2012;

Mirlean *et al.*, 2003). This tidal channel system is connected to the PR by a channel that was artificially opened in the 1960s (Figure 1).

Piauí State is a climatic transitional zone between the Pre-Amazon Wet and NE Semi-Arid zones (Andrade, Jr. *et al.*, 2005). This zone displays a rainy season lasting from January to May, followed by a dry season from June to December. The duration of each season depends on the position of the Intertropical Convergence Zone and the occurrence and intensity of the ENSO phenomena (Hastenrath, 2006).

Along its course, the PR passes through the Parnaíba and Barreirinhas basins, which are two sedimentary basins with different age and formation mechanisms. Phanerozoic sedimentary rocks outcrop along both sedimentary basins as well as along the entire drainage basin of the PR (Feijó, 1994; Figueiredo and Rajagabaglia, 1986; Góes and Feijó, 1994; Pedreira and Waele, 2008; Rossetti and Truckenbrodt, 1992). The PR flows over the Parnaíba Basin through most of its way, reaching the Barreirinhas Basin only in the last tenth of the km distance from its mouth. Regardless of which sedimentary basin it is passing through, unconsolidated sediment is found on the river margins; therefore, a high sediment input to the river is expected. Similarities in the tectonic framework have been observed, with both basins presenting a predominantly SW-NE and NW-SE lineament trend (Almeida Filho *et al.*, 2009; Oliveira and Mohriak, 2003). Several authors have described the occurrence of listric normal faults and strike-slip faults on both basins (Feijó, 1994; Góes and Feijó, 1994; Rossetti and Truckenbrodt, 1992).

4.2. METHODS

In this work, information from two field campaigns was used (February 2009 and March 2010), including collected data on salinity, water temperature, offshore bottom currents, and tidal variation on the PRD and the continental shelf. In addition, the data compiled from governmental agencies includes multispectral satellite images, rainfall, river discharge, and SSC. The methodology used will be discussed in more detail bellow.

4.2.1. Rainfall

The dataset comprises the data from1965–2009 for Parnaiba city; data for 16 months from the years 1989 and 1990 are missing. The mean of precipitation in each month over the 45- year period was estimated to characterize the rainfall season. Single

months were classified as wet or dry. Any month in which the mean was higher than 10% of the maximum mean precipitation (312 mm) was considered a wet month. Inversely, a dry month was defined whenever the mean of the given month was below this threshold (Hastenrath, 2006).

4.2.2. River Discharge

A consistent dataset of river discharge from the PR is available for the cities of Terezina, Luzilândia, and Guadalupe (Boa Esperança water reservoir) from 1982 to 2005 (Figure 1). This data set comprises river discharge daily records from the PR main distributary. Central statistics were applied on the data to describe the general behavior of river discharge in PR. Linear regression was also performed using the data from the three previously mentioned stations to estimate the discharge at the river mouth.

4.2.3. Suspended Sediment Concentration (SSC)

Data for SSC from the stations located at the cities of Terezina and Luzilândia were available and used to evaluate, qualitatively, the contribution of the PR to the continental shelf. The data corresponds to the period between June 1992 and July 2009 for the city of Terezina and from February 1999 to July 2009 for the city of Luzinlândia. Regarding the SSC, not more than four measurements are available for the same year. Therefore, the data were compared according to the rainfall period in which they were classified (wet or dry).

4.2.4. Salinity and Water Temperature

Salinity and water temperature were measured for the PR and the tidal channel complex located westward (Figure 1). For the PR, vertical profiles were measured over 25 hours with a sampling interval of 1 hour. The vertical profiles were sampled at a mooring station (M1) located 5 km upstream of the river mouth. One transect was performed in the western part of the PRD to determine the spatial variability of salinity and temperature in that area (Figure 1). The transect consisted of seven stations distributed at approximately 1 nautical mile apart from each other. The data acquisition was made at 4-Hz frequency, and the data processing of the salinity and water temperature was restricted to bin average to have only one measurement assigned to each depth.

4.2.5. Offshore Bottom Currents

One S4 oceanographic buoy was moored (M2) 4.3 km offshore of the PR mouth to measure the velocity and direction of the bottom currents at that location (Figure 1). The S4 buoy was installed on 7 March 2010, 1 m above the seafloor at a water depth of 10 m, and removed on 4 April 2010. The instrument was set up to continually measure the current velocity and direction for 10 minutes (at a 2-Hz sampling interval) with a 30-minute standby period. The data recorded by the S4 are the average of the measuring time, which results in two data per hour.

4.2.6. Tides

Tide data were obtained from the hydrography department of the Brazilian navy (DHN–Diretoria de Hidrografia e Navegação) for the cities of Luiz Correia, Tutóia, and São Luiz (Figure 1) to evaluate the westward variation of tidal amplitude. In addition, from 16–19 March 2010 (spring tide), a tidal gauge was installed 5 km upstream of the mouth of the PR to record tidal variation. The tidal gauge was set to record variations in water level in 5-minute intervals.

4.2.7. Satellite Images

LANDSAT images were used to evaluate the morphodynamic behavior of the coast line of the PRD during the period between 1981 and 2009 (Table 2). The satellite images were georeferenced, and the coastline morphology was digitized using automated processes in ArcGIS. The total root mean square (RMS) error of the georeferencing was smaller than 13 m for all images. The color composition RGB 543 was used to better differentiate land and water on the images. This allowed the use of automated classification, which reduced the subjectivity in the determination of land and water contact.

Table 2 -Information of the satellite images that were used to assess.

Satellite	Date	Spatial Resolution	Total RMS error
LANDSAT 5TM	08/05/2009	30 m	11.1 m
LANDSAT 5TM	09/11/2005	30 m	10.2 m
LANDSAT 7ETM	07/06/2001	30 m	12.2 m
LANDSAT 5TM	08/04/1997	30 m	11.4 m
LANDSAT 5TM	06/09/1994	30 m	08.2 m
LANDSAT 5TM	06/14/1990	30 m	10.6 m

LANDSAT 5TM	09/20/1985	30 m	12.3 m
LANDSAT 2MSS	08/02/1981	60 m	11.8 m

4.3. RESULTS

Processing and interpretation of the available dataset determined the rainfall seasonality of the PRD area, river dynamics, river mouth morphodynamics, and hydrodynamics.

4.3.1. Rainfall

For the 45-year period, the average of annual cumulative precipitation was 1210 mm/y. Extreme values were observed in 1974 (3127mm) and 1983 (523 mm).Only in 1974 and 1985was the annual cumulative precipitation higher than 2000 mm; therefore, exceptionally high rainfall is rare in this region. Between 1965 and 2009, 36.91% of the months were classified as wet months, whereas 63.09% were considered dry. Annually, the dry period starts in June and extends until December. In turn, the wet period lasts from January to May (Figure 2).

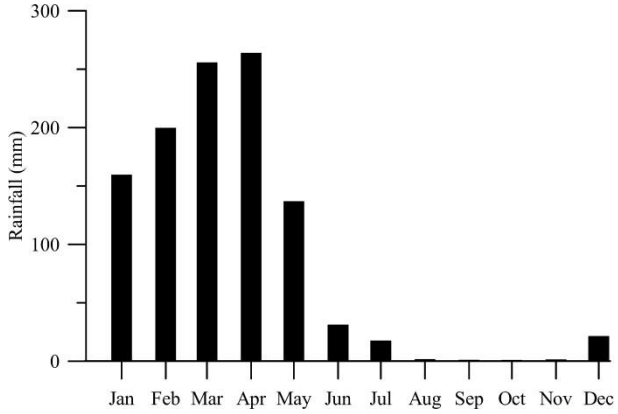

Figure 2 - Graph that shows the monthly averaged precipitation at the city of Parnaíba between 1965 and 2009, from which the wet and dry periods of the delta region were defined.

Normally, there is a rapid increase in rainfall from December to January when rainfall gradually increases until reaching its maximum in April. After April, rainfall decreases rapidly until June until it is practically absent in August, September, October, and November. Harmonic analysis of the rainfall time series displayed fair correlation with ENSO for the stations located at the cities of Terezina, Luzilândia, and Parnaíba (Figure 3).The analysis also revealed that the recurrence period of droughts is approximately 12 years (plus or minus 2 years). The variations in the intensity of the high precipitation and drought periods became smaller after 1991.

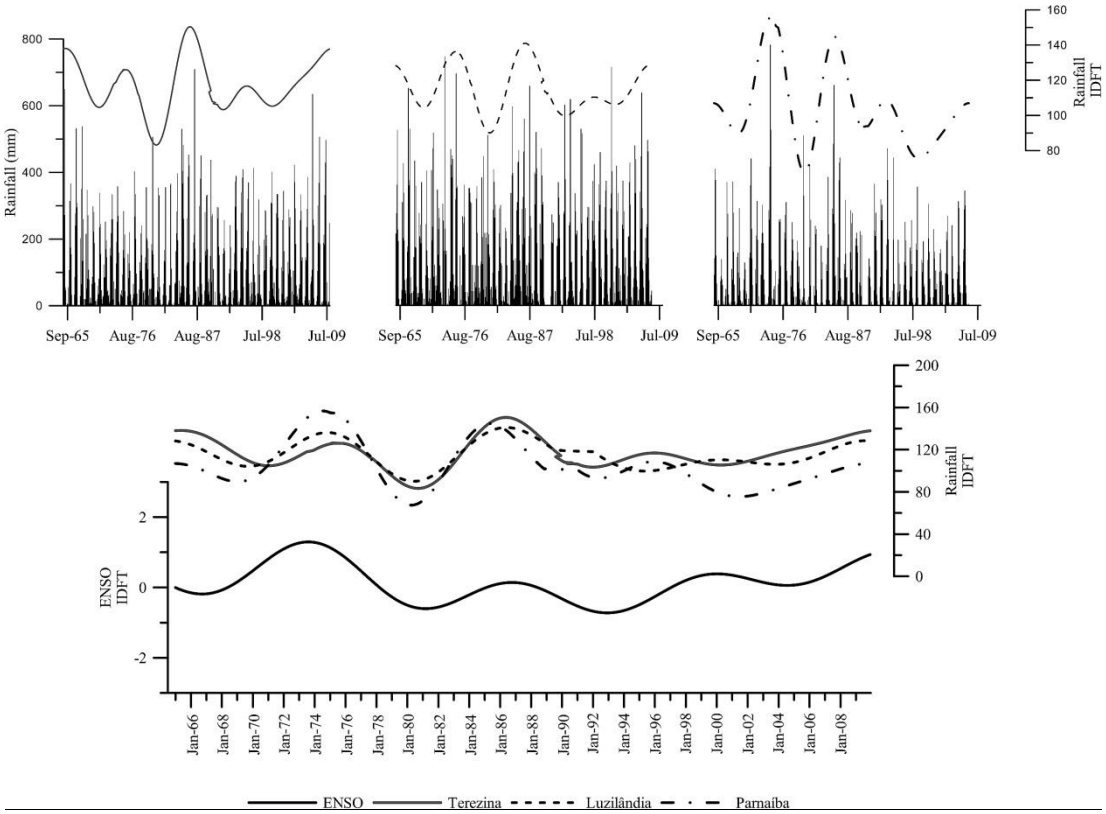

Figure 3 - (top) Graphs of rainfall and related IDFT for the cities of Teresina, Luzilândia, and Parnaíba. (bottom) Graph of IDFT of rainfall and ENSO time series that displays the influence of occurrence and intensity of ENSO on the amount of rainfall for the cities of Teresina, Luzilândia, and Parnaíba.

4.3.2. River Dynamics

The station located at Luzilândia city displayed an annual average discharge of 660 m3/s, with a maximum of 1602 m3/s and minimum of 408 m3/s, which were observed in 1985 and 1998, respectively. For the station located at Terezina, the annual average discharge was 549 m3/s, with extreme values ranging from 228 m3/s to 2764 m3/s registered in 1989 and 1985, respectively. The annual average discharge from the Boa Esperança water reservoir was 445 m3/s, with maximum and minimum values registered in 1985 (1538 m3/s) and in 1986 (242 m3/s), respectively. It is observed that average river discharge increases downstream, indicating that evaporation is compensated by the increase of rainfall toward the coastal zone. Harmonic analysis of the river discharge time series was performed on the data from Luzilândia. The results revealed an increase in river discharge between 1982 and 1986 followed by a decrease until 1991. During the time between 1991 and 2005, small oscillations occurred between the high and low discharge periods. After 1991, the data depicted two cycles of

high and low discharge with an approximately 7-year recurrence period. The same procedure was conducted for the river discharge data from Terezina, in which the same variations were found, such as in the Luzilândia data; however, the oscillations after 1991 were smoother than those observed in Luzilândia (Figure 4).

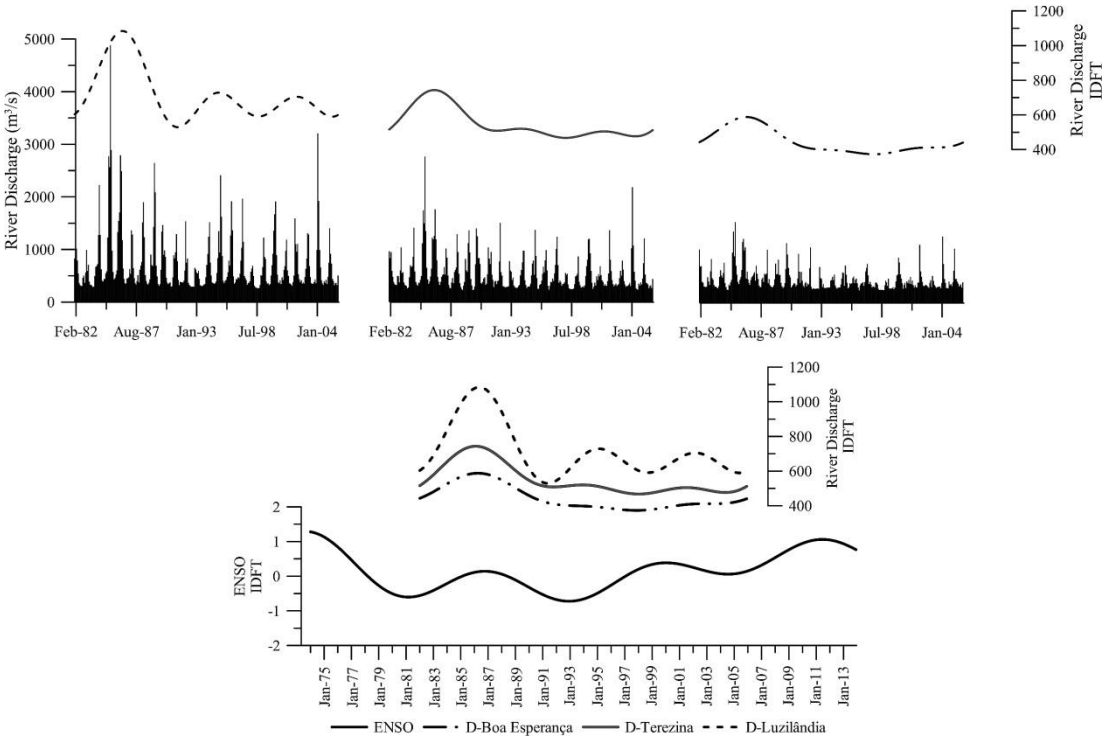

Figure 4 – (top) Graphs of the PR discharge and related IDFT for Boa Esperança water reservoir and Terezina and Luzilândia. (bottom) Graph of IDFT of the PR discharge and ENSO time series that displays the influence of occurrence and intensity of ENSO on the river discharge measured at Boa Esperança water reservoir and Terezina and Luzilândia.

Spatial variation of the mean values of the SSC was noticed between Terezina and Luzilândia, increasing from 103.5 mg/l to 117.2 mg/l, respectively. SSC also increased downstream as the result of the increase of rainfall toward the coastal zone, similarly to what occurred with the river discharge. Temporal variations were also observed between the wet and dry periods on both locations. At Luzilândia, the mean value was 172.2 mg/l during the wet period, decreasing to 84.8 mg/l in the dry period. At Terezina, the mean values varied from 200.2 mg/l and 48.7 mg/l for the wet and dry periods, respectively. Although the dry periods last longer than the wet periods, more than 70% of the sediment yielded by PR occurs during the wet period. Through harmonic analysis of the SSC time series, it was possible to differentiate three periods between 1992 and 2009. There was a high concentration of sediment in suspension in the PR during 1992 and 1996, low concentration between 1996 and 2000, and medium

concentration from 2000 until 2009. Nevertheless, oscillations occurred within each of these periods (Figure 5).

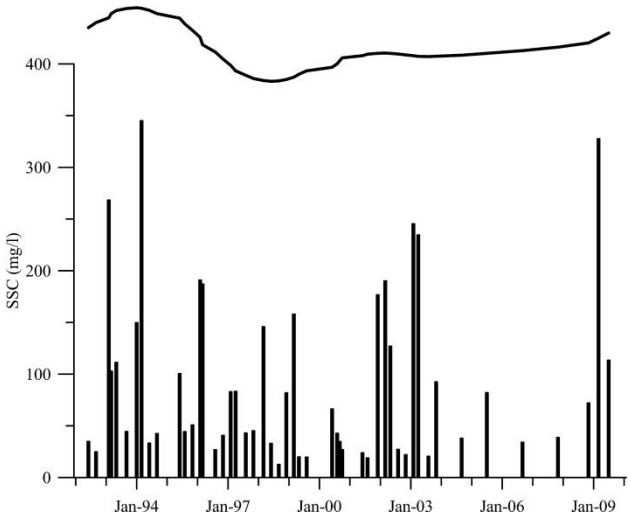

Figure 5 - Graph of the PR SSC measured at Terezina and IDFT of the SSC time series. The IDFT curve reveals three periods of SSC in PR: high, low, and medium, respectively.

4.3.3. Parnaíba River Mouth Hydrodynamics

In this region, the tide is semidiurnal and mesotidal, with a tidal amplitude of 1.70 m at neap tide and 3.06m at spring tide (Figure 6). At Tutóia, which is located approximately 65 km west from Luiz Correia (Figure 1), the tidal amplitude is approximately 3.5 m (DHN), and there is a time lag of 37 minutes (Figure 6). São Luiz, approximately 295 km west from Luiz Correia (Figure 1), has tidal amplitude of 6.1 m and a time lag of 1 hour and 52 minutes (Figure 6). Therefore, between Tutóia and São Luiz, the tidal regime switches from meso- to macrotidal.

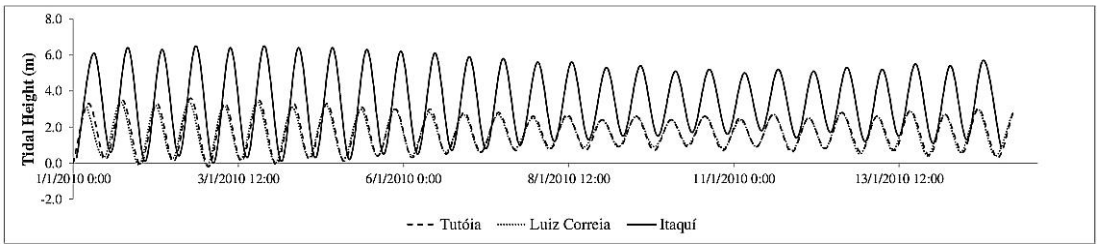

Figure 6 - Tidal curves for the harbors of Luiz Correia, Tutóia, and Itaquí for spring and neap tides showing the differences in tidal amplitude and phase lag for the tidal wave and, therefore, the changes on tidal regime.

During the transition between low tide and high tide, the salinity increases from 0 to 27 PSU at the surface (-1 m) and from 0 to 34 PSU at the bottom (-10 m). Sea water is observed in the estuary during flood and high tide for a total of 8.5/25 hours. Therefore, during most of the time, this region is submitted to fully riverine conditions.

Despite the significant variations in salinity, only small differences in water temperature were observed during either fully marine or fully riverine conditions (Figure 7). The differences between marine and riverine waters ranged from 30.18C to 28.38C at the surface.

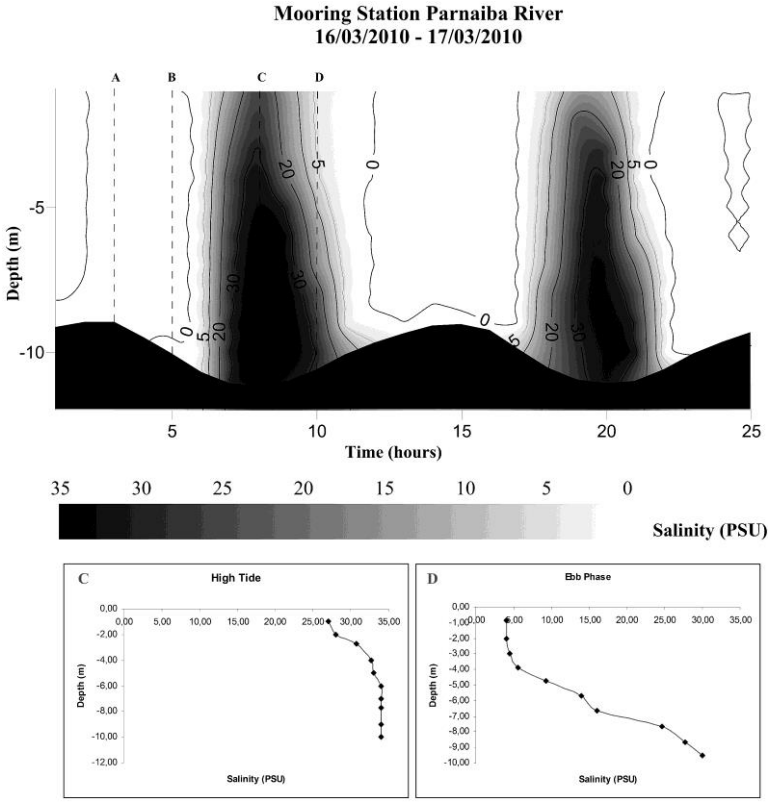

Figure 7 - Plot of the 25-hour time series of salinity at M1 and the salinity vertical profiles on high tide (profile C) and ebb phase (profile D) that show how the salt and fresh water interact on these tidal stages. These figures give an idea of the relation between the river and marine strength on that location of the river over one tidal cycle.

The longitudinal salinity profile depicts a slight decreasing gradient toward the interior of the lagoon. The salinity varies from 35 PSU, closer to the ocean, to 33.1 PSU, closer to the continent (Figure 8). Slight vertical salinity stratification was noticed at the outer stations 1–4, while the vertical profile is more homogeneous at the inner stations 5–7 (Figure 8).

NNE was the principal current direction identified at the M2 location, andmaximum velocities reached 0.52 m/s (mean 0.19 m/s). This is also the direction of the ebb-phase tidal currents and river runoff. SSW currents were also detected but with lower velocities than NNE currents. The SSW currents reached a maximum velocity of 0.22 m/s (mean 0.09 m/s).

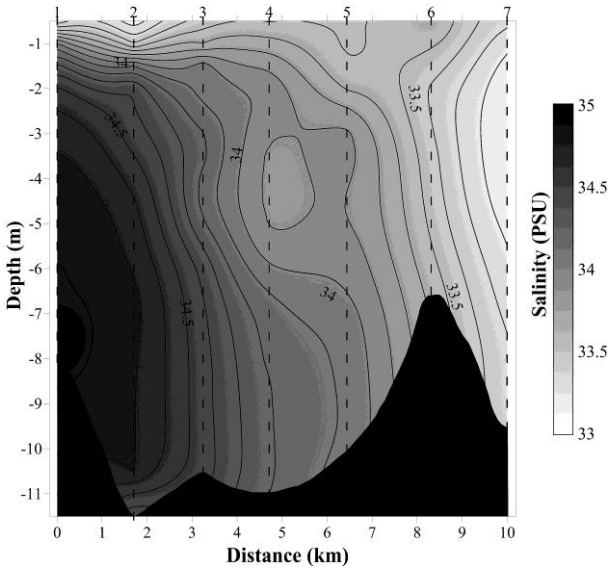

Figure 8 - Plot of the CTD longitudinal profile taken on the west side of the PRD revealing the influence of fresh water input of ephemeral rivers in this part of the delta, characterizing estuarine-lagoonal conditions.

Northern currents reached their maximum velocities during ebb conditions and their minimum during flood conditions. SSW currents only occurred during flood conditions and at the M2 location could only be observed during spring tide, being absent otherwise. The minimum current velocities were observed during neap tide in both the northern and southern directions.

Subordinate currents with WSW/WNW (2508 Az to 2908 Az) directions were found, and their maximum velocity reached 0.41 m/s (Figure 9).

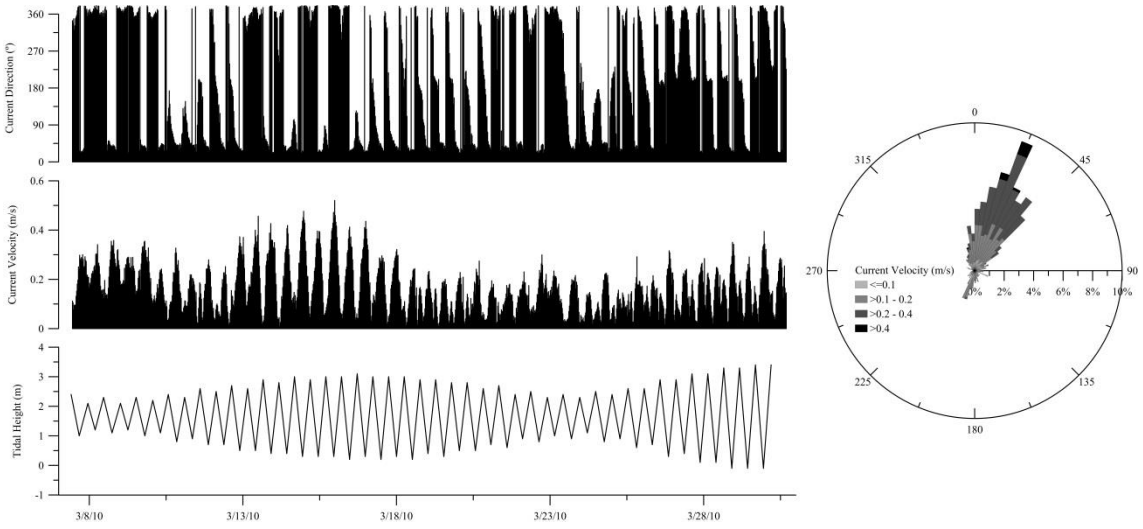

Figure 9 - Graphs of M2 measurements and tidal variation, showing the influence of river discharge at M2 during the different tidal cycles.

This is also the direction of flow of the longshore drift in this region. M2 is located on the edge of the sediment plume of the PR (Figure 10). Despite the predominant influence of NE currents on this location, attributable to PR runoff, the sediment plume from the PR is dispersed westward from its mouth (Figure 10). Shoals are observed at the mouth of PR as well as at the mouth of the tidal channels in a semicircular form (Figure 10). For this region, the waves come from the NE direction during most of the year, with heights varying from 0.5 m to 1.5 m.

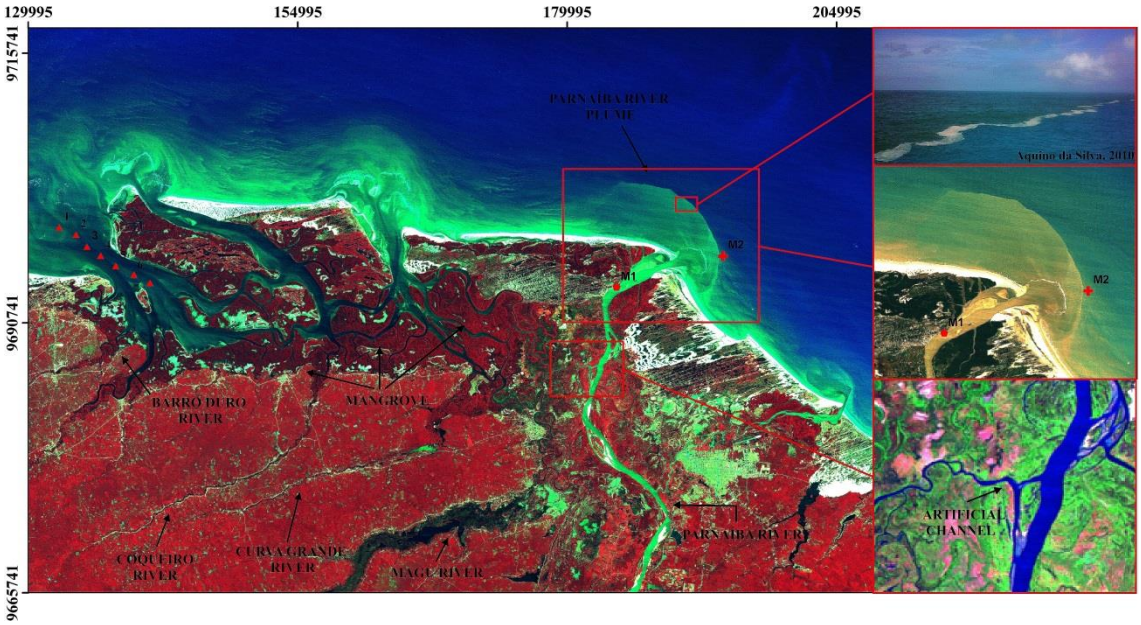

Figure 10 - LANDSAT-TM5 (08/05/2009) color composite RGB-432 highlighting the areas covered by mangrove vegetation, the fresh water input to the lagoonal area by small ephemeral rivers, and the location of theM2 at the edge of the sediment plume. Photo showing the contact between the PR plume and sea water (top right). LANDSAT-TM5 (08/05/2009) color composite RGB-321 showing in detail the sediment plume (middle right). LANDSAT-TM5 (08/05/2009) color composite RGB-542 showing in detail the artificial channel that connects the PR to the lagoonal area. (Color for this figure is available in the online version of this paper.)

4.3.4. Parnaíba River Mouth Morphodynamics

The errors attributed to the georeferencing of the images were quantified in terms of the RMS of the total error. The total RMS error was inferior to 13 m for all images, hence, neglected on the quantification of the coastline changes. This error represents less than 10% of any change reported in this work. Having this in mind, coastline changes were observed along the entire area of the delta (Figure 11). They were more evident in the vicinities of the mouth of the tidal channels (Figure 11, frames 1, 2, and 3). For these locations, the sediment loss caused displacements up to 600 m. Mild shoreline retreat was noticed on the beaches formed between the mouths of the

two tidal channels (Figure 11, frames 1, 2 and 3). On the left margin of the PR mouth, a spit developed that migrated approximately 750 m east from 1985 to 2009 (Figure 11, frame 6). On the right margin of the PR mouth, the shoreline migrated approximately 1600 m NE from 1985 to 2009. Before 1985 (from 1981 to 1985), no changes occurred related to this location.

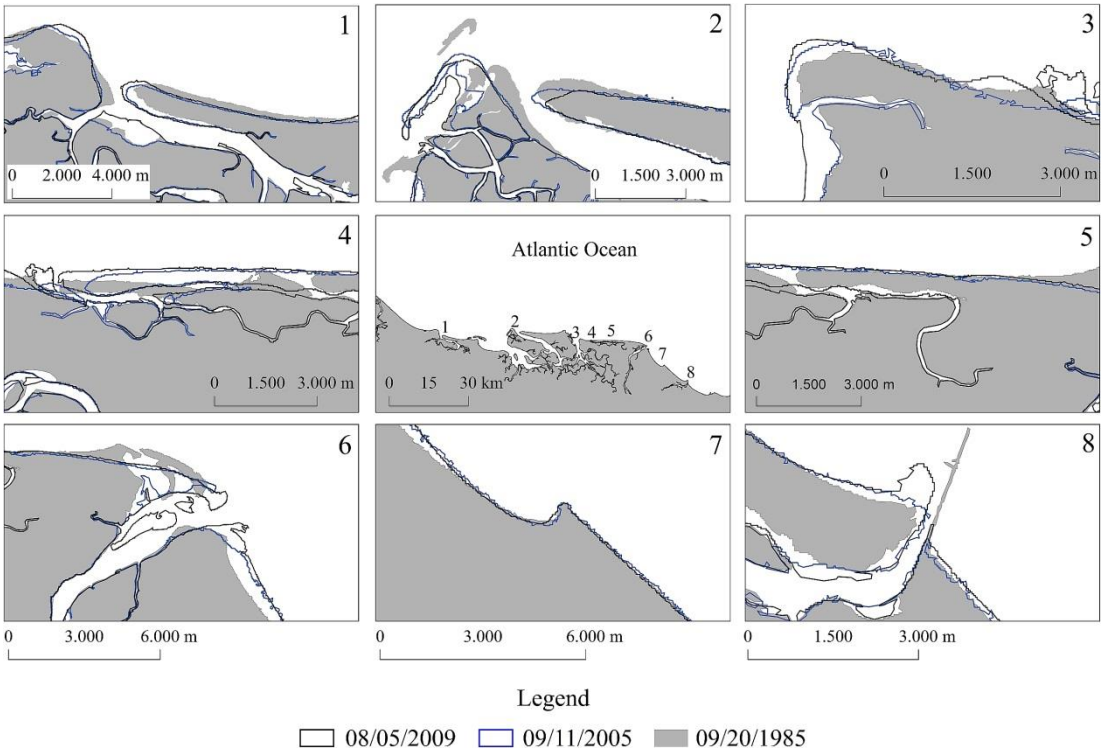

Figure 11 - Shoreline evolution between 1985 and 2009 displaying eight sectors of the PRD region, where progradation, stability, and retreat of the shoreline occurred. The LANDSAT-5TM image from 09/20/1985 is a time-series anchor and is displayed as a gray solid surface.

The position of the margins of the tidal channels in the interior of the lagoonal area did not change between 1981 and 2009; however, some islands located in the mouth of some channels experienced a maximum displacement of more than 2000 m. The migration of the sandy islands occurred predominantly in the western direction (the direction of longshore currents).

The extremity of the spit located westward from the PR mouth (Figure 11, frame 4) migrated approximately 8100 m west and had a maximum shoreline retreat of 180 m between 1981 and 2009. On average, this migration represented a rate of 289 m/y. Three distinct rates of spit migration were observed during this period. Between 1981 and 1990, the spit migrated 1358 m, which represents approximately 150 m/y (Figure 12). The rate of migration increased to 498 m/y between 1990 and 1997, followed by a reduction to 284 m/y until 2009 (Figure 12). The periods when the changes in the

migration rates of this spit occurred fit with the periods of low and high SSC periods established after the application of the harmonic analysis on the SSC time series.

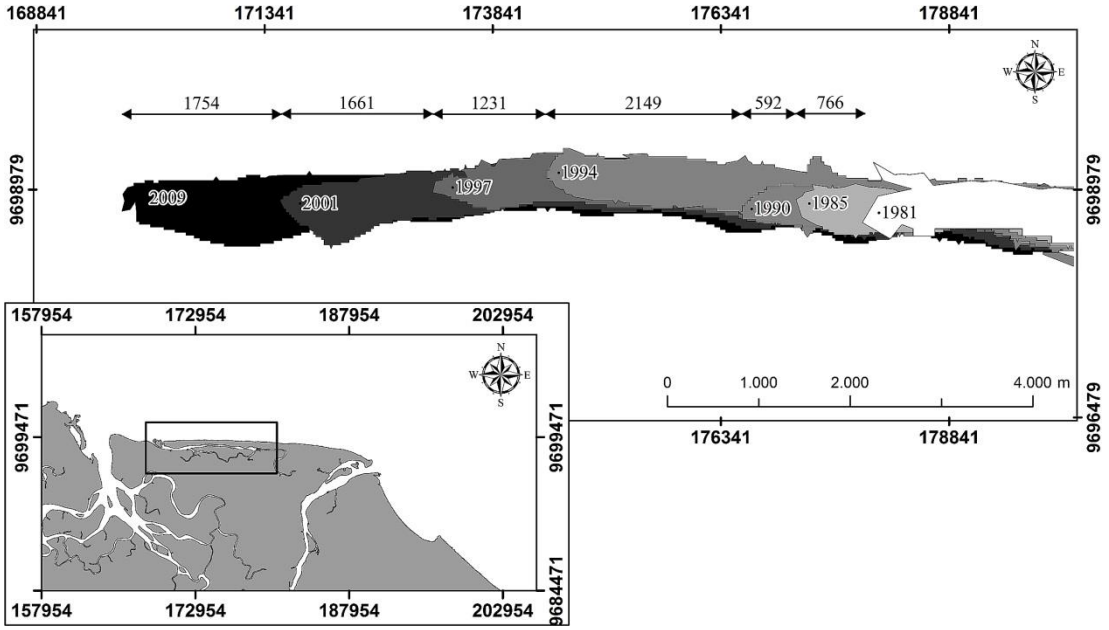

Figure 12 - Detail of the 8153-m spit progradation that occurred between 1981 and 2009 west of the PR mouth.

4.4. DISCUSSION

Considering only its shape, the PRD can be classified as a wave-dominated delta (Bhattacharya and Walker, 1992; Galloway, 1975; Orton and Reading, 1993; Reading and Collinson, 1996; Wright and Coleman, 1973; see Figure 10). Wave influence on PRD development can be observed in the presence of spits and the bedforms formed in the nearshore zone and close to the river and tidal channel mouth. The occurrence of spits growing in the west direction only westward from the PR mouth verifies the asymmetric character of this delta (Bhattacharya and Goisan, 2003). Offshore from the PR mouth (at M2), there is predominance of NE currents, which reflects the influence of the river runoff up to that location. Only during spring tide were southerly currents registered at M2 (Figure 9). Such river runoff strength may act as a hydrodynamic barrier, reducing the bypass of sediment transported E-W by longshore currents close to the coast (Bhattacharya and Goisan, 2003). M2 measurements were taken during a high discharge period; nevertheless, it is expected that the river runoff also continues to influence bottom currents offshore PRD, with less strength, during low discharge periods. This may also contribute to delta asymmetry of the PRD. At M1, riverine conditions prevail for one-third of one tidal cycle, indicating that the river force is

greater than the marine force at that location. This condition is expected to occur also during the period of high river discharge. The location of the incised valley, the shape of its cross-section, and its relative position to the PR mouth suggest a genetic connection between them. The western part of the delta is composed of a tidal channel system with lagoonal-estuarine conditions, such as those found in the Patos Lagoon (Castelao and Moller, Jr., 2006) and Pamlico Sound (Luettich Jr. *et al.*, 2002). There is only one artificial channel connecting this tidal channel area to the PR. Fresh water input to this part of the delta comes either from an artificial channel or from small rivers (Figure 10) that drain into this system (at least during the wet period), influencing the salinity distribution. In this part, the salinity decreases with the increase of the distance from the open ocean (Figure 8). The presence of mangroves indicates that the salinity level does not reach the fresh water limit (Tomlinson, 1986) along the entire western part of the PRD (Figure 10). Older maps (e.g., Imperial Instituto Artistico, 1902; Heck, 1835) show at least three western distributaries diverging from the main PR channel. Because of the currently restricted connection between the western part of PRD and the present course of PR, it is not clear whether the tidal channels in the west have developed independently from PRD or are remnants of older distributaries.

A direct influence of rainfall seasonality was observed on the river discharge over the year, as the highest values coincide with the wet period. Although there is a relation between the amount of rainfall and river discharge, during the dry period the discharge decreases but does not reach values lower than 261 m3/s, which is most likely regulated by the Boa Esperança water reservoir (630 km upstream). The differences of discharges between the wet and dry periods can be attributed to the few ephemeral rivers that drain into PR, such as Poti and Longa Rivers. Such variations in river discharge are also observed on the Yellow River, the Amazon River, the Nile River, and the Ganges/Brahmaputra River (Saito, Yang, and Hori, 2001; Syvitski *et al.*, 2005). Although differences in river discharge did occur between Terezina and Luzilândia, linear regression of the discharge data indicated a correlation coefficient (R2) of 0.91. Therefore, discharge data from either one can used to predict the expected discharge on the other.

Rainfall can also be highlighted as one of the major climatic factors that drives the seasonality of the SSC; however, fluctuation in its value occurs at the beginning of the wet and dry periods. This fluctuation may be dependent on surface soil/sediment erosion mechanisms (Shih and Yang, 2009). The SSC in the PR is not directly related to

the amount of precipitation, although higher precipitation leads to higher water inputs to the river. The occurrence of high SSC is observed during the transition from a wet to dry season (or vice versa). At the beginning of the wet season, the dryer surface sediment is more easily transported into the PR by the first rainfall. At the end of the wet season, surface sediment dries out, attributable to long times without precipitation, and is easily transported by the occasional rainfall that commonly occurs during this period.

The lack of continuity of the SSC time series was a limiting factor for its use; however, the presence of at least one measurement in each season and the absence of exceptional flooding events in this region contributed to a qualitative long term evaluation of the SSC data. The use of harmonic analysis of time series was revealed to be of great importance in establishing general trends on the SSC data given the discontinuity of the data set (Xu and Shen, 2013; Zhou *et al.*, 2012). Harmonic analysis of rainfall, discharge, and SSC time series facilitated the correlation of these parameters to the ENSO. The analysis demonstrated that on the NE Brazilian coast, the intensity and duration of rainfall varied according to the occurrence and intensity of the ENSO (Philippon *et al.*, 2012). The interrelation of shoreline evolution with rainfall and SSC variations was noticed after evaluating the changes in the migration rate of the spit located west from the PR mouth. This interrelation indicated that the ENSO also influences the decadal evolution of the shoreline by regulating its sediment supply (Ruggiero *et al.*, 2010). The influence of the ENSO in shoreline evolution is more evident on the coasts subjected to extreme events such as hurricanes and large storms (Storlazzi and Griggs, 2000). The importance of sediment availability is shown by the shoreline retreat observed at the mouth of the tidal channels located on the west part of the delta. Shoreline retreats up to 1000 m were found for these locations because of the low level of sediment supply and open exposure to waves, tidal, and longshore current action.

4.5. CONCLUSIONS

The PR mouth is a deltaic system; however, its formation, driving forces, and evolution are not completely understood, especially its relation to the tidal channel system in the west. There are geomorphological indications leading to the classification of the PRD as a wave-dominated asymmetric delta. The outline of the PRD and the

presence of features such as spits only west of the PR mouth support this classification. This asymmetry degree, however, has not yet been established.

Harmonic analysis of rainfall, river discharge, and SSC time series data facilitated the determination of the interrelation between these parameters and their influence on decadal shoreline change. It also allowed the correlation of these parameters to the occurrence of the ENSO. Rainfall was determined to be the major climatic force that determines the SSC in PR. Thus, rainfall variation controls the short-term shoreline changes. The geology of the drainage basin has to be considered, though, because it defines how easily sediment will be available and transported to the river. Constructive processes occurred at the PR mouth and in its vicinity, whereas the destructive processes occurred away from it. This indicates that the PR is the primary sediment supplier to the delta region.

PR discharge is likely to be controlled by the Boa Esperança water reservoir during the dry period. M1 and M2 data revealed that, in general, riverine forces are greater than tidal forces at the PR mouth, and the saltwater wedge is restricted to few kilometers upstream. The western part of the PRD can be classified as estuarine-lagoonal because of the small freshwater input of small rivers and its restricted connection to PR. In this area, brackish to sea water conditions prevail. A deltas witching process may explain the geomorphology of the western part of the delta; however, the occurrence of such a process has not yet been proven. For this sector of the NE Brazilian coast, between Luiz Correia and Itaquí, a transition from a meso- to macrotidal regime occurs that is marked by an increase in tidal amplitude from 3.06 m to 6.1 m.

ACKNOWLEDGEMENTS

This work is part of the project ‘‘Northern Brazilian river deltas: River impacts versus pristine discharge,’’ which is funded by the Deutsche Forschungsgemeinschaft (STA 401/16-1). The authors would like to thank the captain and crew of the São Francisco III, as well as all team members, for their efforts to support the study, namely, F. Canindé Soares, Werner F. Tabosa, Pedro Moreia, Gustavo Rocha, Maria Isabel da Rocha, Helmut Beese, Camila Soares, Agata Szczygielski, and Juliana Koenig. The authors also would like to thank CHESF, INMET, and ANA for kindly providing some of the data used on this research. Special thanks for the GGEMMA lab of the Universidade Federal do Rio Grande do Norte for dispose part of the equipment used on

this research and the CNPq for additional for the additional support (Grant PQ CNPq n.8 303481/2009-9).

LITERATURE CITED

Andrade Jr., A. S.; Bastos, E. A.; Barros, A. H. C.; Silva, C. O., and Gomes, A. A. N., 2005. Classificação climática e regionalização do Semi-Árido do Estado do Piauí sob cenários pluviométricos distintos. Revista Ciência Agronômica, 36(2), 143–151.

Almeida Filho, R.; Rossetti, D. F.; Miranda, F. P.; Ferreira, F. J.; Silva, C., and Beisl, C., 2009: Quaternary reactivation of a basement structure in the Barreirinhas Basin, Brazilian Equatorial Margin. Quaternary Research, 72(2009), 103-110.

Becker, J. J.; Sandwell, D. T.; Smith, W. H. F.; Braud , J.; Binder, B.; Depner, J.; Fabre, D.; Factor, J.; Ingalls, S.; Kim, S-H.; Ladner, R.; Marks, K.; Nelson, S.; Pharaoh, A.; Trimmer, R.; Von Rosenberg, J.; Wallace, G., and Weatherall, P., 2009. Global Bathymetry and Elevation Data at 30 Arc Seconds Resolution: SRTM30_PLUS. Marine Geodesy, 32(4), 355-371.

Bhattacharya, J.P. and Walker, R.G., 1992. Deltas. In: Walker, R.G. and N.P. James, (eds.), Facies Models: Response to Sea-Level Change. St Johns: Geological Association of Canada, pp. 157–177.

Castelao, R. M. and Moller Jr, O. O., 2006. A modeling study of Patos lagoon (Brazil) flow response to idealized wind and river discharge: dynamical analysis. Brazilian Journal of Oceanography, 54(1), 1-17.

Feijó, F. J., 1994. Bacia de Barrreirinhas. Boletim de Geociências da Petrobrás, 8(1), 103-109.

Figueiredo, M. F. and Rajagabaglia, G. P., 1986. Sistema classificatório aplicado às bacias brasileiras. Revista Brasileira de Geociências, 16, 351-369.

Galloway, W.E., 1975 Process framework for describing the morphologic and stratigraphic evolution of deltaic depositional systems. In: Broussard, M.L., (ed.), Deltas, Models for Exploration. Houston: Houston Geological Society, pp. 87–98.

Gao, J., 2009. Bathymetric mapping by means of remote sensing: methods, accuracy and limitations. Progress in Physical Geography, 33(1), 103-116.

Góes, A. M. and Feijó, F. J., 1994. Bacia do Parnaíba. Boletim de Geociências da Petrobrás, 8(1), 57-67.

Goisan, L. and Bhattacharya, J., 2003. Wave-influenced deltas: geomorphological implications for facies reconstruction. Sedimentology, 50(1), 187-210.

Gomes, M. P. and Vital, H., 2010. Revisão da compartimentação geomorfológica da Plataforma Continental do Norte do Rio Grande do Norte, Brasil. Revista Brasileira de Geociências, 40(3), 321-329.

Hastenrath, S., 2006. Circulation and teleconnection mechanisms of Northeast Brazil droughts. Progess in Oceanography, 70, 407-415.

Heck, J. G., 1835. Atlas Geographique Astronomique et Historique. Paris: Hammer and Comp., 61p.

Holz, M., 2003. Sequence stratigraphy of a lagoonal estuarine system—an example from the lower Permian Rio Bonito Formation, Parana´ Basin, Brazil. Sedimentary Geology, 162, 305-331.

Kim, H. C. and Montagna, P. A., 2012. Effects of climate-driven freshwater inflow variability on macrobenthic secondary production in Texas lagoonal estuaries: A modeling study. Ecological Modelling, 235-236, 67-80.

Lorenzzetti, J. A.; Negri, E.; Knopers, B., and Medeiros, P. R. P., 2007. Uso de imagens LANDSAT como subsídio ao estudo da dispersão de sedimentos na região da foz do rio São Francisco. Proceedings of 13th Simpósio Brasileiro de Sensoriamento Remoto (Florianópolis, Santa Catarina), pp. 3429-3436.

Luettich Jr, R. A.; Carr, S. D.; Reynolds-Fleming, J. V.; Fulcher, C. W., and McNinch, J. E., 2002. Semi-diurnal seiching in a shallow, micro-tidal lagoonal estuary. Continental Shelf Research, 22(11-13), 1669-1681.

Medeiros, P. R. P.; Souza, W. F. L.; Knoppers, B. A., and Lima, L. L., 2010. Aporte de sedimentos em suspensão no baixo Rio São Francisco (SE/AL), em diferentes condições hidrológicas. Proceedings of the 3rd Congresso Brasileiro de Oceanografia (Rio Grande, Rio Grande do Sul), pp. 2001-2003.

Milliman, J. D. and Farnsworth, K. L., 2011. River Discharge to the Coastal Ocean: A Global Synthesis. Cambridge: University Press, 392p.

Milliman, J. D. and Meade, R. H., 1983. World-wide delivery of river sediment to the oceans. Journal of Geology, 91(1), 1-21.

Milliman, J. D. and Syvitski, J. P. M., 1992. Geomorphic/Tectonic Control of Sediment Discharge to the Ocean: The Importance of Small Mountainous Rivers. Journal of Geology, 100(5), 525-544.

Mirlean, N.; Andrus, V. E.; Baisch, P., and Griep, G., 2003. Arsenic pollution in Patos Lagoon estuarine sediments, Brazil. Marine Polution Bulletin, 46(2003), 1480-1484.

Oliveira, D. C. and Mohriak, W. U., 2003. Jaibaras trough: an important element in the early tectonic evolution of the Parnaıba interior sag basin, Northern Brazil. Marine and Petroleum Geology, 20(2003), 351-383.

Orton, J. G. and Reading, H. G., 1993. Variability of deltaic processes in terms of sediment supply, with particular emphasis on grain size. Sedimentology, 40(1993), 475-512.

Pedreira, A. J. and Waele, B., 2008. Contemporaneous evolution of the Palaeoproterozoic–Mesoproterozoic sedimentary basins of the São Francisco–Congo Craton. Geological Society of London, 294(2008), 33-48.

Pillans, B.; Chappell, J. and Naish, T. R., 1998. A review of the Milankovitch climatic beat: template for Plio–Pleistocene sea-level changes and sequence stratigraphy. *Sedimentary Geology*, 122, 5-21.

Philippon, N; Rouault, M; Richard, Y. and Favre, A., 2012. The influence of ENSO on winter rainfall in South Africa. International Journal of Climatology, 32(15), 2333-2347.

Raposo, M. I. B.; McReath, I., and D'Agrella Filho, M. S., 2006. Magnetic fabrics, rock magnetism, cathodoluminescence and petrography of apparently undeformed Bambui carbonates from São Francisco Basin (Minas Gerais State, SE Brazil): An integrated study. Tectonophysics, 418(1-2), 111-130.

Reading, H. G. and Collinson, J. D., 1996. Sedimentary Environments: Processes, Facies and Stratigraphy. Oxford: Blackwell Science, 704p.

Rossetti, D. F. and Truckenbrodt, W., 1992. Sedimentologia e diagênese dos arenitos da formação Barro Duro (Albiano), área oeste da bacia de Barreirinhas. Boletim de Geociências da Petrobrás, 6(3-4), 201-221.

Ruggiero, P.; Buijsman, M.; Kaminsky, G. M.; Gelfenbaum, G., 2010. Modeling the effects of wave climate and sediment supply variability on large-scale shoreline change. Marine Geology, 273(1-4), 127-140.

Saito, Y.; Yang, Z., and Hori, K., 2001. The Huanghe (Yellow River) and Changjiang (Yangtze River) deltas: A review on their characteristics, evolution and sediment discharge during the Holocene. Geomorphology, 41(2001), 219-231.

Storlazzi, C. D. and Griggs, G. B., 2000. Influence of El Niño–Southern Oscillation (ENSO) events on the evolution of central California's shoreline Geological Society of America Bulletin, February, 112(2), p. 236-249.

Schwarzer, K.; Stattegger, K.; Vital, H., and Becker, M., 2006. Holocene coastal evolution of the Rio Açu Area (Rio Grande do Norte, Brazil). Proceedings of the 8th International Coastal Symposium, Journal of Coastal Research, Special Issue No. 39, pp. 140-144.

Shih, H.-M. and Yang, C. T., 2009. Estimating overland flow erosion capacity using unit stream power. Intern. Jour. of Sediment Research, 24(2009), 46-62.

Syvitski, J. P.; Kettner, A. J.; Correggiari, A., and Nelson, B. W., 2005. Distributary channels and their impact on sediment dispersal. Marine Geology, 222-223(2005), 75-94.

Tassan, S., 1987. Evaluation of the potential of the Thematic Mapper for marine application. Remote Sensing, 8(10), 1455-1478.

Tomlinson, P. B., 1995. The Botany of Mangroves. Cambridge: Cambridge University Press, 436p.

Valladares, C. S.; Machado, N.; Heilbron, M., and Gauthie, G., 2004. Ages of Detrital Zircon from Siliciclastic Successions South of the São Francisco Craton, Brazil: Implications for the Evolution of Proterozoic Basins. Gondwana Research, 7(4), 913-921.

Vital, H.; Furtado, S. F. L., and Gomes, M. P., 2010. Response of Apodi-Mossoro estuary-incised valley system (NE Brazil) to sea-level fluctuations. Brazilian Journal of Oceanography, 58, 13-24.

Vital, H.; Stattegger, K.; Posewang, J., and Theilen, F., 1998. Lowermost Amazon River: Morphology and shallow seismic characteristics. Marine Geology, 152(1998), 277-294.

Wright, L. D. and Coleman, J. M., 1973. Variations in morphology of major river deltas as functions of ocean wave and river discharge regimes. AAPG, 57(1973), 370-398.

Chapter 5

SPECTRAL CALIBRATION OF CBERS 2B MULTISPECTRAL SATELLITE IMAGES TO ASSESS SUSPENDED SEDIMENT CONCENTRATION

André G. Aquino da Silva[1], Venerando E. Amaro[2], Karl Statteger[1], Klaus Schwarzer[1], Helenice Vital[2], Bjorn Heise[3].

[1]*Institute of Geosciences, Kiel University, Germany*

[2]*Departamento de Geologia, UFRN, Brazil*

[3]*TENNET, Germany*

Published in ISPRS International Journal of Remote Sensing and Photogrammetry, reprinted with the permission from the publisher Elsevier

ABSTRACT

In this study, 11 CBERS 2B and 1 LANDSAT 5-TM satellite images from 2008 were used to estimate the suspended sediment concentration and the total suspended sediment load of the Parnaíba River (NE-Brazil). The calculation of the amount of sediment in suspension was performed using Tassan's algorithm, which was originally developed for use on LANDSAT 5-TM images; therefore, the CBERS 2B images were spectrally calibrated using LANDSAT 5-TM at-satellite radiance. The application of atmospheric correction to the images was necessary to account for meteorological influence on the spectral data prior to the calculation of the suspended sediment concentration. Three types of dark object subtraction and the 6S model were tested, and one type of dark object subtraction was chosen as the appropriate atmospheric correction method. Tassan's algorithm requires in situ calibration; therefore, suspended sediment concentrations measured in water samples from the Parnaíba river mouth were used to calibrate the algorithm. The results revealed that the variation of suspended sediment concentration was strongly influenced by seasonal precipitation. In 2008, the suspended sediment released by the Parnaíba River was approximately 2.54 x 106 tons. The discharged sediment formed a sediment plume on the inner continental shelf. The extension of the plume depended on the specific hydrodynamic conditions that were forced mainly by the strength of river runoff, longshore currents, tidal currents and amplitudes, and wind and wave climate.

5.1. INTRODUCTION

The CBERS 2B (China-Brazil Earth Resources Satellite) includes an optical system of a High Resolution Couple Charged Device (CCD) camera that operates in 5 spectral bands with wavelengths ranging from 0.51 to 0.89 μm. The swath of the image scene is 113 km wide with 20 m pixel resolution and a recurrence period of 26 days. Some studies have been carried out to calibrate this sensor for use in assessing coastal, marine, and estuarine areas (Antunes & Tavares Jr., 2005; Ponzoni *et al.*, 2006; Ponzoni *et al.,* 2008a; Ponzoni et al. 2008b; Ferreira *et al.*, in press); however, no studies have targeted the calculation of suspended sediment concentration (SSC). The inclusion of this optical system in the suite of systems that are suitable to remotely estimate SSC will increase the temporal resolution of these data. Temporal resolution is limited by the revisiting period of the given sensor; hence, increasing the number of sensors will increase the amount of suitable data available (i.e., images with low cloud cover, absence of gaps, dates closer to those of in situ measurements, etc.).

Several rivers around the world have been experiencing a decrease in sediment yield over the past decades because of the construction of river dams (Dai *et al.*, 2008; Gupta *et al.* 2012; Luo *et al.,* 2012; Syvitski and Saito, 2007; Syvitski *et al.,* 2005). The reduction of sediment reaching the coast and continental shelf has triggered a progressive erosion on the coastlines located at the vicinities of the river mouths (Bittencourt *et al.,* 2007; Syvitski and Saito, 2007). One example of this is the coastline retreat observed on the São Francisco river delta (NE-Brazil) (Bittencourt *et al.*, 2007).

An important issue in estimating river suspended sediment yield is the availability of SSC data. Traditional data acquisition to estimate SSC by filtration of water samples is costly and time consuming; thus, only sparse measurements are normally available. Remote sensing techniques were developed with the aim of improving the volume of data that measure SSC (Tassan, 1987). The application of remote sensing techniques to monitor water quality in coastal areas is a practice of relatively low costs and high reliability. Several authors (Tassan, 1987; Mertes *et al.,* 1993; Lodhi and Rundquist 1998; Ritchie *et al.,* 2003; Ambarwulan and Hobma, 2004; Lorenzetti et al. 2007) have contributed to increasing the reliability of this type of surface water quality estimation through calibration of algorithms using in situ measurements to validate the results. Lorenzetti et al. (2007) found a consistent correlation between SSC estimated through the filtering of water samples and the data calculated from LANDSAT 5-TM using the

algorithm proposed by Tassan (1987). The accuracy of remotely sensed data depends mostly on the correction of the attenuation effect of the electromagnetic radiation by the atmosphere. This occurs primarily because of the presence of water vapor and aerosol particles. Models were created to compute the behavior of the solar spectrum in the atmospheric pathway to calculate and compensate the losses of the electromagnetic energy due to absorption by gases and scattering by aerosols. The application of the atmospheric correction algorithms reduces the atmospheric attenuation effects, making it possible to compare spectral data from images captured on different dates and under different meteorological conditions (Song et al. 2000). A simpler but more efficient way to account for the atmospheric interference on the electromagnetic signal is the Dark Object Subtraction (DOS) approach (Chaves, 1988; 1996). This method is based on the observation that the dark objects are not completely dark because of atmospheric interference, and the pathway radiance can be estimated. Another effective way to account for and correct the influence of the atmosphere is to use the 6S atmospheric correction model (Kotchenova *et al.*, 2006); however, this method is more complex than DOS because it requires meteorological information from the day of the imagery to input into the model.

In this work, SSC in the Parnaíba River (PR) will be derived from CBERS 2B spectral data using the algorithm proposed by Tassan (1987). To apply this algorithm, the CBERS 2B images have to be spectrally calibrated using LANDSAT 5-TM at-satellite radiance as a reference. In addition, methods for atmospheric correction will be compared, and the use of the results as a validation method for the spectral calibration will be discussed.

5.2. GEOGRAPHICAL SETTINGS

The PR is the second largest river in NE Brazil, only behind the São Francisco River in length and water discharge. The PR is approximately 1,400 km long and has a catchment area of 344.000 km2 that includes the entire Piauí State and parts of Maranhão and Ceará States (Figure 1).

The PR discharges approximately 16 billion m3/year of fresh water into the Atlantic Ocean (data from Agência Nacional de Águas - ANA). Along its course, the PR passes through the Parnaíba and Barreirinhas sedimentary basins, transporting their sediments. The deposition of these sediments at the river mouth over geologic time led

to the formation of an 80 km wide wave dominated asymmetric delta called the Parnaíba River Delta (PRD).

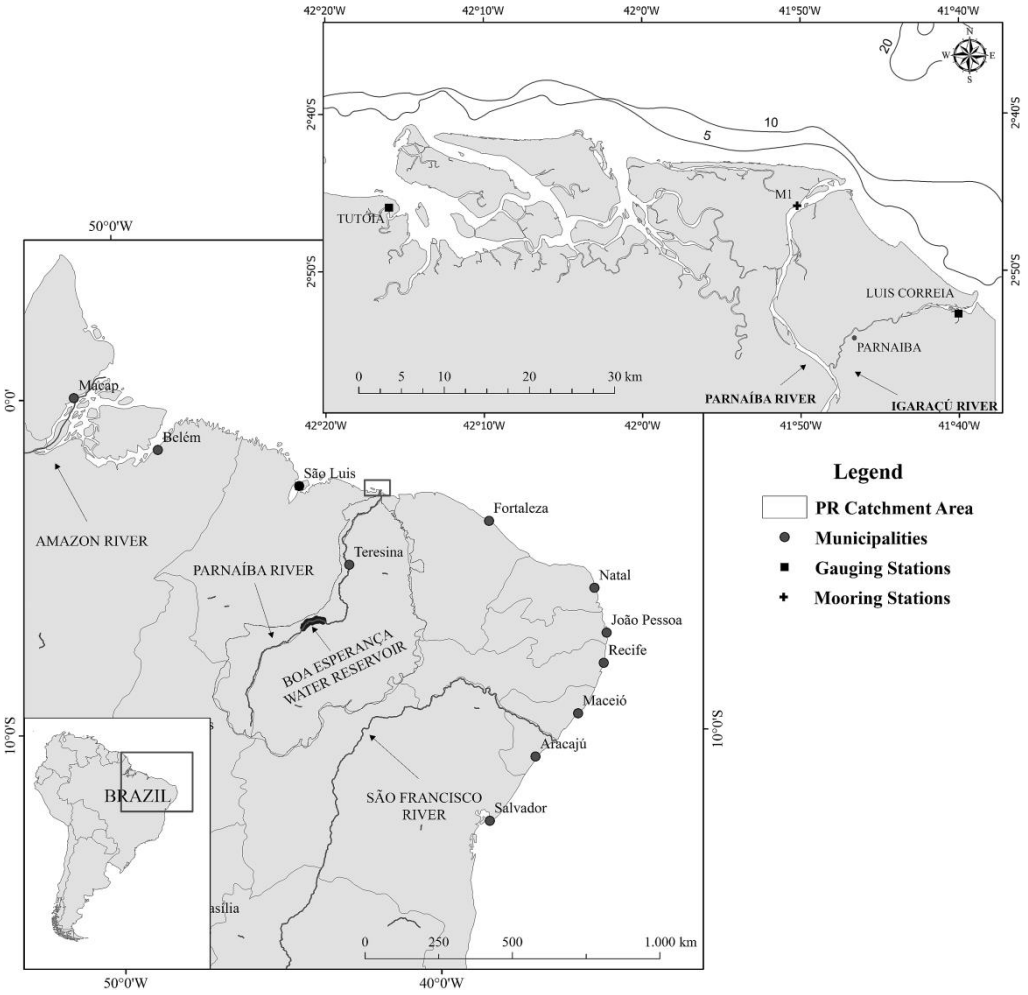

Figure 1 – Location of the Parnaíba River, its catchment area and detail of its lowermost sector with branching off of the Igaraçú River as a second distributary channel.

The continental shelf offshore the PRD is shallow and narrow, which is a common characteristic of NE Brazilian continental shelves (Gomes and Vital, 2010). In this region, the continental shelf is approximately 50 km wide with the shelf break at a 40 m water depth and an average depth of 22 m. The tide is semi-diurnal and mesotidal with a maximum amplitude of 3.06 m at spring tide (Aquino da Silva, in press).

5.3. ENVIRONMENTAL AND SETTINGS

Piauí State is located between the climatic areas characterized as pre-Amazon wet and NE semi-arid zones located on the northeast part of Brazil (Hastenhalt, 2006); therefore, the PR is located in a climatic transition zone in which characteristics of both geoenvironmental domains can be observed. According to the classification proposed by Köppen (Belda *et al.,* 2014; Köppen, 1936), the climate of this region is classified as semi-arid hot type BSW'h, which is characterized by having a monthly average temperature above 18°C. In the coastal region, two distinct seasons are well defined, a wet summer and dry winter (Figure 2). At the coast, the annual average air temperatures range from 26.1oC to 32.9oC, mean wind speed varies from 3.6 m/s to 7.1 m/s (in NE direction), and average relative humidity is 79.1% (data from Instituto Nacional de Meteorologia - INMET).

In this part of the Brazilian northeast coast, the wave climate is dominantly SW-directed with a significant wave height of 1 m and an average period of 5 seconds (Bittencourt *et al.,* 2005). The combination of wind and waves produces an East to West directed longshore current, which is characteristic of the entire NE Brazilian coast (Bittencourt *et al.,* 2005)

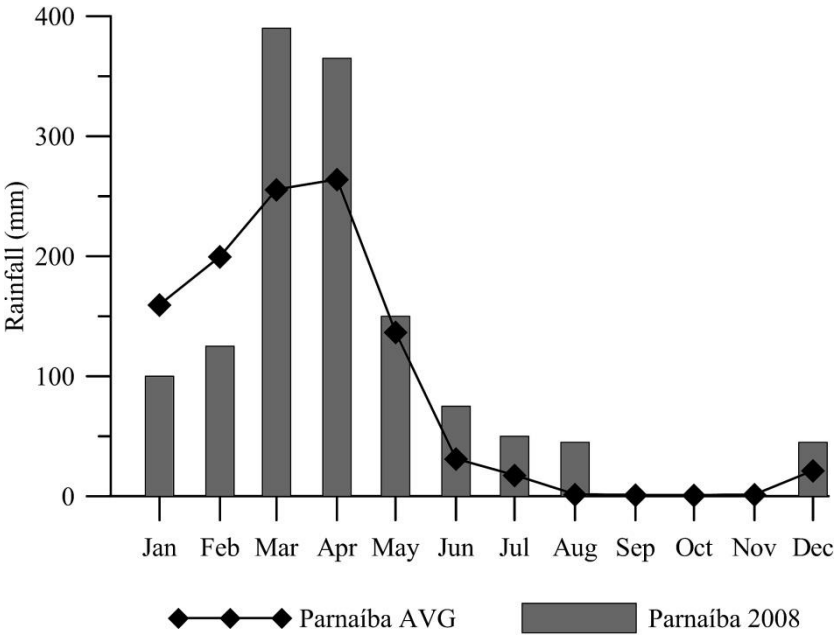

Figure 2 - Monthly average precipitation time series (1965-2009) and data from 2008 showing wet and dry periods at the Parnaíba coastal region.

5.4. MATERIAL AND METHODS

The estimation of SSC for the PR was performed using 12 multispectral satellite images that covered the period between January and December, 2008. One CBERS 2B image from 08/05/2008 and one LANDSAT 5-TM from 08/02/2008 were used to perform the CBERS 2B to LANDSAT 5-TM spectral calibration. The calibration of Tassan's algorithm was performed using five CBERS images in which imagery dates were closest to the in situ measurement dates (Table 1)

Table 1 - Dates of the *in situ* measurements of SSC in PR and the closest CBERS image available.

In situ	Closest image
10/25/2004	11/05/2004
07/06/2005	06/30/2005
10/28/2005	11/07/2005
11/12/2008	11/02/2008
03/16/2010	03/06/2010

5.4.1. Spectral Calibration of the CBERS 2B

The CBERS 2B and the LANDSAT 5-TM have similar spectral and spatial resolution (Table 2), and direct comparison of their products could be performed for visual purposes (e.g., definition of point bar migration, shoreline evolution, lowering of lake level margin position during drought periods, etc.). However, a calibration of the spectral range of the sensors was necessary to compare the products derived from the spectral information of their pixels (radiance or reflectance); therefore, the CBERS 2B images were calibrated using at-satellite radiance of the LANDSAT 5-TM images as a reference (Antunes and Tavares Jr. 2005). It was verified that the same meteorological conditions occurred during the imagery time of these two sensors, decreasing (or eliminating) the error intrinsic to this variable. This calibration allowed for the use of the algorithm developed by Tassan (1987) on the CBERS 2B images. The CBERS 2B digital numbers (DN) were calibrated using the LANDSAT 5-TM at-satellite radiance at four sites: dry quartzose sand (Sand), a fresh water lake without sediment in suspension (Coastal Lake), salt water without sediment in suspension (Deep Water), and a fresh water lake with high sediment in suspension (Lake Sediment) (Figure 3). In addition, the maximum and minimum DN of the images were used.

Table 2 - Characteristics of the LANDSAT 5-TM and the CBERS 2B satellite images.

Spectral Band	LANDSAT TM 5		CBERS 2B	
	Spectral Range (μm)	Spatial Resolution	Spectral Range (μm)	Spatial Resolution
1	0.452 - 0.518	30 m	0.45 - 0.52	20 m
2	0.528 - 0.609	30 m	0.52 - 0.59	20 m
3	0.626 - 0.693	30 m	0.63 - 0.69	20 m
4	0.776 - 0.904	30 m	0.77 - 0.89	20 m
5	1.567 - 1.784	30 m		
6	10.45 - 12.42	60 m		
7	2.097 - 2.349	30 m		
PAN			0.51 - 0.73	20 m

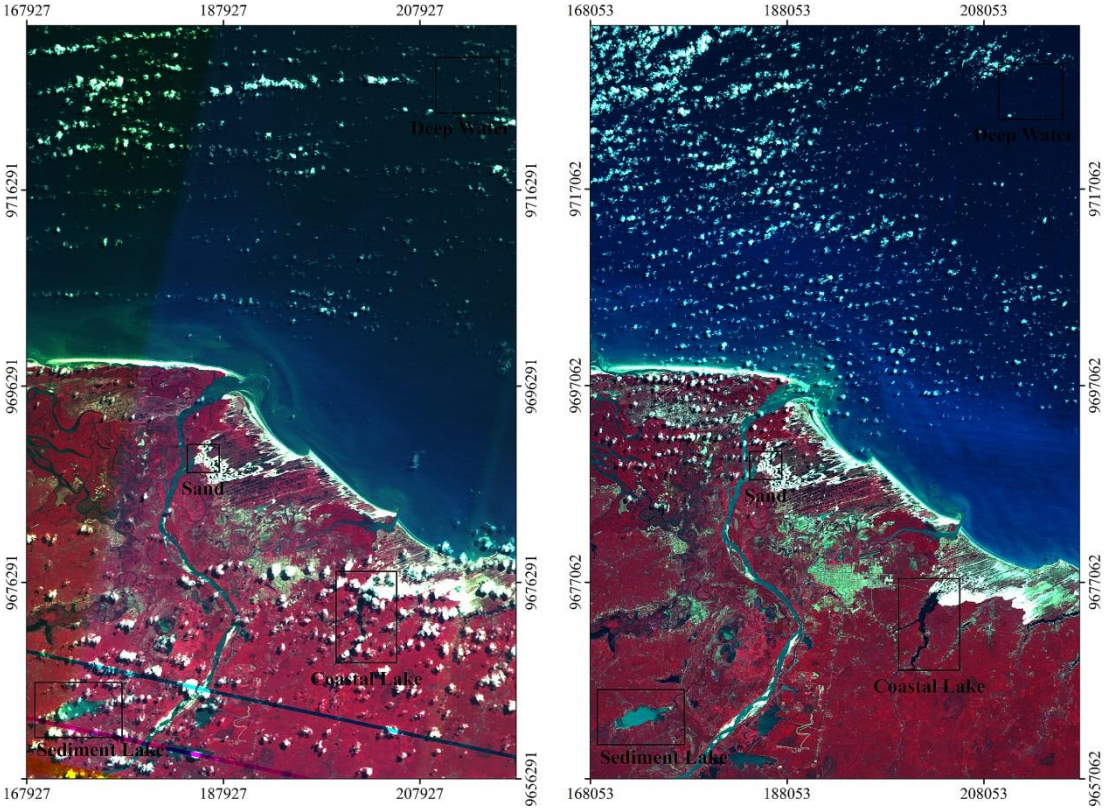

Figure 3 - Location of the sites used for the CBERS 2B to LANDSAT 5-TM calibration.

From each site, the average radiance of the LANDSAT 5-TM image and the DN of the CBERS 2B image were calculated for a group of pixels in the same geographic location in both images. The calibration equation was obtained through linear regression between the averages of the LANDSAT 5-TM at-satellite radiance and the CBERS 2B DN (Figure 4). The calibration was focused on band 2 and band 3, and those data were used in Tassan's algorithm (Table 3).

Table 3 - The values of the CBERS 2B DN and LANDSAT 5-TM at-satellite radiance (W/m2 sr μm).

Site	CBERS 2B DN 08-16-2009		LANDSAT 5TM at-Satellite 08-05-2009	
	B2	B3	B2	B3
Min DN	0.00	0.00	-2.84	-1.17
Sand	106.50	160.50	141.98	133.50
Coastal Lake	40.00	45.00	25.40	15.53
Deep Water	32.00	40.00	26.12	15.53
Lake Sediment	62.00	85.00	72.47	66.69
Max DN	255.00	255.00	365.00	264.00

The results of the linear regression were as follows: y = 1.5419 x – 26.613 and y = 1.1411 x – 34.576 for bands 2 and 3, respectively.

a **b**

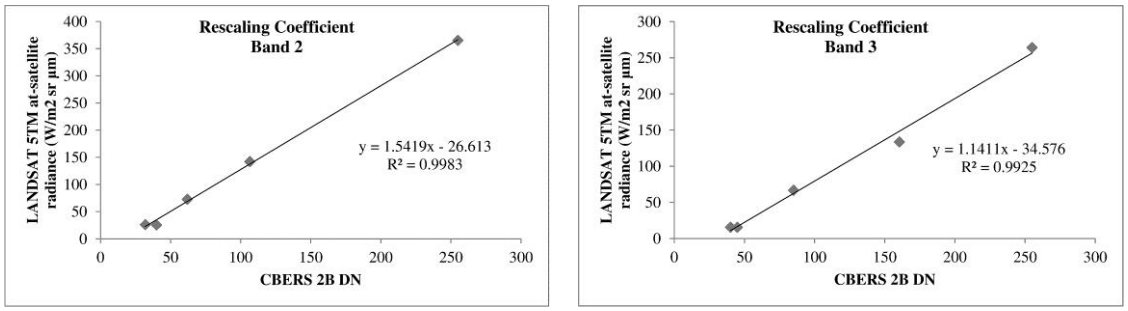

Figure 4 – Graph of the LANDSAT 5-TM at-satellite radiance vs CBERS 2B DN for the chosen sites and the respective calibration coefficients used to calculate the calibrated at-satellite radiance of the CBERS 2B for band 2 (a) and band 3 (b).

5.4.2. Atmospheric Correction

To work with radiance and reflectance of orbital sensors from different dates (or periods), it was necessary to remove the atmospheric effects of the passage of the electromagnetic wave through the atmosphere (Song *et al.*, 2000; Singh and Shanmugam, 2014; Hilker *et al.*, 2012; Themistocleous *et al.*, 2013). In this case, radiance had to be converted into reflectance prior the calculations of the SSC using the satellite images. Kaufman and Sendra (1988) found a relation between the at-satellite radiance and surface reflectance for a uniform Lambertian surface in a cloudless atmosphere, as expressed in Equation 1 below:

$$Lsat = Lp + [(\rho FdT\upsilon)/\pi(1-s\rho)] \qquad \text{(Equation 1)}$$

In Equation 1, Lsat is the at-satellite radiance, Lp is the path radiance, Fd is the irradiance received at the surface, Tυ is the atmospheric transmittance from the target

toward the sensor, s is the factor of the radiation back-scattered upward by the atmosphere to the surface, and ρ is the surface reflectance.

The irradiance reaching the Earth's surface follows Equation 2 (Song *et al.*, 2000):

$Fd = Eb + Edown$ (Equation 2)

In Equation 2, Edown is the downwelling diffuse irradiance, Eb is the beam irradiance, and $Eb = E0 \cos(\theta z)\, Tz$. In this last equation, E0 is the exoatmospheric solar constant, Tz is the atmospheric transmittance in the illumination direction, and θz is the solar zenith angle. sρ was assumed to be small in Equation 1 and could be neglected. Equation 1 can be solved for ρ and surface reflectance and written as follows:

$\rho = [\pi (Lsat - Lp)]/[T\upsilon (E0 \cos(\theta z))\, Tz + Edown]$ (Equation 3)

According to Chavez (1988, 1996) and Moran et al. (1992), the path radiance can be computed by using Equation 4:

$Lp = G\, DNmin + B - 0.01\, [E0 \cos(\theta z)\, Tz + Edown]\, T\upsilon/\pi$ (Equation 4)

In Equation 4, G is the sensor gain, B is the bias used for converting the sensor digital numbers (DN) to at-satellite radiance, and DNmin is the minimum digital number recorded by the satellite in the entire scene.

Using these equations on the calibrated CBERS 2B and on the LANDSAT 5-TM images, the consistency of the atmospheric correction methods was tested using Dark Object Subtraction (DOS) and the 6S ATM model. The aim was to choose the best method to be applied to the satellite images before calculating SSC. For DOS, three different input parameters were used in equations 3 and 4, as proposed by Song et al. (2000) (Table 4).

Table 4 - Settings for the parameters used to calculate the atmospherically corrected reflectance in the Dark Object Subtraction (DOS) approaches (modified from Song *et al.*, 2000).

Methods	T_υ	T_z	E_{down}
DOS_1	1,0	1,0	0,0
DOS_2	1,0	cos (θz)	0,0
DOS_3	$e^{-\tau r/\cos(\theta\upsilon)}$	$e^{-\tau r/\cos(\theta z)}$	Rayleigh (6S)

5.4.3. SSC and Suspended Sediment Load (SSL) Calculations

The set of images used to calculate SSC in the PRD region included 11 CBERS 2B images and 1 LANDSAT 5-TM image. The LANDSAT 5-TM image was used to complete the data set because of cloud cover issues for the CBERS 2B image from March, 2008 (Table 5).

Table 5 - Table of the dates and images used to assess the PR SSC in 2008 with the precipitation of each month.

Date	Satellite	PR Discharge (m^3)	Precipitation (mm)	
		1982-2005	2008	1971-2012
01/10/2008	CBERS 2B	948.5	95	131.4
05/02/2008	CBERS 2B	1138.4	157.2	203.5
02/03/2008	CBERS 2B	1847.7	389.9	285.9
28/04/2008	LANDSAT 5-TM	1930.4	366.2	281.5
19/05/2008	CBERS 2B	1028.2	151.6	183.2
14/06/2008	CBERS 2B	540.3	76.5	56.3
10/07/2008	CBERS 2B	394.7	51.5	37.6
05/08/2008	CBERS 2B	385.2	44.6	3.3
26/09/2008	CBERS 2B	377.3	0.0	1.5
22/10/2008	CBERS 2B	401.1	0.0	3.2
17/11/2008	CBERS 2B	475.3	0.0	4.9
13/12/2008	CBERS 2B	634.7	47.5	26.8

Tassan (1987) showed that there is a relation between the water reflectance of bands 2 and 3 in the LANDSAT 5-TM and the SSC measured in situ. Following his methodology, the algorithm was calibrated using a CBERS 2B image (after spectral calibration) and SSC in situ measurements in the PR. The SSC was first established by filtering surface water samples collected on 03/16/2010 at the mooring station in the river mouth (Figure 1). In total, 25 surface water samples were collected during 25 hours at hourly sampling intervals, covering a complete tidal cycle. The water samples were collected using a plastic bottle submerged approximately 0.5 m from the surface. Exactly 100 ml were filtered through pre-weighed 4 µm fiber glass filters. The filters were dried at 60ºC in an oven for 24 hours, and the weight difference was the amount of suspended sediment per 100 ml.

The CBERS 2B image from 03/06/2010 (at 13:12) was the satellite image with the closest date to that of the in situ measurements and was used to calibrate Tassan's algorithm for that location. The CBERS 2B imagery was taken during an ebb phase and two hours after high tide according to the tidal table of the imagery date and time. The value of the SSC measured on 03/16/2010, also at two hours after high tide, was used to calibrate the algorithm. The validation of this calibration was performed by comparing four in situ SSC measurements with the SSC calculated using the calibrated algorithm on four images (11/05/2004, 06/30/2005, 11/07/2005, and 11/02/2008).

To calculate the suspended sediment load (SSL), the SSC was calculated in 2008 for each month and the PR's average discharge was used assuming that no variations in

SSC occurred in the period between two consecutive images. The SSL was then calculated as described in the Equation 5 below:

$SSL = Qavg \times \Delta t \times SSCimage$ (Equation 5)

In Equation 5, Qavg is the monthly average river discharge in m3/s, Δt is the time in seconds and SSCimage is the calculated SSC; therefore, the summation of the SSL for each month was considered an approximation of the total yearly sediment discharge of the river to the inner continental shelf as suspended load..

5.5. RESULTS

5.5.1. Atmospheric Correction

The results of the atmospheric correction methods applied to the CBERS 2B and the LANDSAT 5-TM images (those that were used for the CBERS 2B to LANDSAT 5-TM spectral calibration) were compared to demonstrate the consistency between DOS and the 6S model (Figure 5). Sites of low reflectance had more consistent results than those of high reflectance (Figure 5).

The 6S model was considered the most accurate method for performing atmospheric correction (Kotchenova *et al.*, 2006); hence, the accuracy of the DOS method was estimated in relation to the 6S model. The choice of the DOS method was based on the accuracy and simplicity of application. With this in mind, the standard deviation of the differences between the DOS methods and the 6S model was computed (Table 6). The results revealed that DOS-2 provided more accurate results than the other two methods (Table 6). The other two methods under- or overestimated ρ because of different approaches used to estimate Tυ, Tz, and Edown (Table 4), although all results were fairly close to those obtained using the 6S model, as shown by highly significant R2-values (Table 6).

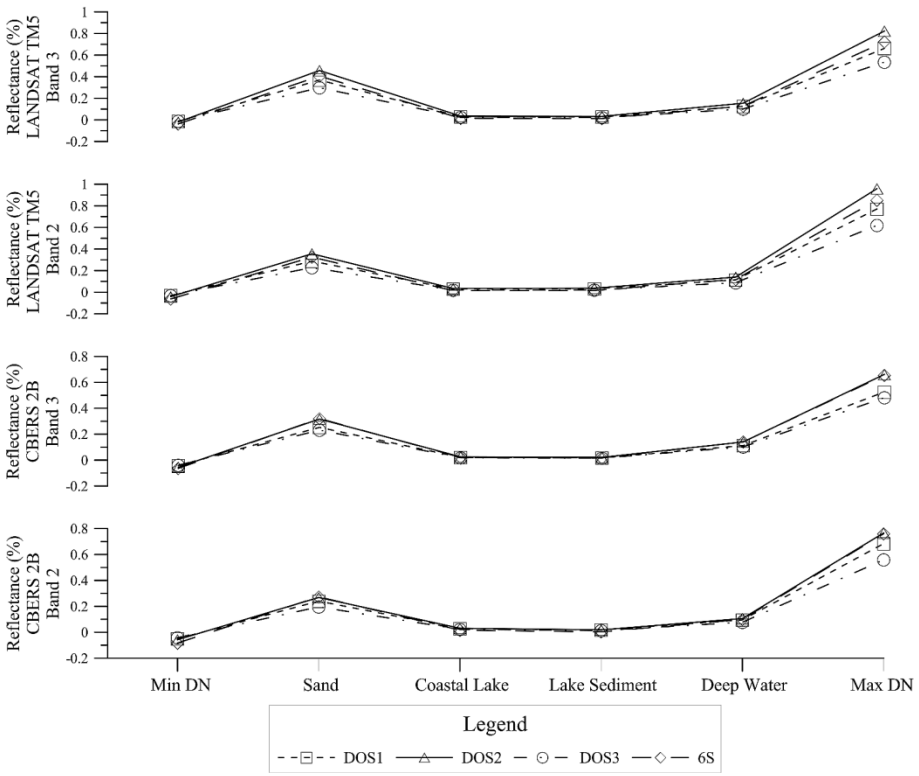

Figure 5 – Plots of the atmospherically corrected reflectance, using the different atmospheric correction methods, for the CBERS 2B image in bands 2 and 3 and for the LANDSAT 5-TM image in bands 2 and 3.

The comparison between the atmospherically corrected reflectance of the CBERS 2B and the LANDSAT 5-TM images successfully validated the spectral calibration applied to the CBERS 2B image, regardless of the divergences previously described (Figure 6). In addition, the divergences of the atmospherically corrected reflectance were smaller in band 2 than in band 3, although they increased as reflectance increased in both spectral bands (Figure 6).

Table 6 - Comparison between the three types of DOS and the 6S model.

Sensor and spectral sites	**ρ**				**Error of ρ related to 6S model**		
CBERS 2B - B2	DOS-1	DOS-2	DOS-3	6S	DOS-1	DOS-2	DOS-3
Min DN	-0.0505	-0.0579	-0.0420	-0.0834	0.0329	0.0255	0.0414
Sand	0.2400	0.2682	0.1956	0.2730	-0.0331	-0.0048	-0.0774
Coastal Lake	0.0284	0.0306	0.0225	0.0166	0.0118	0.0141	0.0059
Deep Water	0.0175	0.0184	0.0136	0.0029	0.0146	0.0155	0.0107
Lake Sediment	0.0953	0.1058	0.0773	0.0996	-0.0042	0.0063	-0.0223
Max DN	0.6837	0.7664	0.5587	0.7605	-0.0769	0.0059	-0.2018
Standard Deviation	0.2706	0.3039	0.2215	0.3097	0.0399	0.0104	0.0885
R^2					0.9988	0.9989	0.9989
CBERS 2B - B3							

Min DN	-0.0423	-0.0546	-0.0396	-0.0638	0.0215	0.0092	0.0242
Sand	0.2523	0.3169	0.2311	0.3207	-0.0684	-0.0038	-0.0896
Coastal Lake	0.0206	0.0247	0.0182	0.0205	0.0001	0.0042	-0.0023
Deep Water	0.0177	0.0211	0.0155	0.0167	0.0010	0.0044	-0.0011
Lake Sediment	0.1118	0.1398	0.1020	0.1406	-0.0288	-0.0008	-0.0386
Max DN	0.5258	0.6617	0.4824	0.6554	-0.1295	0.0064	-0.1730
Standard Deviation	0.2118	0.2671	0.1946	0.2679	0.0562	0.0048	0.0734
R^2					0.9997	0.9997	0.9996
LANDSAT 5 TM - B2							
Min DN	-0.0311	-0.0412	-0.0297	-0.0626	0.0315	0.0214	0.0329
Sand	0.2875	0.3559	0.2279	0.3254	-0.0379	0.0305	-0.0975
Coastal Lake	0.0296	0.0344	0.0193	0.0140	0.0156	0.0204	0.0053
Deep Water	0.0315	0.0368	0.0209	0.0164	0.0151	0.0204	0.0045
Lake Sediment	0.1144	0.1402	0.0880	0.1190	-0.0046	0.0212	-0.0310
Max DN	0.7711	0.9588	0.6191	0.8530	-0.0819	0.1058	-0.2339
Standard Deviation	0.3006	0.3748	0.2432	0.3421	0.0424	0.0341	0.0993
R^2					0.9991	0.9989	0.9988
LANDSAT 5 TM - B3							
Min DN	-0.0140	-0.0199	-0.0120	-0.0376	0.0237	0.0178	0.0256
Sand	0.3688	0.4573	0.2976	0.4055	-0.0367	0.0518	-0.1080
Coastal Lake	0.0298	0.0347	0.0234	0.0148	0.0150	0.0199	0.0086
Deep Water	0.0280	0.0325	0.0220	0.0127	0.0153	0.0198	0.0092
Lake Sediment	0.1257	0.1542	0.1009	0.1280	-0.0024	0.0261	-0.0271
Max DN	0.6622	0.8231	0.5348	0.7228	-0.0606	0.1002	-0.1880
Standard Deviation	0.2653	0.3308	0.2146	0.2987	0.0338	0.0245	0.0843
R^2					0.9992	0.9993	0.9991

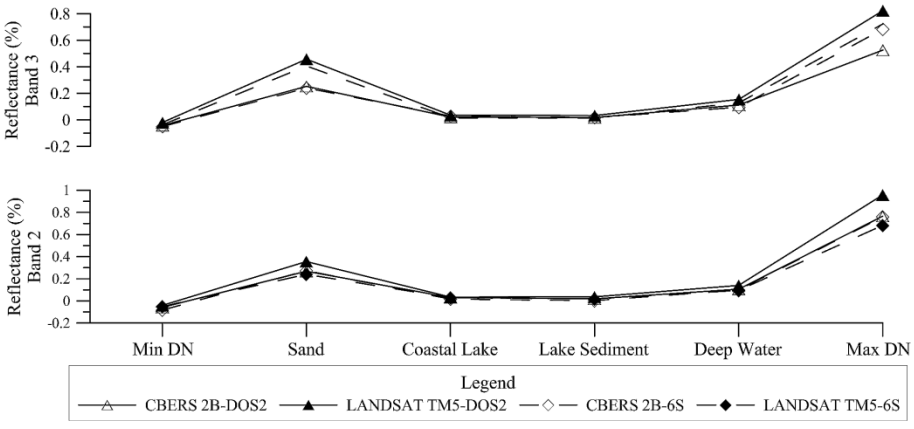

Figure 6 – Comparison of the atmospherically corrected reflectance calculated using 6S code and DOS_2 for the CBERS 2B and LANDSAT 5-TM images in bands 2 and 3.

5.5.2. Calibration of the Algorithm

The calibration of the algorithm was performed for bands 2 and 3 using the in situ SSC measured in the PR and the CBERS 2B satellite image. The calculated SSC from both spectral bands underestimate or overestimate the measured values on different occasions (Table 7). The jackknife test revealed that the tuned algorithm, in general, underestimated the results for both spectral bands (-0.0214 for band 3 and -0.0310 for band 2). For band 2, the calculated SSC had results that underestimated the measured values by up to 28.0%, whereas for band 3, the underestimation was up to 12.8%. The overestimation of the calculated SSC for band 3 was higher than those that resulted from band 2, 11.7% and 8.0% for bands 3 and 2, respectively (Table 7). The best performance of the tuned algorithm was observed in band 3, which showed smaller discrepancies between measured and calculated values (R2=0.93 for band 3 compared to R2=0.90 for band 2); therefore, band 3 was used to calculate the SSC in the PR for 2008. The performance of the algorithm, after tuning, was satisfactory for both high and low concentrations and validated its application in the Parnaíba coastal zone (Table 7).

Table 7 - Table showing the dates of in situ measurements and satellite imagery, their respective SSC values and the error of the calculated SSC.

in situ Date	Image Date	*In situ* SSC (mg/l)	SSC Band 2 (mg/l)	SSC Band 3 (mg/l)	SSC Band 2 Error %	SSC Band 3 Error %
10/25/2004	11/05/2004	75.9	67.0	74.2	-11.8	-2.3
07/06/2005	06/30/2005	99.8	85.1	87.1	-14.8	-12.8
10/28/2005	11/07/2005	70.3	75.9	78.5	8.0	11.7
11/12/2008	11/02/2008	66.5	67.2	67.6	1.1	1.7
03/16/2010	03/06/2010	136.7	98.4	137.8	-28.0	0.9

5.5.3. SSC in PR During 2008

In 2008, the months when maximum and minimum SSC occurred were February (135.9 mg/l) and September (56.3 mg/l). The maximum SSC occurred during the rainy period, whereas the minimum occurred during the dry period (Table 8).

A threshold value of 84.0 mg/l was established from defined periods of low and high turbidity in the PR. This threshold was defined based on the median SSC value of a given year. The low turbidity period occurred whenever the SSC was more than 10% lower than the median of the year, and the opposite was defined as the high turbidity period. According to this threshold, the period of high turbidity started in December, when rainfall increased rapidly compared to the previous month, and ended in July.

Thus, the period from August until November was classified as the low turbidity period (Figure 7). The turbidity and the rainy periods were not equal. The rainy period lasts for 6 to 7 months each year, while in 2008, the high turbidity period lasted for 8 months. Moreover, the occurrence of the maximum was displaced. In 2008, maximum turbidity occurred in February, while precipitation reached its peak in April. The minimum SSC and rainfall occurred concomitantly (Figure 7). The maximum SSL occurred in March (532,608.4 tons), although the maximum SSC occurred in February and the maximum river discharge in April (Table 8). The minimum SSL (50,850.0 tons) and river discharge occurred in September. In 2008, the PR discharged approximately 2.53 x 106 tons of sediment to the continental shelf. The average of the SSL during the period of low SSC was 6.50 x 104 tons, resulting in a total of 2.60 x 105 tons of sediment (from August until November), which represented only 10.3% of the total sediment yield by the PR in 2008. In 2008, the PR released most of the sediment (89.7%) to the inner continental shelf during the period of high SSC (December until July). The mean SSL for this period was 2.84 x 105 tons/month, which resulted in a total of 2.27 x 106 tons of sediment during this period.

Table 8 - Calculated SSC from 2008 using the satellite images, cumulative precipitation in 2008, monthly average River discharge (1982-2005), and total SSL of PR.

Month (2008)	SSC (mg/l)	Cumulative precipitation 2008 (mm)	Discharge (m3/s)	SSL (tons)
Jan	87.1	171.5	948.5	210,223.2
Feb	135.9	188.5	1,138.4	362,225.2
Mar	112.0	263.5	1,847.7	532,608.4
Apr*	107.9	305.0	1,930.4	518,116.3
May	103.8	152.5	1,028.2	273,875.8
Jun	101.73	83.0	540.3	136,398.9
Jul	99.7	31.5	394.7	100,774.5
Aug	63.1	6.5	385.2	60,663.7
Sep	56.3	6.5	377.3	50,850.0
Oct	69.8	8.5	401.1	70,337.8
Nov	67.6	5.5	475.3	77,933.4
Dec	85.0	58.0	634.7	137,064.8

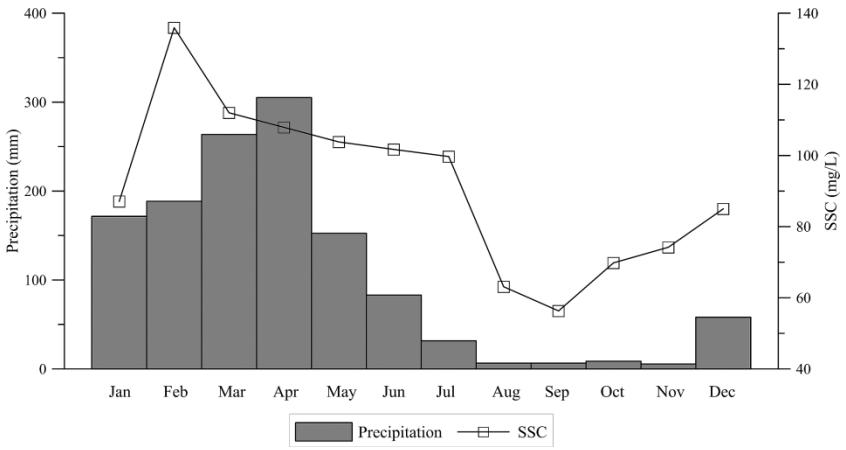

Figure 7 - Plot of satellite derived SSC for the location of the mooring station M1 and the precipitation in the region of Parnaíba city in 2008.

5.5.4. The SSC on the Continental Shelf

During the ebb phase and low tide, the river sediment plume was pushed offshore (northward) approximately 10 km off the PR mouth (Figure 8). The offshore and eastward limits of the river plume were well defined by an abrupt change between the high turbidity river plume and the low turbidity sea water (Figure 8). Contrarily, the SSC gradually decreased westward, and its limit could not be clearly defined (Figure 9). In addition, further west from the PR mouth, areas with high SSC were noted close to the shoreline, and they decreased gradually offshore.

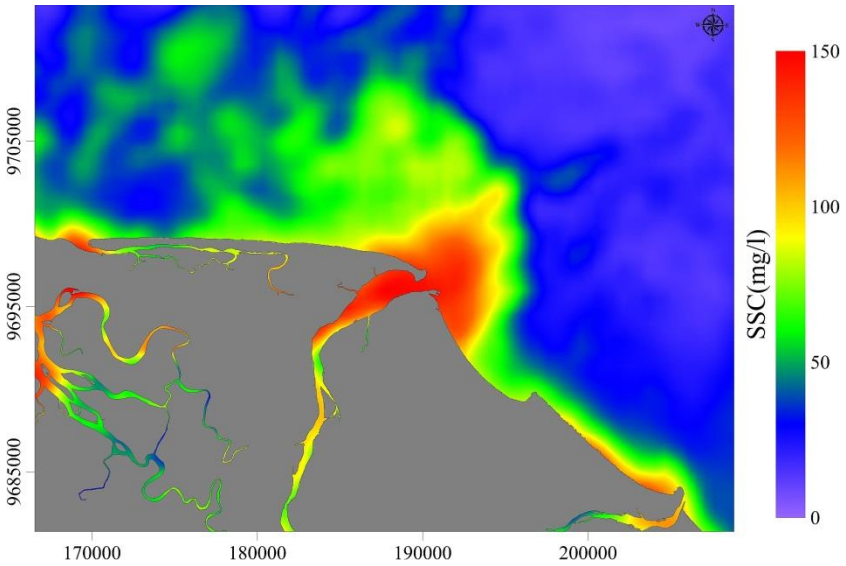

Figure 8 – The map of the SSC calculated from the CBERS 2B image of 02/05/2008 (imagery during ebb phase).

During the flood phase and high tide, the river sediment plume was pushed toward the coastline and into the river. In these periods, the areas with high SSC were well defined and occurred close to the shoreline and upstream in the PR (Figure 10). The SSC near the shoreline was always greater than 20 g/m3 in both high and low turbidity periods. The dissipation of the sediment plume occurred in the same manner during both periods, however, with different characteristics (e.g., size of the plume, offshore, eastward and westward extent).

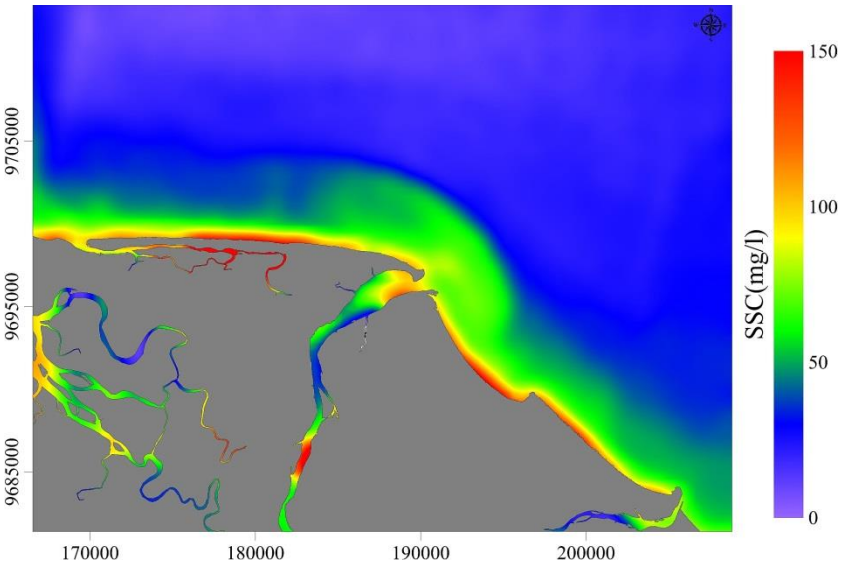

Figure 9 - The map of the SSC calculated from the CBERS 2B image of 09/26/2008 (imagery during low tide).

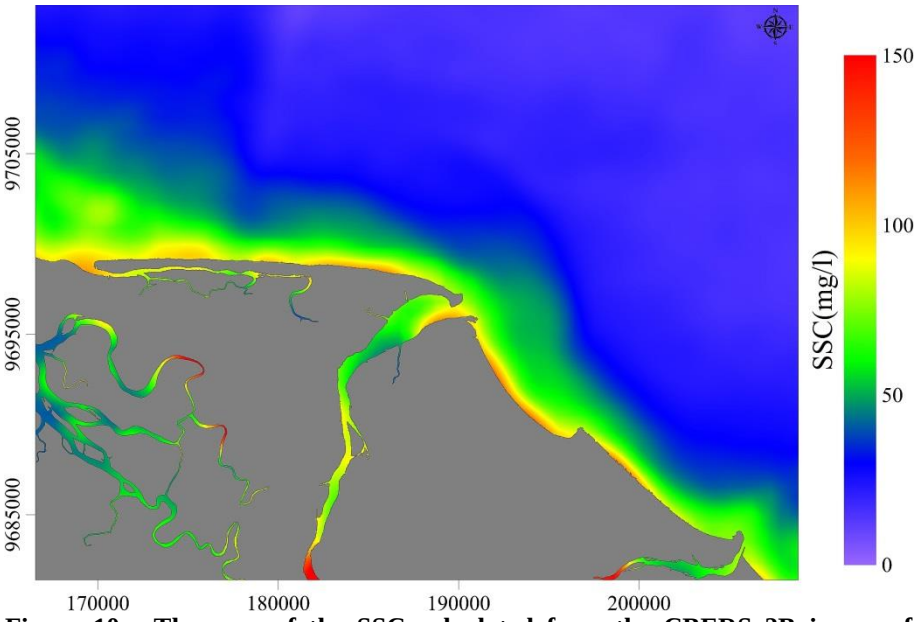

Figure 10 - The map of the SSC calculated from the CBERS 2B image of 07/10/2008 (imagery during flood phase).

5.6. DISCUSSIONS

The spectral calibration of the CBERS 2B images yielded a significant correlation coefficient (R2) of 0.9983 for band 2 and 0.9925 for band 3 with the LANDSAT 5-TM. The spectral band similarities between the sensors contributed to the consistency of the spectral calibration of the CBERS 2B image using LANDSAT 5-TM at-satellite radiance. The consistency between the atmospherically corrected reflectance from the LANDSAT 5-TM (08/02/2008) and the CBERS 2B (08/05/2008) images in the selected sites can be interpreted as a validation method for the spectral calibration of the CBERS 2B images. In addition, the comparison of the atmospherically corrected reflectance between the sensors was used to evaluate the different atmospheric correction methods according to their simplicity of application and accuracy in comparison to the 6S model. This methodology turned out to be a reliable validation technique suitable for testing the consistency of the spectral data from different sensors.

The satellite derived SSC was more consistent with field measurements using band 3 (R2=0.93) than using band 2 (R2=0.90), in contrast to the findings of Lorenzetti et al. (2007) on studies carried out in the São Francisco River (Northeast Brazil). This difference could be attributed to the lower SSC found in the São Francisco River. Tassan's algorithm (Tassan, 1987) was developed in a site where low SSC occurred. In the PR, considerably higher SSC was measured than those found by Lorenzetti (Lorenzetti *et al.*, 2007) in the São Francisco River and by Tassan (Tassan, 1987) in the Adriatic Basin. In the high turbidity period, SSC between these sites differed by up to a factor of 10. The differences in SSC may be one of the reasons it was necessary to change some of the coefficients in the original algorithm that resulted in the best performance obtained in band 3. Tassan also suggested that band 3 should perform better when calculating low concentrations (approximately 1 mg/l) (Tassan, 1987) than the other bands, which was not the case at our sample site. In our study, when calculating high concentrations, the algorithm provided better results in band 3 than in band 2 after tuning sensitivity analysis using low and high SSC (Table 7). Better correlation with in situ measurements occurred when SSC was calculated using band 3 in areas of high SSC, which was also reported by other authors (Harrington *et al.*, 1992; Ritchie *et al.*, 2003). The addition of CBERS 2B images to assess the SSC may increase the temporal resolution of this information because it depends on the satellite recurrence period, which is 26 days for CBERS 2B and 16 days for LANDSAT 5-TM (Chander *et*

al., 2009). In addition the CBERS 2B images have a higher spatial resolution than the LANDSAT 5-TM images (Table 2).

After calibration, the algorithm was used to calculate the SSC for 2008, in which it was found that the increase of the SSC in response to the increase of precipitation was not linear. The SSC in the river also depended on the transport mechanisms of the fine sediment (Beuselinck *et al.,* 2002; Shih and Yang, 2009) from the river bank and adjacent areas. This was demonstrated by the rapid increase in SSC during the first rainfall immediately after the dry period (Beuselinck *et al.,* 2002; Shih and Yang, 2009); therefore, higher concentrations had a tendency to occur before the peak of precipitation. The surface sediment/soil erosion mechanism described by Shih & Yang (2009) could be highlighted as one of the major factors that contribute to this phenomenon. During the dry season, the wind was responsible for maintaining the minimum SSC concentration (56.3 mg/l in September, 2008). In the early stage of the rainy season, the SSC reached the maximum (135.9 mg/l in March).

In 2008, the average SSC in the PR was 91.4 mg/l, which was low compared to other rivers; for example, the average SSC of 190 mg/l in the Orinoco and Amazon rivers (Venezuela and Brazil, respectively), 310 mg/l in the Fitzroy-East river (Australia), 610 mg/l in the Amo river (Italy), and 810 mg/l in the Mississippi river (USA) (Table 9), as described by Syvitski and Saito (2007). Nevertheless, the PR yielded approximately 2.54 x 106 ty-1 of sediment to the inner continental shelf because of its water discharge (approximately 26 billion m3y-1), whereas, the Fitzroy-East and the Amo rivers yields 2.20 x 106 ty-1 and have higher average SSC. Similar situation is observed in the Amazon River, which has lower SSC than the Yangtze (190 mg/l against 540 mg/l), even though it yields 1,200 x 106 ty-1 of sediment to the ocean, whereas the Yangtze river yields 4,800 x 105 ty-1. Thus, the total amount of sediment yield by a river is more influenced by the river discharge than by the SSC. The discharge of the river sediment to the continental shelf depends on the local hydrodynamic conditions. In the case of the PRD, the occurrence of a westward directed longshore current caused the westward drift (Bittencourt *et al.,* 2005; Warrick *et al.,* 2007) of the sediment plume. Longshore currents and NE trade winds (Bittencourt *et al.,* 2005) were also responsible for the well-defined eastward contact between the sediment plume and the sea water, as well as its gradational westward alongshore dispersion pattern. On the west side of the PR mouth, the NE wind and waves pushed the suspended sediment toward the coast, resulting in high SSC observed close to the

shoreline over the entire year. The across-shore extent of the sediment plume offshore of the PRD depended on the SSL yield and the strength of the river discharge.

Table 9 - Example of river characteristics and hydrographic parameters in different geological and climatological environments. The data were compiled from Syvitski and Saito, 2007.

River	Country	Catchment Area (km^2)	Length (km)	Water Discharge (m3/s)	ssc (mg/l)
Parnaíba	Brazil	344,112	1,400	841	91
São Francisco	Brazil	638,576	2,700	2,528	34
Amazon	Brazil	6,183,507	6,516	198,676	190
Paraná	Brazil	2,887,069	4,500	14,506	180
Arno	Italy	7,969	240	57	680
Danube	Italy	778,499	2,850	6,420	330
Ebro	Spain	756,86	930	1,400	1,040
Ganhes/Brahma	India	1,568,702	2,840	31,000	1,120
Mekong	Vietnam	792,245	4,425	17,345	340
Mississipi	United States	3,208,025	6,020	15,452	1,110
Nile	Egypt	2,786,902	6,669	3,484	1,400
Orinoco	Venezuela	962,373	2,500	34,500	160
Rhone	France	87,857	820	1,700	1,310
Yangtze	China	1,807,000	6,380	28,278	540

5.7. CONCLUSIONS

The presence of clouds is an important limiting factor in the use of multi-spectral satellite images to monitor seasonally changing parameters derived from ocean color; therefore, the possibility of using more than one orbital sensor, for instance to calculate the SSC, improves the chances to obtain images suitable for performing this task. It is necessary to correct the images for atmospheric effects to compare the spectral data of images taken at different dates because of differences in atmospheric conditions during imagery. The absence of atmospheric correction will significantly impact the results. Any of the atmospheric correction methods that were tested could be applied to remove the atmospheric effects of the images to calculate the SSC without a significant loss of accuracy. The use of DOS to perform atmospheric correction significantly reduced the computational time for image correction compared to the 6S model. Tassan's algorithms allow the calculation of SSC from spectrally calibrated CBERS 2B images.

The rainfall is the major factor that influences the seasonality of the SSC in the PR; however, the relation between rainfall and SSC is not linear. The apex of the SSC in the river occurs before the maximum precipitation because of the high input of fine sediments at the beginning of the rainy season and the variations in the surface

sediment/soil erosion mechanism caused by water saturation of the ground. The comparison of the SSC and the SSL of the PR with other rivers around the world revealed that the SSL is more influenced by the river discharge than by the SSC itself. Local hydrodynamic conditions and trade winds were the major forces that defined the dispersion pattern of the river sediment plume in the inner continental shelf; however, the strength of the river discharge defined the characteristics of the river sediment plume and its offshore extent in the continental shelf. The combined action of wind and waves was responsible for the high SSC near the coastline during the low turbidity period.

ACKNOWLEDGEMENTS

This work is part of the project "Northern Brazilian river deltas: River impacts versus pristine discharge" which is funded by the Deutsche Forschungsgemeinschaft (STA 401/16-1). The authors would like to thank the captain and crew of the São Francisco III, as well as all team members, for their efforts to support the study, namely, F. Caninde´ Soares, Werner F. Tabosa, Pedro Moreia, Gustavo Rocha, Maria Isabel da Rocha, Helmut Beese, Camila Soares, Agata Szczygielski and Juliana Köenig. The authors also would like to thank CHESF, INMET, ANA for have kindly provided some of the data used on this research. Special thanks for the GGEMMA lab of the Universidade Federal do Rio Grande do Norte for dispose part of the equipment used on this research and the CNPq for additional for the additional support (Grant PQ CNPq n.º 303481/2009-9).

LITERATURE CITED

Ambarwulan, W. and Hobma, T.W., 2004. Bio-optical Model for Mapping Spatial Distribution of Total SuspendedMatter from Satellite Imagery. 3rd FIG *Regional Conference*, Jakarta, Indonesia.

Antunes, M.A.H. and Tavares Jr., J.B., 2005. Calibração do sensor CCD-CBERS II com dados do ASTER1. Anais XII *Simpósio Brasileiro de Sensoriamento Remoto*, Goiânia, Brasil.

Aquino da Silva, A. G.; Stattegger, K.; Schwarzer, K.; Vital, H., and Heise, B., 2014. The influence of climatic variations on river delta hydrodynamics and morphodynamics in the Parnaíba Delta, Barzil. *Journal of Coastal Research*, in press.

Belda, M.; Holtanová, E.;Halenka, T., and Kalvová, J., 2014. Climate classification revised: from Köppen to Trewartha. *Journal of Climate Rersearch*, 59, 1-13.

Beuselinck, L.; Govers, G.; Hairsine, P. B.; Sander, G. C. and Breynaert, M., 2002. The influence of rainfall on sediment transport by overland flow over areas of net deposition. *Journal of Hydrology*, 257(1-4), 145-163.

Bittencourt, A.C.S.P.; Dominguez, J.M.L.; Martin, L. and Silva, I.R., 2005. Longshore transport on the northeastern Brazilian coast and implications to the location of large scale accumulative and erosive zones: An overview. *Marine Geology*, 219, 219-234.

Bittencourt, A. C. S. P.; Dominguez, J. M. L.; Souza, L. C. D. L.; Silva, I. R. and Silva, F. R., 2007. Wave Refraction, River Damming, and Episodes of Severe Shoreline Erosion: The São Francisco River Mouth, Northeastern Brazil. *Jounal of Coastal Research*, 23(4), 930-938.

Chander, G.; Marjham, B. L., and Helder, D. L., 2009. Summary of current radiometric calibration coefficients for Landsat MSS, TM, ETM+, and EO-1 ALI sensors. *Remote Sensing of Environment*, 113, 893-903.

Chavez Jr., P.S., 1988. An improved dark-object subtraction technique for atmospheric scattering correction of multispectral data. *Remote Sensing of Environment*. 24, 459–479.

Chavez Jr., P.S., 1996. Image-based atmospheric correction-revisited and improved. *Photogrammetric Engineering and Remote Sensing*, 62, 1025–1036.

Dai, S.; Yang, S. and Cai, A., 2008. Impacts of dams on the sediment flux of the Pearl River, southern China. Catena, 76, 36-43

Gomes, M.P. and Vital, H., 2010. Revisão da compartimentação geomorfológica da Plataforma Continental Norte do Rio Grande do Norte, Brasil. *Revista Brasileira de Geosciências*, 40(3), 321-329.

Gupta, H.; Kao, S.-J. and Dai, M., 2012. The role of mega dams in reducing sediment fluxes: A case study of large Asian rivers. *Journal of Hydrology*, 464-465, 447-458.

Harrington, J.A.; Schiebe, Jr. and Schiebe, F.R.,1992. Remote Sensing of Lake Chicot, Arkansas: Monitoring Suspended Sediments, Turbidity, and Secchi Depth with Landsat MSS Data. *Remote Sensing of Environment*, 39, 15-27.

Hastenrath, S., 2006. Circulation and teleconnection mechanisms of Northeast Brazil droughts. *Progress in Oceanography*, 70, 407-415.

Hilker, T.; Lyapustin, A.I.; Tucker, C.J.; Sellers, P.J.; Hall, F.G. and Wang, Y., 2012. Remote sensing of tropical ecosystems: Atmospheric correction and cloud masking matter. *Remote Sensing of Environment*, 127, 370-384.

Kaufman, Y.J. and Sendra, C., 1998. Algorithm for automatic Radioatmosphericcorrections to visible and near-IR satellite imagery. *Remote Sensing*, 9, 1357-1381.

Köppen, W., 1936. Das geographische System der Klimate. In: Köppen W, Geiger R (eds) Handbuch der Klimatologie. Gebrüder Borntraeger, Berlin, p 1−44

Kotchenova, S.Y.; Vermote, E.F.; Matarrese, R. and Klemm Jr., F.J., 2006. Validation of a vector version of the 6S radiative transfer code for atmospheric correction of satellite data. Part I: Path radiance. *Applied Optics*, 56(26), 6762-6774.

Lodhi, M.A. and Rundquist, D.C., 1998. Estimation of Suspended Sediment Concentration in Water Using Integrated Surface Reflectance. *Geocarto International*, 13(2), 11-15.

Lorenzzetti, J.A.; Negri, E.; Knopers, B. and Medeiros, P.R.P., 2007. Uso de imagens LANDSAT como subsídio ao estudo da dispersão de sedimentos naregião da foz do rio São Francisco. Anais XIII *Simpósio Brasileiro de Sensoriamento Remoto*, Florianópolis, Brasil.

Luo, X.; Yang, S. and Zhang, J., 2012. The impact of the Three Gorges Dam on the downstream distribution and texture ofsediments along the middle and lower Yangtze River (Changjiang) and its estuary,and subsequent sediment dispersal in the East China Sea. *Geomorphology*, 179, 126-140.

Mertes, L.A.K.; Smith, M.O. and Adams, J.B., 1993. Estimating Suspended SedimentConcentrations in Surface Waters of theAmazon River Wetlands from Landsat Images. *Remote Sensing of Environment*, 43, 281-301

Moran, M.S.; Jackson, R.D.; Slater, P.N. and Teillet, P.M., 1992. Evaluation of simplified procedures for retrieval of land surface reflectance factors from satellite sensor output. *Remote Sensing of Environment*, 41, S. 169-184.

Ponzoni, F.J.; Junior, J.Z. and Lamparelli., R.A.C., 2006. Transformações radiométricas dos dados dos sensores do satélite CBERS-2. Anais 1º *Simpósio de Geotecnologias no Pantanal*, Campo Grande, Brasil.

Ponzoni, F.J. and Albuquerque, B.F.C., 2008a. Pre-Launch Absolute Calibration of CCD/CBERS-2B Sensor. *Sensors*, 8, 6557-6565.

Ponzoni, F.J.; Junior, J.Z. and Lamparelli, R.A., 2008b. In-flight absolute calibration of the CBERS-2 CCD sensor data. Annals of the *Brazilian Academy of Sciences* 80(2), 373-380.

Ritchie, J.C.; Zimba, P.V. and Everitt, J., 2003. Remote sensing techniques to assess water quality. *Photogrammetric Engineering and Remote Sensing*, 69(6), 695-704.

Singh, R. K. and Shanmugam, P., 2014. A novel method for estimation of aerosol radiance and its extrapolation in the atmospheric correction of satellite data over optically complex oceanic waters. *Remote Sensing of Environment*, 142, 188-206.

Shih, H.-M. and Yang, C.T., 2009. Estimating overland flow erosion capacity using unit stream power. Int. *Jour. of Sediment Research*,24(1), 46-62.

Song, C.; Woodcock, C.E.; Seto, K.C.; Lenney, M.P. and Macomber, S.A., 2000. Classification and Change Detection Using Landsat TM Data: When and How to Correct Atmospheric Effects? *Remote Sensing of Environment*,75, 230-244.

Syvitski, J. P. M. and Saito, Y., 2007. Morphodynamics of deltas under the influence of humans. *Global and Planetary Change*, 57, 261-282.

Syvitski, J.P.; Kettner, A.J.; Correggiari, A., and Nelson, B.W., 2005. Distributary channels and their impact on sediment dispersal. *Marine Geology*, 222-223, 75-94.

Tassan, S., 1987. Evaluation of the potential of the Thematic Mapper for marine application. *International Journal of Remote Sensing*, 8(10), 1455-1478.

Themistocleous, K.; Hadjimitsis, D.G.; Retails, A.; Chrysoulakis, N. and Michaelides, S., 2013. Precipitation effects on the selection of suitable non-variant targets intended for atmospheric correction of satellite remotely sensed imagery. *Atmospheric Research*, 131, 73-80.

Warrick, J.A.; DiGiacomo, P.M.; Weisberg, S.B.; Nezlin, N.P.;Mengel, M.; Jones, B.H.; Ohlmann, J.C.; Washburn, L.; Terrill, E.J. and Farnsworth, K.L., 2007. River plume patterns and dynamics within the Southern California Bight. *Continental Shelf Research*, 27, 2427-2448.

Chapter 6

LATE PLEISTOCENE AND HOLOCENE SEISMIC STRATIGRAPHY OFFSHORE THE PARNAIBA DELTA, NE BRAZIL, AS INDICATOR OF SEA LEVEL CHANGE

André G. Aquino da Silva[1], Karl Stattegger[1], Klaus Schwarzer[1], Helenice Vital[2]

[1]Institute of Geosciences, Kiel University, Germany
[2]Departamento de Geologia, UFRN, Brazil

Submitted to the International Journal of South American Earth Sciences

ABSTRACT

The late Pleistocene Holocene stratigraphic architecture on the northeastern Brazilian continental shelf off the Parnaíba Delta has been explored by high resolution seismic profiles. The seismic surveys reveal the widespread distribution of incised valleys of different size in offshore continuation of the present-day Parnaiba delta. According to the morphology two types can be distinguished: U-shaped channels in the eastern part and V-shaped channels in the western part. The stratigraphic successions were grouped into four seismic units of different seismic facies. The characteristics of the seismic boundaries and internal reflectors were used to distinguish between marine, transitional estuarine and riverine sedimentation. The incised-valleys architectural elements were used to make a link between the sedimentation processes and variations in base level from late Pleistocene channel avulsion and channel infill in the lowermost course of the paleo-Parnaíba River to marine sediments of the present-day inner shelf. The change of the depositional environments in relation to deglacial sea-level rise is compared to incised valley infills of the Mekong River and Red River systems in southeast Asia.

6.1. INTRODUCTION

Incised valleys are common features that mark the variations in sea level, which can be recognized on many continental shelves around the world (e.g. Dalrymple and Zaitlin, 1994; Gupta, 1995; Smith and Read, 2000; Hori *et al.*, 2002; Hou *et al.*, 2003).

These features are commonly formed at times of shelf exposure during sea level lowstand (regression) and their lower surface represents the subaerial uncorformity due to the extension of the drainage system (Nordfjord *et al.*, 2005). The morphological depression produced by the river may be completely, or partially, filled containing deposits of the following transgression and highstand (Zaitlin *et al.*, 1994). Valley and valley-infill represent the stratigraphic record of maximum fall of base-level and early to transgressive phase during sea level rise. This record indicates the changes in the depositional system and may contain internal structures that represent deposits of riverine, estuarine or open marine settings (Vail, 1987; Van Wagoner *et al.*, 1988; Allen and Posamentier, 1993; Dalrymple *et al.*, 1992; Foyle and Oertel, 1997; Nordfjord, 2006). Dimensions of the incised valleys can range from tens to thousands of meters wide and one to tens of meters deep and their sedimentary evolution depends primarily on the sediment supply, hydrodynamic forcing at the site and sea level changes (Dalrymple *et al.*, 1992; Harris and Collins, 1985; Gupta *et al.*, 2012; Harris *et al.*, 2002).

Incised-valley infills of the Açu River on the shelf of Rio Grande do Norte state in NE Brazil were described by Schwarzer *et al.* (2006) and Gomes & Vital (2010).

The aim of the present study is to describe the architecture of incised valleys which were found on the continental shelf offshore Parnaíba River Delta (PRD). The analysis is based on the processing, evaluation and interpretation of high-resolution shallow-seismic profiles acquired offshore PRD. Through this data it was possible to map the occurrences of the incised valleys, characterization of their filling pattern, the depositional environment (i.e. riverine, estuarine or marine) and its correlation to sea level.

This study focused on high resolution shallow seismic to define seismic facies and seismic boundaries (through the description of their form, continuity, amplitude and frequency) to interconnect seismic stratigraphy to system tracts and sea level variations.

6.2. GEOLOGICAL SETTINGS

The PRD is an asymmetric wave dominated delta (Wright *et al.*, 1973; Orton and Reading, 1993; Reading and Collinson, 1996; Bhattacharya and Giosan, 2003; Szczygielski *et al.*, 2014) forming the mouth of the Parnaíba River (PR). The PRD is located at the NE Brazilian coast at the border of the states of Piauí and Maranhão approximately 1,100km east of the Amazon River and around 1,200km northwest of the

São Francisco River Delta (Figure 1). The PR is the largest river system of NE Brazil between those two rivers in terms of river discharge and dimension of the drainage basin.

The continental shelf offshore PRD is approximately 58km wide and the shelf break occurs at 40 m water depth (Aquino da Silva *et al.*, 2015). It is gently sloped (0.04°), shallow (average depth of 22m) and narrow that is a common characteristic of NE Brazilian shelves (Gomes and Vital, 2010; Vital *et al.*, 2008; Vital, 2014).

PR flows mostly over sedimentary rocks from Parnaíba Basin and enters the Barreirinhas Basin in its lowermost section and delta.

The Parnaíba Basin covers an area of approximately 400.000 km2 and is composed mainly of Paleozoic sedimentary rocks (Goes and Feijó, 1994). The tectonic framework of Parnaíba Basin is formed by listric normal faults of WNW-ESE and NW-SE directions, which define a distensive system cut by younger NE-SW strike-slip faults.

Barreirinhas basin is a coastal basin that has a total area of approximately 40.000km2 of the coastal and continental shelf portion of Maranhão and Piauí States. On the surface mostly Quaternary sedimentary rocks crop out that were deposited on top of a rift and passive margin system. The onshore part of Barreirinhas basin shares the tectonic framework with the Parnaíba Basin (Feijó, 1994). Its offshore part is linked to the Pará-Maranhão Basin and characterized by NW-SE normal faults. The tectonic influence on the landscape can be noticed by the course of PR. The river has long straight sections in N to NE direction and an “elbow-like” turning to ENE near the river mouth (Fig.1), which is a typical feature of tectonically controlled river courses (Rachna, 2012; Kirby and Whipple, 2012; Ramasamy *et al.*, 2011). Almeida Filho *et al.* (2009) also recognized the differences in the drainage pattern east and west of Pirapemas lineament formed by small rivers.

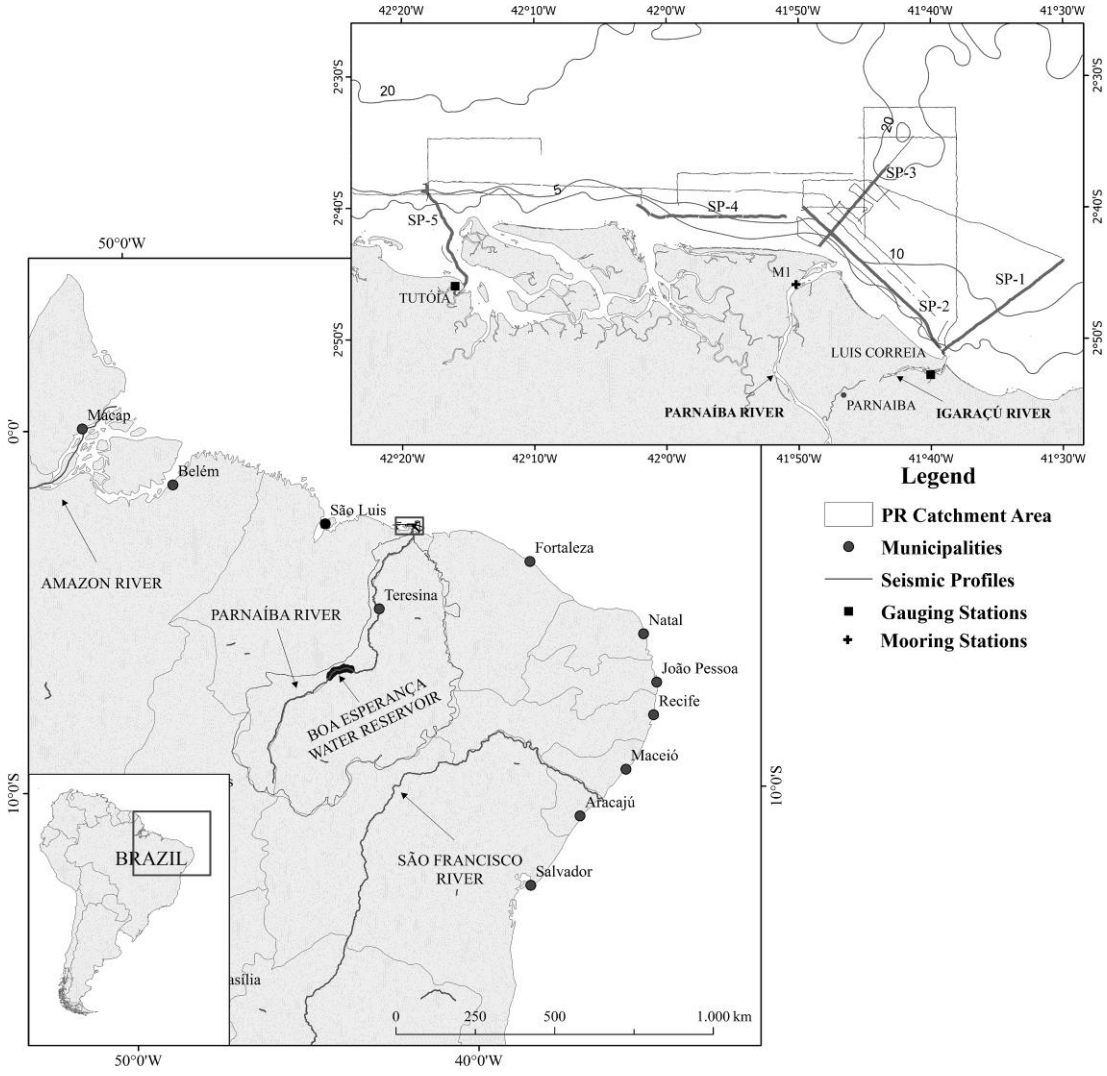

Figure 1 - Location map of PRD and its continental shelf .

6.3. METHODS

This study is based on high resolution offshore reflection seismic profiles acquired using a sub-bottom profiler SES 2000 Standard from INNOMAR. This equipment uses dual frequency chirp technology recording both low and high frequency (LF and HF, respectively) signals. LF signal ranges from 4-15 kHz, HF signal is set as 100 kHz and both were acquired using a ping rate of 8 Hz. During the survey, done in March of 2009 and January of 2010, 580 km of seismic lines were collected (Figure 1). A dynamic motion sensor (DMS) was used to compensate pitch and roll originated by wave interference. The DMS was installed immediately aside the SES 2000 Standard transducer as well as the GPS antenna, in order to minimize post-acquisition positioning corrections.

Seismic lines were surveyed along the entire area offshore PRD (Figure 1) to acquire substantial data about the sub-bottom features. Processing of the seismic lines was restricted to the use of bandpass filters and time-varying gain to minimize the spherical divergence effects. For depth calculation the sound velocity for average sea water (1500 m/s) was used, given the simplicity of the depth conversion which was successfully applied in other areas (Schwarzer *et al.*, 2000; Schwarzer *et al.*, 2006).

The interpretation of the seismic lines focused on the identification of seismic facies (SF), which were defined based on the architecture, continuity, amplitude and frequency of their seismic reflectors. The depositional environment of each SF was interpreted on the basis of the architecture of the seismic reflectors and stratigraphic superposition (Catuneanu *et al.*, 2009; Scott *et al.*, 2004; Tang *et al.*, 2010).

The correlation between system tract and sea level (Figure 2) was made as proposed by Catuneanu *et al.* (2010). Moreover, the architecture of the seismic reflectors was used to associate the SF and seismic boundaries (SB) to a correlated system tract.

The positions of the incised-valleys were plotted on the map in Figure 3, wherever they occur, for visualization of their spatial distribution. This procedure provided a better overview of the position of the incised-valleys cross section and helped on the identification of the type of fluvial system that has formed them.

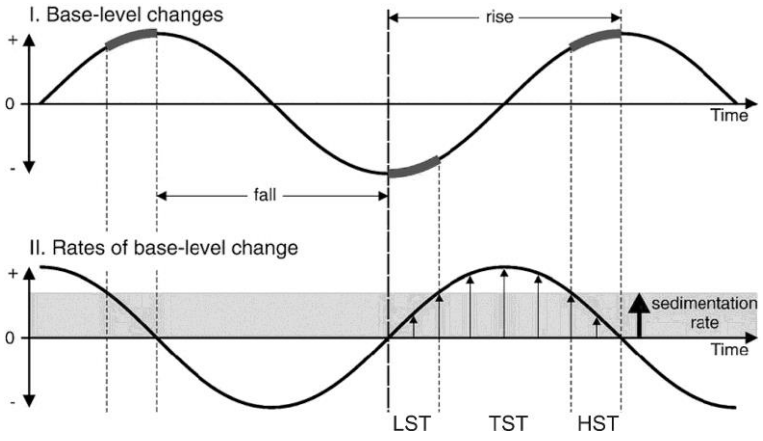

Figure 2 - - Definition of the system tracts as a function of the variations in base level (here in considered as synonymous of sea level variation). Figure modified from Catuneanu *et al.* (2009).

6.4. RESULTS

Several incised-valleys were identified on the seismic profiles recorded on the continental shelf offshore PRD. On the seismic profiles, locations of the identified incised-valleys are highlighted to provide a regional visualization that facilitated the interpretation of the depositional conditions under which they were formed (Figure 3).

Analyzing the channel's internal structures and limiting surfaces, four seismic facies and four seismic boundaries were identified.

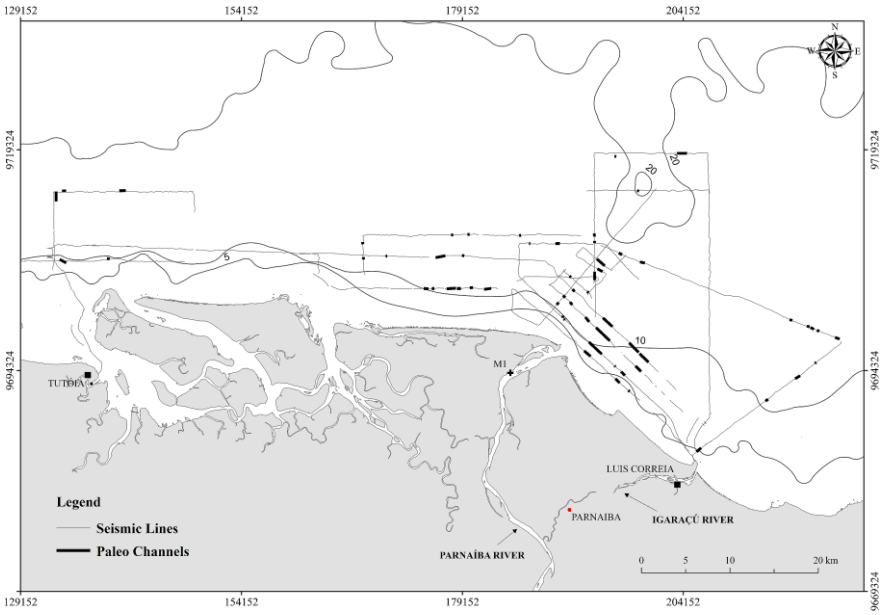

Figure 3 - Map showing the location of the identified incised-valleys along the seismic lines.

The profiles SP-1 to SP-4 were surveyed in the open shelf in front of PRD while the profile SP-5 is located in the western tidal channel (Figure 1). The seismic profiles SP-1 to SP-4 depict a high amplitude reflector of regional occurrence (R) that shows good lateral continuity indicating parallel horizontal to sub-horizontal stratification (Figures 4 and 5).

The R horizon is not distinguishable in SP-5 that depicts V-shape channels, bar and point bar migration as major sub-bottom features, which are characteristics inherent to, both, fluvial and tidal channels.

Delta front deposits were recognized on seismic profiles SP-3 and SP-4, in which shallow gas effect is observed preventing the clinoform reflectors of being tracked toward the delta (Figures 4 and 5).

A reflector of high amplitude, moderate lateral continuity that outlines an irregular surface was the deepest reflector found in the surveyed area and is related to an old landscape (OL) which probably corresponds to the late Pleistocene sea-level lowstand.

In all seismic profiles, two types of incised-valleys were recognized and classified as V- and U-like channels. Considering their morphology and the seismic stratigraphy of the reflectors, lateral channel migration and vertical stacking are the two types of filling patterns that are distinguished in the incised-valleys.

The incised-valleys were identified in all seismic lines few kilometers from the coastline and extending until 25km offshore and 20 m water depth (Figure 3). When incision was completed the most prominent U-shaped channel was 1.129m wide and ~10m deep which are approximately the dimensions of the PR at its mouth nowadays. Other incised-valleys of similar shape were found in different positions offshore and east of the PR mouth (Figure 4). Incised-valleys are widespread on the investigated area; however, U-shaped channels occur only on the east and close to the PR whereas the V-shaped channels occur predominantly on the west and farer from it. West of PR mouth the V-shaped incised-valleys are narrow (up to 900m) and deep (maximum depth of 19m). The slope range of the terrain influences the type of channel developed, hence, it can be estimated by the channel's cross section. According to the classification proposed by Rosgen (1994), the geomorphic configuration of the channels found offshore PRD refer to a slope of the terrain smaller than 4%.

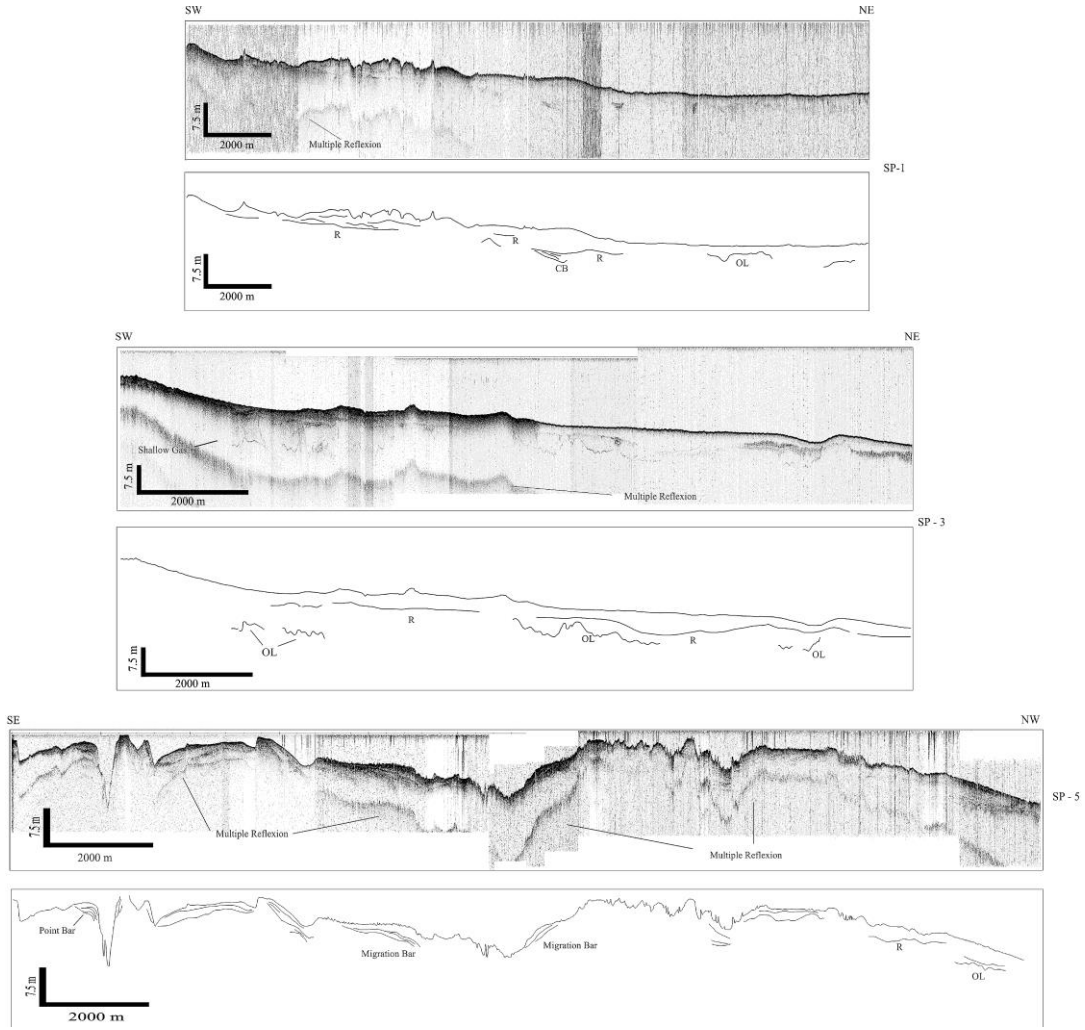

Figure4 - Shore-perpendicular seismic profiles (SP-1, SP-3, SP-5; location in Fig.1) revealing the regional seismic reflectors. OL - Old Landscape; R - Regional Reflector and CB - Channel Boundary.

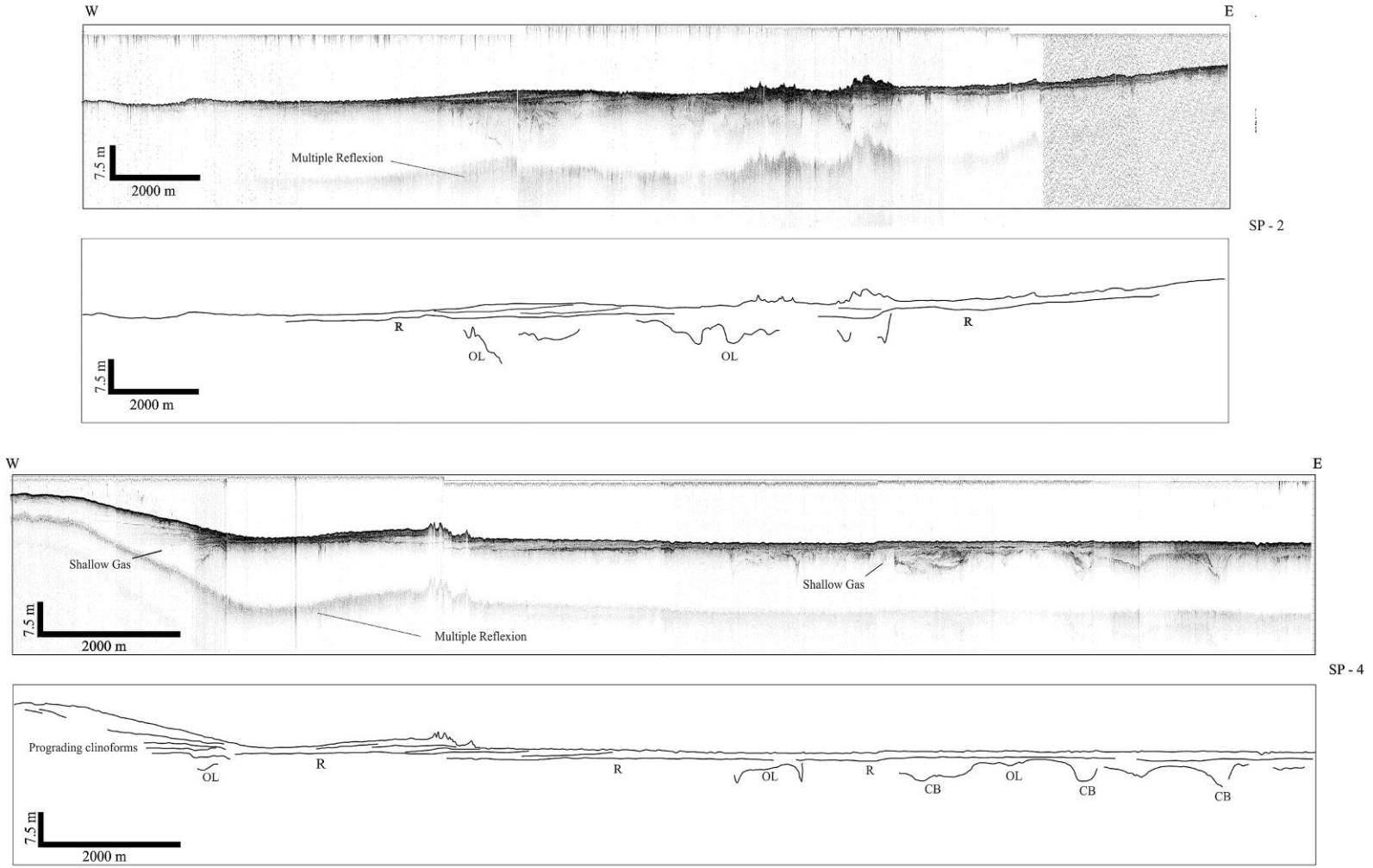

Figure5 - Shore parallel seismic profiles east (SP-2) and west (SP-4) of PR mouth (location in Fig. 1) revealing the regional seismic reflectors. OL - Old Landscape; R - Regional Reflector and CB - Channel Bounda

6.4.1. Seismic Units

Four SU were distinguished offshore PRD based on their seismic facies: character of the bounding surface, stratigraphic superposition and geometry of seismic reflectors and were named SU1 to SU4 from bottom to top (Figure 6).

SU1 is stratigraphically underneath the incised-valleys and it is represented by acoustically transparent and chaotic reflectors (Figure 6). It is only distinguishable where the incised-valleys occur. The seismic facies is on the limit of detection of the SES 2000, due to its operating frequency and power.

SU2 is composed by parallel to sub-parallel high amplitude continuous reflectors and by inclined reflectors with downlap termination that are intercalated by chaotic reflectors (Figure 4). The inclined reflectors converge toward the deepest part of the channel. The variation of the deeper parts of the incised-valley indicates changes in channel morphology because of point-bar development and evolution and accretion. Channel levees, that represent the maximum flooding surface on a river channel, were eroded prior to the deposition of SU3. Nevertheless, sigmoidal features were found in SU2. The bottom limit of SU2 is the reflector that marks the shape of the incised-valleys and a truncation surface that corresponds to the bottom of SU3. Two different evolutional stages of the channel burial process can be recognized in SU2 which are defined as lateral point-bar progradation and infill as well as subsequent vertical aggradation in the remaining channel (Figure 6).

The reflectors of SU3 are characterized as low amplitude and chaotic (or acoustically transparent in some locations). SU3 is bounded at the bottom by the truncation surface that marks the contact with SU2 and at the top by a horizontal reflector of high amplitude and good lateral continuity. The thickness of SU3 decreases in onshore direction until it pinches out completely.

SU4 is observed in all lines and it is characterized by low amplitude chaotic reflectors that are limited on top by the present sea floor (Figure 6). Occasionally horizontal to sub-horizontal high amplitude layered reflectors were found. SU4 is the youngest SU of the area, based on its stratigraphic position.

6.4.2. Seismic Boundaries

The SU are bounded by seismic boundaries (SB) identified as: present sea floor (PSF), transgressive surface (T), channel boundary (CB) and regional horizon (R) (Figure 6).

PSF is the uppermost SB which represents the interface between the youngest deposited sediment and the water column. It is the top limiting surface of SU4.

The R horizon is the bottom limit of SU4 and top limit of SU3, whenever it occurs. This surface is flat and regionally observable landward of 15m water depth.

The T horizon is the top limiting surface of the SU2, and SU1 in some locations. This horizon truncates the top layers of these two lower SU and can also be observed throughout the entire area. This SB is flat and recognizable due to the truncation of the reflectors that define the channel migration observed on SU2 below.

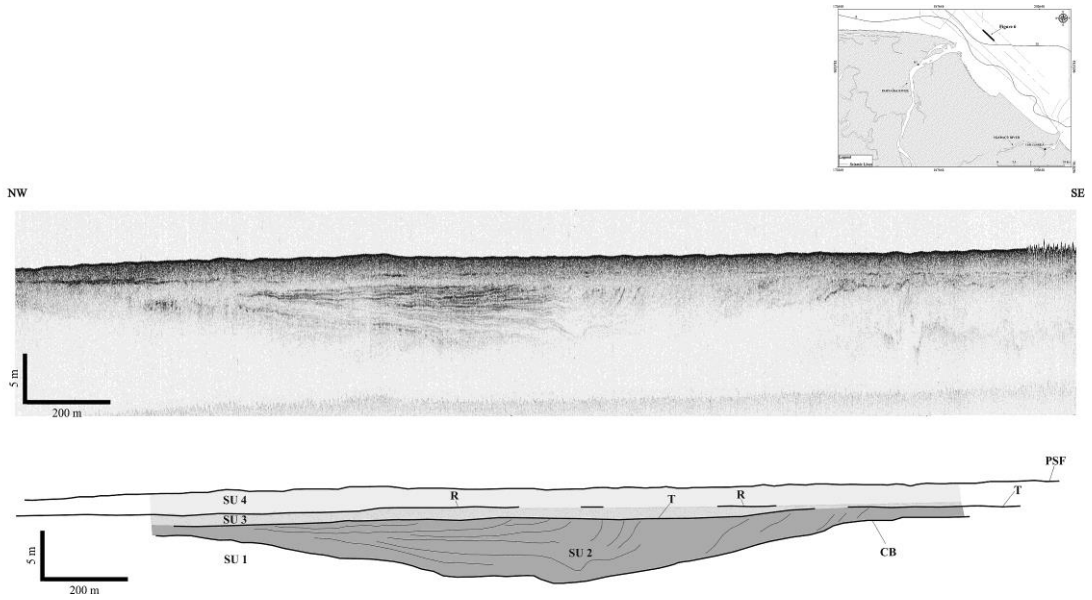

Figure 4 - Seismic profile showing a incised-valley where the four SF and the three SB can be individualized.

CB is the bottom boundary of the SU2 CB is defined by the lower boundary of SU2 reflectors, however, in this case marking the base of their seismic facies downlaps. The outline of the incised-valley is depicted by CB, which occurs in both coastal perpendicular and coastal parallel sections, and both U and V shaped channels indicating channel bending.

6.4.3. Incised-valleys Morphology and Fill Pattern

Two types of channels were identified V and U shaped channels (Figures 7 and 8). V-shaped channels occur on the western part of PRD while U-shaped channels occur on the eastern part (see Figure 3 for location). Stratification observed on the V-shaped paleo channels show vertical accretion (Abreu *et al*., 2003) as the infill process occurred during continuous drowning and rising base level of the valley (Figure 7).

U-shaped channels are wider than the V-shaped, though, shallower. The internal structures of these channels show two different patterns of channel fill: vertical accretion and lateral accretion by progradation of point-bar foresets. Vertical accretion is the first fill pattern observed and positioned concordantly underneath the section where lateral point-bar accretion by sigmoidal foresets is characterized as the major fill pattern. (Figure 7)

In both types of channels sediments deposited on horizontal to sub-horizontal layers marking the R horizon are considered as being marine from their stratification pattern (Figures. 7 and 8).

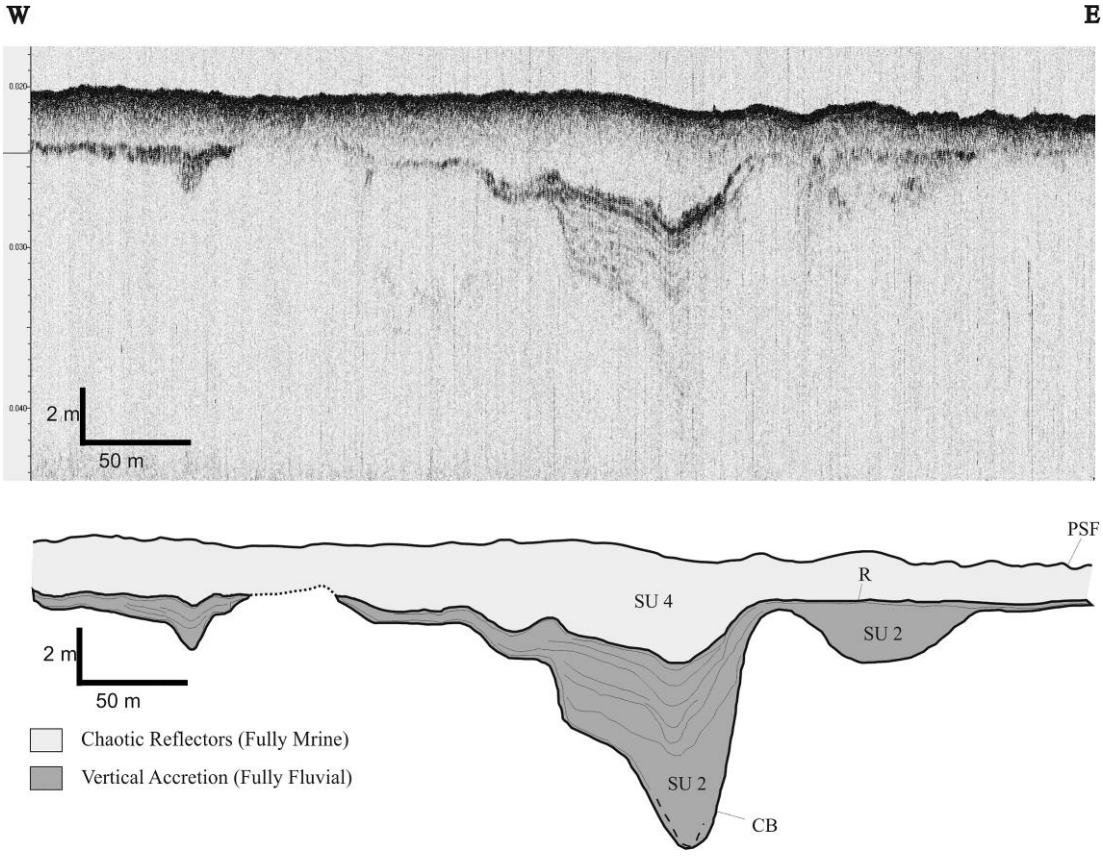

Figure 5 - Seismic profile revealing a V-shaped channel on the eastern side of PRD with internal structures showing vertical accretion, covered by chaotic reflectors deposited in fully marine environment. Cross-reference to Figure3.

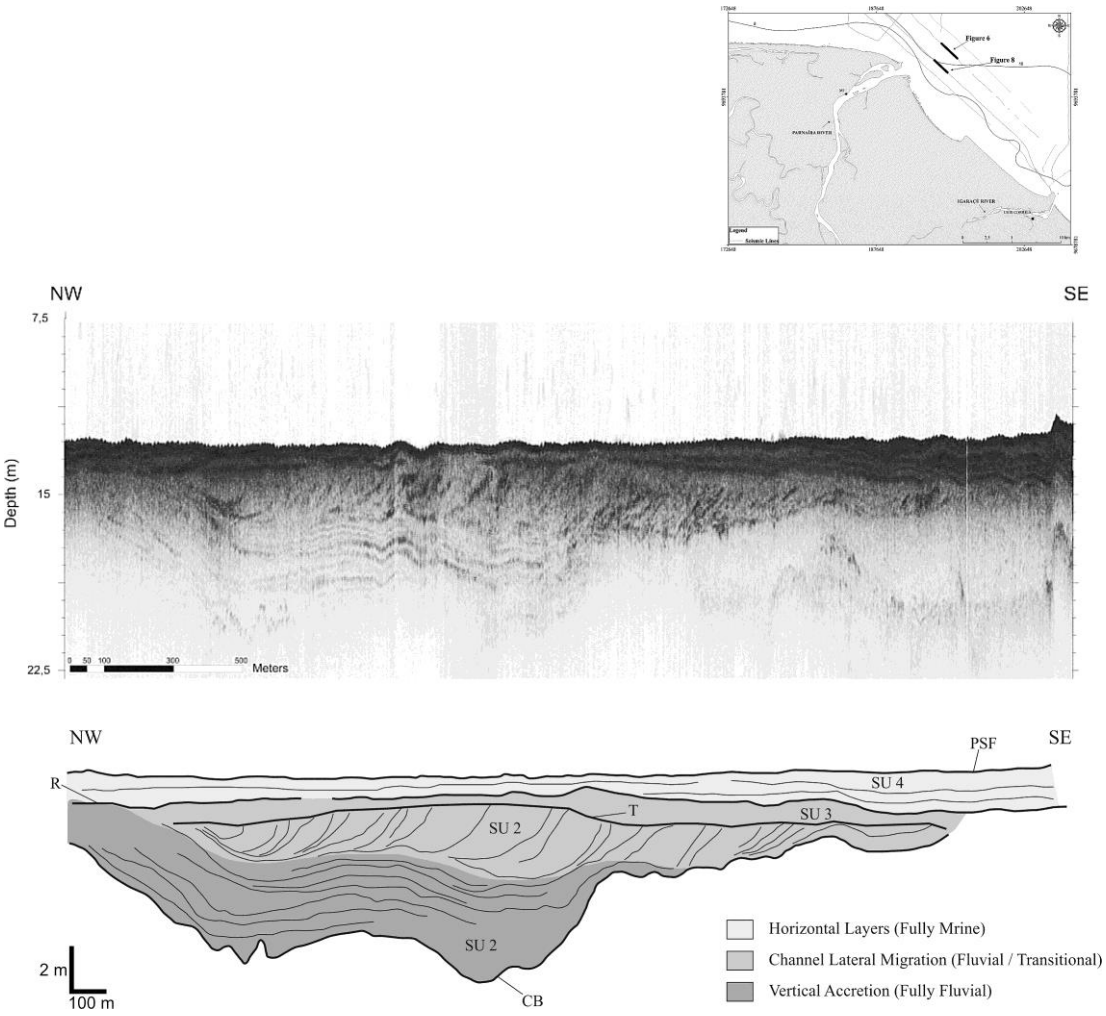

Figure8 – Seismic profile revealing a U-shaped channel with internal structures showing vertical accretion on the base, lateral point-bar migration concordantly above, chaotic reflectors and horizontal layers. Cross reference to Fig.3

6.5. DISCUSSIONS

Schwarzer *et al.* (2006) and Vital *et al.* (2010) found incised-valleys in the continental shelf of Rio Grande do Norte (NE Brazil). Schwarzer *et al.* (2006) identified an incised-valley in seismic profiles in which the sub-surface structures depicted similar shape of those found in the incised-valleys offshore PRD. Vital *et al.* (2010) recognized a channel like feature (using mid-resolution satellite images and bathymetrical models) that was later defined as an incised-valley in seismic profiles. This incised-valley was interpreted as the path of Apodí-Mossoró River, over the continental shelf, during the last sea level lowstand. Such surface and sub-surface features were also found at the continental shelf offshore PRD using the same methods (satellite images, bathymetric models and seismic data). However, in the region of PRD, more than one incised-valley,

as well as channel type, was identified in seismic profiles. It is likely that the U-shaped channel corresponds to the main distributary of the PR and depicts the river path over the continental shelf during the last sea level lowstand. On the other hand, the V-shaped channels can be interpreted as smaller distributaries that deviate from (or drain into) the PR main distributary during sea level lowstand. The presence of incised-valleys on both east and west sides is an indication that the delta area extended from Tutóia to east of Igaraçú River mouth.

Szczygielski *et al.* (2014) found strong evidences on sediment cores that the tidal channels on the west of PR were active river distributaries approximately 6.0 kyr BP. The occurrence of incised-valleys offshore the tidal channels support this hypothesis.

Moreover, the occurrence and spatial distribution of V-shaped channels and absence of the U-shaped indicates that on that location meandering system predominated. Similarly, offshore Igaraçú River mouth (eastward) V-shaped channels occurred and U-shaped channels were absent. Their spatial distribution suggests meandering channel system as formating mechanism. Therefore, the PR was the delta's main distributary during sea level lowstand.

Wetzel et al. (in prep.) discussed the relation of incised-valleys and their infill with variations in sea level. He also suggests that channel sinuosity is highly dependent of shelf slope and that channel lateral migration is correlated to periods of relative stable sea level. Using the same criteria the incised-valleys offshore PRD, as well as their infill, were correlated to variations of sea level. Indications of three distinct stages of sea level were found: lowstand, transgression (rising in sea level) and "maximum transgression". These sea level stages were obtained by analyzing the architectural elements of the incised-valleys found offshore PRD and the strata on top of them. The system tracts related to these sea level stages are lowstand system tract (LST), transgressive system tract (TST) and highstand system tract (HST) (Catuneanu *et al.*, 2010).

The position and the shape of the cross section of incised-valleys (Figure 4) suggest a genetic connection with the PR. These features developed during the lowering of sea level below -40 m, when the shelf became sub-aerially exposed until the lowstand during the Last Glacial Maximum in the time period 70 to 20 kyr BP. During this time the river continued to incise and to cross the exposed shelf, because of the decrease of base level (Green *et al.*, 2013; Lin et al., 2005; Nordfjord *et al.*, 2005).The CB can be interpreted as the lower boundary surface of LST.

The T horizon was probable made under shallow water condition when wave action eroded the top of the sigmoidal foresets forming the point bar succession, during TST (Catuneanu *et al.*, 2009). Horizontal to sub-horizontal stratifications found on top of "T" depicts a reduction of energy (possibly wave energy) caused by increase in water depth. This allowed the deposition of such low energy deposits.

The fill of the incised-valleys indicates a decrease in river flow competence caused by elevation of base level during TST (Catuneanu *et al.*, 2009), which resulted on vertical aggradation (Figure 7). During this phase, base level rose rapidly not allowing the channel to laterally move and sedimentation was concentrated on the deeper parts of the channel. The formation of point-bars (Figure 7) in the lower reaches of a sinuous river system with several distributary channels can also be related to TST (Catuneanu *et al.*, 2009), however, with slow rise in base level and rapid lateral accretion of point-bars. During LST and TST (until the complete fill of the channel) only riverine sediment was deposited under fluvial conditions (Catuneanu *et al.*, 2009).

R horizon marks the maximum flooding surface (which is the base of SU4) and it is related to HST (Catuneanu *et al.*, 2009). During HST only marine sediment was deposited in horizontal to sub-horizontal layers.

Features such as point bar migration and channel avulsion are common features in meandering fluvial channels (James and Dalrymple, 2010). The presence of these features on the incised-valleys infer relative positions to the shoreline and suggest the lowermost diverging parts of a meandering fluvial system as suitable depositional model to explain their formation (Cserkész-Nagy *et al.*, 2012).

Bui *et al.* (2013) found similar relation between the incised-valley fill and sea level variation at the Mekong Delta. He stated that LST ended with the beginning of deglacial sea-level rise at 19.6 kyr BP in the western South China Sea and that HST began at 8.0 kyr BP after the last phase of accelerated sea-level rise in the early Holocene (cf. Tjallingii *et al.*, 2010). Caldas *et al.* (2006), investigating beach rocks on the NE Brazilian coast, defined the mid-Holocene highstand as period of the maximum deglacial flooding around 5.5 kyr BP. Considering the similarities between the incised-valleys found offshore PRD and those at the Mekong and Red River (Tjallingii *et al.*, 2010; Wetzel *et al.*, in prep.; Wiesner *et al.*, 2012) one can correlate their formation and evolution. The specific situation of the shallow and narrow shelf region suggests that the flooding of the shelf with the aggradational infill of the incised valleys started when sea-level rose above -40 m, approximately 10000 years BP. The transgression ended

with the mid-Holocene sea-level highstand around 5.5 kyr BP. However, the acquisition of more precise chronostratigraphic information at PRD incised-valleys is necessary to confirm this hypothesis.

6.6. CONCLUSIONS

The identification and interpretation of seismic boundaries and architectural elements are valuable information that can be used to correlate the incised-valleys to episodes of sea level variation as well as to identify the ancient channels types.

A fluvial meandering system is likely to be the system that formed the incised-valleys found offshore PRD. This definition was based on the analysis of the seismic facies, architectural elements and the position of their cross sections in relation to the shoreline.

Similar features found at the continental shelf of the Mekong and Red River suggest that marine deltas and estuaries around the world were subjected to similar processes during the late Pleistocene-Holocene period. This occurred because of the large rise in sea level and the change from lowstand to highstand conditions during that period. The infill of incised-valleys is likely to have preserved records of deglacial sea-level rise. Such records are expected to remain restricted to the last ten thousand years since the shelf break off the PRD occurs at 40 m water depth and complete infill may not have occurred under steep continental slope conditions.

A regional SB, herein named as “R”, depicts the maximum flooding surface at PRD continental shelf. It also represents the change from higher to lower-energy hydrodynamic conditions caused by the increase in water depth. Conversely, the CB represents the maximum regression surface. These SB should be traced offshore until 120 m water depth at the upper continental slope corresponding to the eustatic sea-level lowstand during the Last Glacial Maximum 20,000 years ago.

ACKNOWLEDGEMENTS

This work is part of the project “Northern Brazilian river deltas: River impacts versus pristine discharge” which is funded by the Deutsche Forschungsgemeinschaft (STA 401/16-1). The authors would like to thank the captain and crew of the São Francisco III, as well as all team members, for their efforts to support the study, namely, F. Caninde´ Soares, Werner F. Tabosa, Pedro Moreia, Gustavo Rocha, Maria Isabel da Rocha, Helmut Beese, Camila Soares, Agata Szczygielski and Juliana Koenig. The

authors also would like to thank CPRM for kindly providing some of the data used on this research. Special thanks for the GGEMMA lab of the Universidade Federal do Rio Grande do Norte for disposing part of the equipment used on this research.

LITERATURE CITED

Abreu, V., Sullivan, M., Pirmez, C. and Mohrig, D., 2003. Lateral accretion packages (LAPs): an important reservoir element in deep water sinuous channels. *Marine and Petroleum Geology*, 20, pp.631–648.

Allen, G. P. and Posamentier, H.W., 1993. Sequence stratigraphy and facies model of an incised valley fill: the Gironde Estuary, France. *Journal of Sedimentary Petrology*, 63, pp.378–391.

Almeida-filho, R., Rossetti, D. F., Miranda, F. P., Ferreira, F. J., Silva, C., Beisl, C., 2009. Quaternary reactivation of a basement structure in the Barreirinhas Basin , Brazilian Equatorial Margin. *Quaternary Research*, 72(1), pp.103–110. Available at: http://dx.doi.org/10.1016/j.yqres.2009.02.010.

Aquino da Silva, A. G., Stattegger, K., Schwarzer, K., Vital, H. and Heise, B., 2015. The Influence of Climatic Variations on River Delta Hydrodynamics and Morphodynamics in the Parnaíba Delta ,. *Journal of Coastal Researchsearch*, in press.

Bhattacharya, J.P. & Giosan, L., 2003. Wave-influenced deltas : geomorphological implications for facies reconstruction. *Sedimentology*, 50, pp.187–210.

Bui, V. D.; Stattegger, K.; Unverricht, D.; Phach, P. V., and Thanh, N. T., 2013. Late Pleistocene–Holocene seismic stratigraphy of the Southeast Vietnam Shelf. *Global and Planetary Change*, 110, 156-169.

Caldas, L. H. O., Stattegger, K., and Vital, H., 2006. Holocene sea-level history: Evidence from coastal sediments of the northern Rio Grande do Norte coast, NE Brazil. *Marine Geology*, 228(1-4), pp.39–53.

Catuneanu, O., Abreu, V., Bhattacharya, J.P., Blum, M.D., Dalrymple, R.W., Eriksson, P.G., Fielding, C.R., Fisher, W.L., Galloway, W.E., Gibling, M.R., Giles, K.A., Holbrook, J.M., Jordan, R., Kendall, C. G. St. C., Macurda, B., Martinsen, O.J., Miall, A.D., Neal, J.E., Nummedal, D., Pomar, L., Posamentier, H.W., Pratt, B.R., Sarg, J.F., Shanley, K.W., Steel, R.J., Strasser, A., Tucker, M. E. and Winker, C., 2009. Towards the standardization of sequence stratigraphy. *Earth-Science Reviews*, 92, pp.1–33.

Catuneanu, O., Bhattacharya, J. P., Blum, M. D., Dalrymple, R. W., Eriksson, P. G. and Fielding, C.R., 2010. Sequence stratigraphy : common ground after three decades of development. *First Break*, 28(January), pp.21–34.

Cheng, T.; Zhou, D.; Endler, R.; Lin, J., and Harff, J., 2010. Sedimentary Development of the Pearl River Estuary Based on Seismic Stratigraphy. *Journal of Marine Systems*, 82 3–16. DOI:10.1016/j.jmarsys.2010.02.001.

Cserkész-Nagy, Á., Thamó-Bozsó, E., Tóth, T. and Sztanó, O., 2012. Reconstruction of a Pleistocene meandering river in East Hungary by VHR seismic images, and its climatic implications. *Geomorphology*, 153-154, pp.205–218.

Dalrymple, R.W., Zaitlin, B.A., Boyd, R., 1992. Estuarine facies models: conceptual basis and stratigraphic implications. *Journal of Sedimentary Petrololgy*, 62, 1130–1146.

Dalrymple, R. W., Zaitlin, B.A., 1994. High-resolution sequence stratigraphy of a complex, incised valley succession, the Cobequid Bay–Salmon River estuary, Bay of Fundy, Canada. *Sedimentology*, 41, pp.1069–1091.

Feijó, F.J., 1994. A Bacia de Barreirinhas. *Boletim de Geociências de PETROBRAS*, 8(1), pp.103–109.

Fielding, C. R., 1993. A review of recent research in fluvial sedimentology. *Sedimentary Geology*, 85, 1–4, 3-14.

Foyle, A. M. and Oertel, G.F., 1997. Transgressive systems tract development and incised-valley fills within a Quaternary estuary-shelf system: Virginia inner shelf, USA. *Marine Geology*, 137, pp.227–249.

Galloway, W.E., 1975. Process framework for describing the morphological and stratigraphic evolution of deltaic depositional systems. In: Broussard, M.E. (Ed.), Deltas. *Houston Geological Society*, Houston, Texas, pp. 87–98.

Góes, A. M. and Feijó, F.J., 1994. Bacia do Parnaíba. *Boletim de Geociências da PETROBRAS*, 8(1), pp.57–67.

Gomes, M.P. & Vital, H., 2010. Revisão da compartimentação geomorfológica da Plataforma Continental Norte do Rio Grande do Norte , Brasil. , 40(3), pp.321–329.

Green, A. N., Dladia, N. and Garlick, G.L., 2013. Spatial and temporal variations in incised valley systems from the Durban continental shelf, KwaZulu-Natal, South Africa. *Marine Geology*, 335, pp.148–161.

Gupta, A., 1995. Magnitude, frequency and special factors affecting channel form and processes in the seasonal tropics. In P. Costa, J. E., Miller, A. J., Potter, K. W. and Wilcock, ed. *Natural and Anthropogenic Influences in Fluvial Geomorphology*. American Geophysical Union, Monograph 89, pp. 125–136.

Gupta, H., Kao, S-J. and Dai, M., 2012. The role of mega dams in reducing sediment fluxes: A case study of large Asian rivers. *Journal of Hydrology*, 464-465, pp.447–457.

Harris, P. T. and Collins, M.B., 1985. Bedform distributions and sediment transport paths in the Bristol Channel and Severn Estuary, U.K. *Marine Geology*, 62, pp.153–166.

Harris, P. T., Heap, A. D., Bryce, S. M., Porter-Smith, R., Ryan, D. A. and Heggie, D.T., 2002. Classification of Australian clastic coastal depositional environments based upon a quantative analysis ofwave, tidal, and river power. *Journal of Sedimentary Research*, 72, pp.858–870.

Hori, K., Saito, Y., Zhao, Q. and Wang, P., 2002. Architecture and evolution of the tide-dominated Changjiang (Yangtze) River delta, China. *Sedimentary Geology*, 146, pp.249–264.

James, N. P. and Dalrymple, R.W., 2010. *Facies Models 4*, Newfoundland: Memorial University of Newfoundland Press.

Kirby, E. and Whipple, K.X., 2012a. Expression of active tectonics in erosional landscapes. *Journal of Structural Geology*, 44, pp.54–75.

Kirby, E. and Whipple, K.X., 2012b. Expression of active tectonics in erosional landscapes. *Journal of Structural Geology*, 44, pp.54–75.

Li, C., Wang, P., Sun, H., Zhang, J., Fan, D., Deng, B., 2002. Late Quaternary incised-valley fill of the Yangtze delta (China): its stratigraphic framework and evolution. *Sedimentary Geology*, 152, 133–158.

Lin, C-M., Zhuo H-C. and Gao, S., 2005. Sedimentary facies and evolution in the Qiantang River incised valley, eastern China. *Marine Geology*, 219(4), pp.235–259.

Nordfjord, S., Goff, J. A., Austin Jr., J. A. and Gulick, S.P.S., 2006. Seismic facies of incised-valley fills , New Jersey continental shelf : implications for erosion and preservation processes acting during latest pleistocene – holocene transgression. *Journal of Sedimentary Research*, 76, pp.1284–1303.

Nordfjord, S., Goff, J. A., Austin, J. A. and Sommerfield, C.K., 2005. Seismic geomorphology of buried channel systems on the New Jersey outer shelf : assessing past environmental conditions. , 214, pp.339–364.

Orton, G. J. and Reading, H.G., 1993. Variability of deltaic processes in terms of sediment supply, with particular emphasis on grain size. *Sedimentology*, 40, pp.475–512.

Rachna, R., 2012. Late Quaternary tectonic history of the Vatrak River basin, western India: morphometric and morphostructural approach. *Quaternary International*, 279-280, p.392–.

Ramasamy, S. M., Kamanan, C. J., Selvakumar, R. and Saravanevel, J., 2011. Remote sensing revealed drainage anomalies and related tectonics of South India. *Tectonophysics*, 501(1-4), pp.41–51.

Reading, H. G. and Collinson, J.D., 1996. Clastic Coasts. In H. G. Reading, ed. *Sedimentary Environments: Processes, Facies and Stratigraphy*. Oxford: Blackwell Science, pp. 154–231.

Rosgen, D.L., 1994. A classification of natural rivers. *Catena*, 22, pp.169–199.

Rosseti, D. F., Góes, A. M. and Truckenbrodt, W., 2001. *O Cretáceo da Bacia de São Luís-Grajaú*, Belém: Museu Emílio Goeldi.

Schwarzer, K., Stattegger, K., Vital, H. and Becker, M., 2006. Holocene Coastal Evolution of the Rio Açu Area (Rio Grande do Norte , Brazil). In *Proceedings, 8th International Coastal Symposium*. Itajaí, SC, Brazil: Journal of Coastal Research, Special Issue No. 39, pp. 140–144.

Schwarzer, K.; Diesing, M. And Trieschmann, B., 2000. Nearshore facies of the southern shore of the Baltic Ice Lake, example from Tromper Wiek (Rügen Island). *Baltica*, 39, pp.140–144.

Scott, G. H, King, P. R. and Crundwell, M.P., 2004. Recognition and Interpretation of Depositional Units in a Late Neogene Progradational Shelf Margin Complex, Taranaki Basin, New Zealand: Foraminiferal Data Compared with Seismic Facies and Wireline Logs. *Sedimentary Geology*, 164(1-2), pp.55–74.

Smith, L. B. Jr. and Read, J.F., 2000. Rapid onset of late Paleozoic glaciation on Gondwana: Evidence from Upper Mississippian strata of the Midcontinent, United States. *Geology*, 28(3), pp.279–282.

Tjallingii, R., Stattegger, K., Wetzel, A., Van Phach, P., 2010. Infilling and flooding of the Mekong River incised valley during deglacial sea-level rise. *Quaternaru Science Reviews*, 29(11-12), pp.1432–1444.

Vail, P.R., 1987. Seismic stratigraphy interpretation using sequence stratigraphy, Part I: Seismic stratigraphy interpretation procedure. In A. W. Bally, ed. *Atlas of Seismic Stratigraphy*. Atlas of Seismic Stratigraphy: American Association of Petroleum Geologists, Studies in Geology 27, pp. 1–10.

Vital, H., Furtado, S. F. L. and Gomes, M.P., 2010. Response of Apodi-Mossoro Estuary-Incised Valley System (Ne Brazil) To Sea-Level Fluctuations. *Brazilian Journal of Oceanography*, 58, pp.13–24.

Vital, H., Stattegger, K., A, aro, V. E., Schwarzer, K., Frazão, E. P. and Tabosa, W.F., 2008. Inner continental shelf off northern Rio Grande do Norte, NE Brazil. In R. Hampson, G. and Dalrymple, ed. *Recent advances in shoreline –shelf Stratigraphy*. Tulsa, Okla.: SEPM Special Issue n. 90.

Van Wagoner, J. C., Posamentier, H. W., Mitchum, R. M., Vail, P. R., Sarg, J. F., Loutit, T. S. and Hardenbol, K., 1988. An overview of the fundamentals of sequence stratigraphy and key definitions. In J. C. Wilgus, C. K., Hastings, B. S., Kendall, C. G. St. C., Posamentier, H. W., Ross, C. A. and Van Wagoner, ed. *Sea-Level Changes: An Integrated Approach*. SEPM, Special Publication 42, pp. 39–46.

Wetzel, A., Szczygielski, A., Unverricht, D., Tjallingii, R. and Stattegger, K., 2015. *Environmental significance of bent incised-valley fill-deposits*, Basel, Switzerland.

Wiesner, M.G., Stattegger, K., Pohlmann, T., Chen, F., Heddaeus, A., Heyckendorff, K., Jechlitschek, H., Lahajnar, N., Liskow, I., Li, X., Liu, Z., Lorenc, S., Metzke, M., Müller, M., Peleo-Alampay, A., Schönke, M., Schwarzer, K., Szczygielski, A., Steen, Y., 2012. *Cruise Report RV Sonne 220 – Land-Ocean-Atmosphere Interactions in the Gulf of Tonkin*, Institut für Geowissenschaften Universität Kiel, 101 pp.

Wright, L. D., Coleman, J. M. and Thom, B.G., 1973. Processes of channel development in a high-tide-range environment: Cambrige Gulf-Ord River delta, western Australia. *Journal of Geology*, 81, pp.15–41.

Zaitlin B. A., Dalrymple, R. W. and Boyd, R., 1994. The stratigraphic organization of incised valley systems associated with relative sea-level change. In B. A. Dalrymple, R. W., Boyd, R. and Zaitlin, ed. *Incised-Valley Systems: Origin and Sedimentary Sequences*. SEPM, Specail Publication 51, pp. 45–60.

Chapter 7 – GENERAL DISCUSSIONS

The PRD is located on a transition zone in terms of continental shelf morphology, climatic and oceanographic conditions. The continental shelf on this area is shallow and narrow as most of the NE continental shelf (Gomes and Vital, 2010). However, this characteristic gradually changes with the proximity to the Amazon River where the continental shelf has its maximum width. Tidal amplitude also increases approximately 3 m in 295 km, between the cities of Luiz Correia and Itaquí. Hence, the tidal regime switches from meso-tidal to macro-tidal although the semi-diurnal character remains. This can be attributed to the gigantic discharge of the Amazon River that influences the variations in tidal amplitude. Moreover, wave influence on coastal morphodynamics decreases with the increase of the tidal influence and coastal morphology starts to show typical features of such tidal dominated environment. Westward from Itaquí coastline morphology changes from long strait beaches with occasional presence of barrier islands giving place to a coast dominated by islands elongated perpendicular to the coast (parallel to tidal current direction). The increase in tidal amplitude caused the change on coastal morphology because of changes in the morphodynamic conditions.

Rainfall distribution along the drainage basin influences the amount of sediment that is transported by rivers, regulating the amount of water and sediment that "feeds" the river, hence, determining its competence and capacity. Nevertheless, the geology of the drainage basin has to be considered.

According to the classification proposed by Köppen the entire drainage basin of PR is classified as Tropical Aw with the dry season occurring during winter. Seasonality of rainfall on the study area depicts two distinct periods which were defined as wet and dry. The wet period last from January to May while the dry period last from June to December. River discharge is directly affected by the seasonal oscillations of rainfall, therefore, the period of high and low river discharges follow the rainfall seasonality. Although, a river dam on PR headwaters (Boa Esperança water reservoir) may regulate the river discharge during the dry period or long periods of drought. ENSO is the climatic factor that controls the rainfall and its seasonality on that area (Davey *et al.*, 2002; Davey *et al.*, in press; Hastenrath, 2006; Pasquini *et al.*, 2012), where a decadal analysis of rainfall revealed a recurrence period of approximately 7 years (plus or minus 2 years) for droughts on the area.

Rainfall influences the amount of sediment transported to river (Pasquini *et al.*, 2012), hence, seasonality in SSC in PR was noticed as well. However, seasonality of SSC do not perfectly match the rainfall seasonality, although, is highly influenced by it. Therefore, the occurrence and strength of ENSO indirectly influences the SSC (Pasquini *et al.*, 2012), sediment yield and short term (decadal) coastline change.

Average SSC of PR (50 mg/l) is higher than of São Francisco (34 mg/l) and smaller than Paraná (180 mg/l) and Amazon (190 mg/l) rivers; however, they are longer and have larger drainage basins than PR. Nevertheless, approximately 1.44 x 10^6 tons of sediment is yielded annually by PR and this high sediment yield is attributed to the geology of PR's drainage basin (Phanerozoic sedimentary rocks) and the land use close to the river margins (plantations and livestock activities). The discharged sediment is transported westward by longshore currents, northward by ebb phase tidal currents and southeastward (toward the coast) flood phase tidal currents. A spit was developed westward from PR mouth as result of alongshore sediment transport and wave climate, which migrates at 291 m/year in down drift longshore current direction between 1981 and 2009. The importance of waves on coastline development on this region is evidenced by the shape of PRD. Regarding only its shape, this delta can be classified as asymmetric and wave dominated (Bhattacharya and Walker, 1992; Galloway, 1975; Orton and Reading, 1993; Reading and Collinson, 1996; Wright and Coleman, 1973); however, the degree of asymmetry was not yet defined. It is likely that river runoff contributes to this asymmetry by forming a hydrodynamic groin (Bhattacharya and Walker, 1992). This assumption is supported by the predominance of NE and SE currents at 4 km directly offshore PR mouth (data from on mooring station) reaching approximately 0.5 m/s and demonstrating river influence on that location. This hydrodynamic groin acts as a barrier reducing the bypass of sediment that is transported by the longshore current (Bhattacharya and Giosan, 2003). The prevention of alongshore sediment transport by the river, as well as by the tidal channels, is the main cause of coastline retreat observed in some sectors of further west of PR mouth shoreline.

West of PR there is an estuarine-lagoonal area composed by several tidal channels (Luettich Jr. *et al.*, 2002; Castelao and Moller Jr., 2006). The fresh water input to this area is made by an artificial connection to PR, made on 1960's, and by ephemeral rivers that drain into this area during wet period. The geomorpholgy of the tidal channels suggests that they were old distributaries of PR that were abandoned

during a process of channel switching. Szczygielski *et al.* (2014) found evidences, on sediment cores of collected in the tidal channels, that such connection existed approximately 6.0 kyr. BP. In this case, tectonics can be pointed out as a possible reason cause of the channel switching process on this area. Tectonic control on PR flow is evident and can be seen as the long strait sections of the river and "elbow" like turns, whose directions coincide with the major tectonic framework of Parnaíba and Barreirinhas sedimentary basis (Almeida Filho *et al.,* 2009; Feijó, 1994; Goes and Feijó, 1994; Rosseti *et al.,* 2001).

On the inner continental shelf directly offshore PR mouth was found an incised-valley which was probable formed during low sea level. Morphological characteristics such as channel width and depth are similar to those found on some section of PR nowadays, supporting their genetic correlation (Nordfjord *et al.,* 2005; Green, 2009; Green *et al.,* 2013; Gutierrez *et al.,* 2003; Schwarzer *et al.,* 2006). This feature cannot be seen on depths shallower than -20 m (approximately 11 km from modern shoreline). The presence of incised-valleys offshore the entire delta area indicates shelf exposure during low sea level together with sufficient riverine strength (Estournès *et al.,* 2012; Schwarzer *et al.,* 2006). Moreover, the incised-valleys can be interpreted as paleo-climatic indicator periods of moderate to high precipitation along the PR drainage basin. The shape of the cross section of the paleo-channels (U-shaped or V-shaped) suggests different conditions of river discharge and sediment load (bed and suspended load) for their formation. The proximity and morphology of the U-shaped paleo-channels to the PR indicate that they are likely to be genetically correlated. Moreover, considering the position of all paleo-channels cross sections, in relation to the shoreline, and their architectural elements it is reasonable to assume that they were formed by a meandering fluvial system (James and Dalrymple, 2010).

The filling patterns and SU's found on the paleo-channels indicate at least three stages of sea level: lowstand, transgression and "maximum transgression". The sea level stages related to these sea levels are LST, TST and HST (Catuneanu *et al.,* 2010). The SB CB represents the LST and corresponds to the river incision on the exposed shelf (Nordfjord *et al.,* 2005; Green, 2009; Green *et al.,* 2013; Gutierrez *et al.,* 2003; Schwarzer *et al.,* 2006). TST is characterized by the gradual increase in sea level that reduced the river strength due to increase of tidal influence on the river mouth. This stage is characterized, on seismic data, by accretion and point bar migrating deposits (Tjallingii *et al.,* 2010). These features were result of adjustments of channel

morphology due to reduction in hydrodynamic conditions caused by increase of base level (Bahrami, 2013; North and Davidson, 2012; Schumm, 1993). The relation of incised-valleys and sea level was discussed by Wetzel *et al.* (in prep.), in which he suggests that the increase in channel sinuosity is related to stability in sea level. On the investigation area, the channel sedimentation initially occurred completely under riverine condition, followed by a gradual changed to transitional (with the increase of tidal influence) and subsequent fully marine conditions. The riverine conditions are represented in seismic profiles by vertical accretion and progradation of point bars. The "T" horizon is evidence that (during a certain period) the channel was under transitional conditions located at the shoreline or close to it. The "T" horizon possibly represents the action of waves eroding the topmost part of the sigmoidal strata that characterize the point bar deposits. The sediment composing SU3 may represent very shallow marine deposits formed under wave influenced (surf zone). The "R" horizon represents low energy marine deposits characterized by horizontal to sub-horizontal stratification corresponding to middle or outer continental shelf. The offshore increase of the thickness of SU3 indicates that sea level did not rise linearly (considering that they occurred under similar sediment availability conditions and sedimentation rate). Thicker layers of SU3 may indicate low rates of sea level rise while thinner layers are correlated to high rates of sea level rise.

Chapter 8 – GENERAL CONCLUSIONS

There is a relation between rainfall and both river discharge and suspended sediment concentration on PR's drainage basin. Annual seasonality of river discharge is directly related to the total amount of rainfall of a given month. However, during long drought periods the discharge of PR is influenced by water release from Boa Esperança reservoir. Rainfall regulates the seasonality of SSC, although, not in a simple manner. Other factors such as the geology of the drainage basin and land use close to the river margins affect the amount of sediment that is transported into the river as well. Minimal rainfall after the dry period is capable of substantially increase the SSC. Because of this the high turbidity period is longer than the wet period. The PR is the primary sediment source for the coast and inner continental shelf; hence, oscillations on SSC directly influence the variations on sediment yield affecting coastal morphodynamics. Therefore, the occurrence and intensity of ENSO indirectly affects sediment yield and

short term (inter-annual to decadal) morphodynamics by directly influencing the rainfall intensity and seasonality.

Incised-valleys are the records of sea level variations on the continental shelf offshore PRD. Although it is rather difficult to approximate the time when these features were developed due to lack geochronological information (stable isotopes), interpretation of seismic profiles allow to establish a relative chronology of the incised-valleys SU and changes in sea level. A key point to achieve this was to use seismic stratigraphy based on the recognition of seismic units, seismic boundaries, seismic facies, architectural elements and strata termination of the paleo-channels layers. The stratigraphic record suggests that only one event of valley incision have occurred. Therefore, one hypothesis is that CB occurred during the last glacial maximum (~20.000 yr. BP) when sea level was approximately 120 m bellow the present level (Fleming *et al.,* 1998; Rabineau *et al.,* 2006; Yokoyama *et al.,* 2001). The R horizon is interpreted as the surface of "maximum transgression", hence, deposited during sea level high stand which occurred at about 5.600 – 6.000 yr. BP (Bezerra *et al.,* 2003; Caldas *et al.,* 2006). In this case the development of the fluvial system that originated the incised-valleys started during the Late Pleistocene.

This work pointed out strong indications that the tidal channels west of PR are its older distributaries and a process of channel switching occurred. However, its controlling factors were not established. Moreover, ENSO can be one climatic factor that influences short term coastal morphology in terms of shoreline evolution.

GENERAL ACKNOWLEDGEMENT

This work represents the end of a long (really long) journey and the beginning of a new one. Along the way I had the privilege of meeting many people and all had their share in contributing to this outcome. However, some of them substantially influenced my pathway to which I would like to write a few words to express my gratitude.

First I would like to thank my parents (Canindé and Ducila) that always supported, helped and cheered for me. Without them I would certainly not have achieved what I did so far. My brother, Vinícius, that I know will always be there whenever I need him. My wife, Carina, and my sister, Viviane, without they two my life in Kiel it would had been much more difficult. Their love and friendship gave strength and tranquility to overcome the difficult times. More recently to my son, Matheus, that gave inspiration and to whom I want to be a good person, good father,

best friend, and, more importantly, a good example (as my father and my mother have been to me).

To my mentors, Prof. Dr. Helenice Vital, Prof. Dr. Karl Stattegger (and his wife Heidi) and Dr. Klaus Schwarzer, my deepest gratitude for the patience, guidance and help on this journey. Without you I could not have accomplished this.

To my colleagues of the institute; Daniel Unverricht, Christophe Heinrich, Fabiana Santos, Camille Traini, Peter Feldens, Peter Richter, Svenja Pimpke, Agata Szczygielski and Juliana Koenig, many thanks. I extend my thanks also to all my friends of the GGEMMA group in Brazil (which I will not list because it would be a long list).

Last but not least I would like to thank my friends: David Rose and Jan Carstens, thank you my friends. To Frederico Schwarz, Darumwan Sakuna, Eliene and Stephan Hazemberg, and Björn Heise I would like to say that I can never thank you enough for what you have done for me.

In these brief words wish to have expressed my gratitude for all that directly or indirectly contributed to this achievement.

LITERATURE CITED

Almeida-filho, R., Rossetti, D. F., Miranda, F. P., Ferreira, F. J., Silva, C., Beisl, C., 2009. Quaternary reactivation of a basement structure in the Barreirinhas Basin , Brazilian Equatorial Margin. *Quaternary Research*, 72(1), pp.103–110. Available at: http://dx.doi.org/10.1016/j.yqres.2009.02.010.

Andrade Júnior, A. S., Bastos, E. A., Barros, A. H. C., Silva, C. O. and Gomes, A.A.N., 2005. Classificação climática e regionalização do semi-árido do Estado do Piauí sob cenários pluviométricos distintos 1 Climatic classification and semiarid zone regionalization of the Piauí State , Brazil , Material e Métodos. *Revista Ciência Agronômica*, 36(2), pp.143–151.

Bahrami, S., 2013. Tectonic controls on the morphometry of alluvial fans around Danehkhoshk anticline, Zagros, Iran. *Geomorphology*, 180-181, pp.217–230.

Becker, J. J., Sandwell, D. T., Smith, W. H. F., Braud, J., Binder, B., Depner, J., Fabre, D., Factor, J., Ingalls, S., Kim, S-H., Ladner, R., Marks, K., Nelson, S., Pharaoh, A., Trimmer, R., Von Rosenberg, J., Wallace, G. and Weatherall, P., 2009. Global Bathymetry and Elevation Data at 30 Arc Seconds Resolution: SRTM30_PLUS. *Marine Geodesy*, 32, pp.355–371.

Bezerra, F. H. R., Barreto, A. M. F. and Suguio, K., 2001. Holocene sea-level history on the Rio Grande do Norte State coast, Brazil. *Marine Geology*, 196, pp.73–89.

Bhattacharya, J.P. & Giosan, L., 2003. Wave-influenced deltas : geomorphological implications for facies reconstruction. *Sedimentology*, 50, pp.187–210.

Bhattacharya, J.P. And Walker, R.G., 1992. Deltas. In Walker, R.G. and James, N. P., ed. *Facies Models: Response to Sea-Level Change*. St. Jhons: Geological Association of Canada, pp. 157–177.

Caldas, L. H. O., Stattegger, K., and Vital, H., 2006. Holocene sea-level history: Evidence from coastal sediments of the northern Rio Grande do Norte coast, NE Brazil. *Marine Geology*, 228(1-4), pp.39–53.

Castelao, R.M. & Moller Jr, O.O., 2006. A modeling study of Patos lagoon (Brazil) flow response to idealized wind and river discharge: dynamical analysis. *Brazilian Journal of Oceanography*, 54(1), pp.1–17.

Catuneanu, O., Bhattacharya, J. P., Blum, M. D., Dalrymple, R. W., Eriksson, P. G. and Fielding, C.R., 2010. Sequence stratigraphy : common ground after three decades of development. *First Break*, 28(January), pp.21–34.

Davey, M. K., Brookshaw, A. and Ineson, S., 2014. The probability of the impact of ENSO on precipitation and near-surface temperature. *Climate Risk Management*, 1, pp.5–24. Available at: http://dx.doi.org/10.1016/j.crm.2013.12.002.

Davey, M., Huddleston, M., Sperber, K., Braconnot, P., Bryan, F., Chen, D., Colman, R., Cooper, C., Cubasch, U., Delecluse, P., DeWitt, D., Fairhead, L., Flato, G., Gordon, C., Hogan, T., Ji, M., Kimoto, M., Kitoh, A., Knutson, T., Latif, M., Le Treut, H., S. and Z.S., 2002. STOIC: a study of coupled model climatology and variability in tropical ocean regions. *Climate Dynamics*, 18(5), pp.403–420.

Estournès, G., Menier, D., Guillocheau, F., Le Roy, P., Paquet, F. and Goubert, E., 2012. The paleo-Etel River incised valley on the Southern Brittany inner shelf (Atlantic coast, France): Preservation of Holocene transgression within the remnant of a middle Pleistocene incision? *Marine Geology*, 329-331, pp.75–92. Available at: http://dx.doi.org/10.1016/j.margeo.2012.08.005.

Feijó, F.J., 1994. A Bacia de Barreirinhas. *Boletim de Geociências de PETROBRAS*, 8(1), pp.103–109.

Fleming, K., Jhonston, P., Zwartz, D., Yokoyama, Y., Lambeck, K. and Chappell, J., 1998. Refining the eustatic sea-level curve since the Last Glacial Maximum using far- and intermediate-field sites. *Earth and Planetary Science Letters*, 163, pp.327–342.

Galloway, W.E., 1975. Process framework for describing the morphologic and stratigraphic evolution of deltaic depositional systems. In M. L. Broussard, ed. *Deltas, Models for Exploration*. Huston, TX: Houston Geological Society, pp. 87–98.

Góes, A. M. and Feijó, F.J., 1994. Bacia do Parnaíba. *Boletim de Geociências da PETROBRAS*, 8(1), pp.57–67.

Gomes, M.P. & Vital, H., 2010. Revisão da compartimentação geomorfológica da Plataforma Continental Norte do Rio Grande do Norte , Brasil. , 40(3), pp.321–329.

Green, A.N., 2009. Palaeo-drainage, incised valley fills and transgressive systems tract sedimentation of the northern KwaZulu-Natal continental shelf, South Africa, SW Indian Ocean. *Marine Geology*, 263(1-4), pp.46–63. Available at: http://dx.doi.org/10.1016/j.margeo.2009.03.017.

Green, A. N., Dladia, N. and Garlick, G.L., 2013. Spatial and temporal variations in incised valley systems from the Durban continental shelf, KwaZulu-Natal, South Africa. *Marine Geology*, 335, pp.148–161.

Gutierrez, B. T., Uchupi, E., Driscoll, N. W. and Aubrey, D.G., 2003. Relative sea-level rise and the development of valley-fill and shallow-water sequences in Nantucket Sound, Massachusetts. *Marine Geology*, 193, pp.295–314.

Hastenrath, S., 2006. Progress in Oceanography Circulation and teleconnection mechanisms of Northeast Brazil droughts. *Progress in Oceanography*, 70, pp.407–415.

James, N. P., and Dalrymple, R., 2010. *Facies Models 4* R. W. James, N. P. and Dalrymple, ed., Newfoundland: Memorial University of Newfoundland Press.

Luettich Jr., R.A., Carr, S.D., Reynolds-Fleming, J.V., Fulcher, C.W. and McNinch, J.E., 2002. Semi-diurnal seiching in a shallow, microtidal lagoonal estuary. *Continental Shelf Research*, 22, pp.1669–1681.

Nordfjord, S., Goff, J. A., Austin, J. A. and Sommerfield, C.K., 2005. Seismic geomorphology of buried channel systems on the New Jersey outer shelf : assessing past environmental conditions. , 214, pp.339–364.

North, C. P. and Davidson, S.K., 2012. Unconfined alluvial flow processes: recognition and interpretation of their deposits, and the significance for paleogeographic reconstruction. *Earth Sciences Reviews*, 111, pp.199–223.

Orton, G. J. and Reading, H.G., 1993. Variability of deltaic processes in terms of sediment supply, with particular emphasis on grain size. *Sedimentology*, 40, pp.475–512.

Pasquini, A.I., Niencheski, L.F.H. and Depetris, P.J., 2012. The ENSO signature and other hydrological characteristics in Patos and adjacent coastal lagoons, south-eastern Brazil. *Estuarine Coastal and Shelf Science*, 111, pp.139–146.

Rabineau, M., Berné, S., Oliviet, J.-L., Aslanian, D., Guillocheau, F. and Joseph, P., 2006. Paleo sea levels reconsidered from direct observation of paleoshoreline position during Glacial Maxima (for the last 500,000 yr). *Earth and Planetary Science Letters*, 252, pp.119–137.

Reading, H. G. and Collinson, J.D., 1996. Clastic Coasts. In H. G. Reading, ed. *Sedimentary Environments: Processes, Facies and Stratigraphy*. Oxford: Blackwell Science, pp. 154–231.

Rosseti, D. F., Góes, A. M. and Truckenbrodt, W., 2001. *O Cretáceo da Bacia de São Luís-Grajaú*, Belém: Museu Emílio Goeldi.

Schumm, S.A., 1993. River Response to Baselevel Change: Implications for Sequence Stratigraphy. *The Journal of Geology*, 101(2), pp.279–294.

Schwarzer, K., Diesing, M. and Trieschmann, B., 2000. Nearshore facies of the southern shore of the Baltic Ice Lake, example from Tromper Wiek (Rügen Island). *Baltica*, 13, pp.69–79.

Schwarzer, K., Stattegger, K., Vital, H. and Becker, M., 2006. Holocene Coastal Evolution of the Rio Açu Area (Rio Grande do Norte , Brazil). In *Proceedings, 8th International Coastal Symposium*. Itajaí, SC, Brazil: Journal of Coastal Research, Special Issue No. 39, pp. 140–144.

Szczygielski, A., Stattegger, K., Schwarzer, K., Aquino da Silva, A. G., Vital, H. and Koenig, J., 2014. Evolution of the Parnaíba Delta (NE Brazil) during the late Holocene. *Geo-Marine Letters*, in press. Available at: http://link.springer.com/10.1007/s00367-014-0395-x.

Tassan, S., 1987. Evaluation of the potential of the Thematic Mapper for marine application. *International Journal of Remote Sensing*, 8(10), pp.1455–1478.

Wetzel, A., Szczygielski, A., Unverricht, D., Tjallingii, R. and Stattegger, K., *Environmental significance of bent incised-valley fill-deposits*, Basel, Switzerland.

Wright, L. D., Coleman, J. M. and Thom, B.G., 1973. Processes of channel development in a high-tide-range environment: Cambrige Gulf-Ord River delta, western Australia. *Journal of Geology*, 81, pp.15–41.

Yokoyama, Y, De Deckker, P., Lambeck, K, Jhonston, P. and Fifield, L.K., 2001. Sea-level at the Last Glacial Maximum: evidence from northwestern Australia to constrain ice volumes for oxygen isotope stage 2. *Palaeogeography, Palaeoclimatology, Palaeoecology*, 165, pp.281–297.